

DRY SEPARATION OF PYRITE FROM COAL

By

W. T. Abel, M. Zulkoski and G. J. Gountlett
U. S. Department of the Interior, Bureau of Mines
Morgantown Energy Research Center
Morgantown, West Virginia 26505

ABSTRACT

A dry separation process for removing pyrite from fine coal utilizing centrifugal and electrostatic methods removed 35 to 55 percent of the total pyritic sulfur (amounting to 70 to 100 percent of available pyritic sulfur) in rejects of 10 to 15 percent. Both separation methods are benefited by restricting the particle-size range and keeping the pyrite particles as large as possible. Removal efficiency is increased, therefore, by integrating the separation and grinding operations, as in stage grinding.

INTRODUCTION

Relatively coarse coal can be cleaned quite effectively at the mine by wet processes. However, the removal of fine pyrite cannot be completed until the coal is finely pulverized. Because of transportation losses, this final pulverization is usually carried out at the point of use rather than the mine. Furthermore, if these fines were to be cleaned by wet methods, problems of coal drying and wet waste disposal would be introduced.

In the dry process reported here and shown in figure 1, the coal is ground then subjected to centrifugal separation for removal of the fines as light, pyrite-depleted fractions leaving a heavy, pyrite-enriched fraction. The light fractions amounting to 10 to 50 percent of the feed are taken as a clean product. The heavy fraction is passed to an electrostatic separator that concentrates the pyrite in a reject fraction of about 10-15 percent.¹

¹ Minutes of the "Removal of Pyrite from Coal" Conference, U. S. Bureau of Mines, Pittsburgh Coal Research Center, Bruceton, Pa., April 22, 23, 24, 1968, pages 69-91.

Centrifugal Separation

A cross section of the centrifugal separator is shown in figure 2. Particles of coal drop down the hollow drive shaft onto the spinning spreader disk and are thrown off into the rising stream of recirculated air. Particles that are too heavy to become entrained drop into the tailings cone and out the heavy product exit. Particles whose density and shape allow entrainment are carried into the swirl of air created by the centrifugal fan and are classified according to particle mass. The lighter particles are carried into the annular space between the inner and outer cones from where they drop out the light product exit. The heavier particles are thrown to the walls of the chamber where they fall in the stagnant air layer near the wall and leave the separator via the heavy product exit. The size of fines carried into the air swirl of the classifying fan can be limited by adjusting the velocity of the recirculated air. Starting at the lowest setting of recirculated air velocity and refeeding the heavy fraction with each increase in air velocity, a series of fine cuts may be obtained.

Electrostatic Separation

Electrostatic separations utilize the difference in conductivity or dielectric properties of coal and associated material, such as pyrite, to maintain or adequately lose an induced charge under dynamic conditions. Figure 3 shows the separation section of a "high intensity" electrostatic separator. A sufficiently dispersed layer of feed is maintained on the electrically grounded rotor for individual particle contact. The feed passes under an active electrode for exposure to ionic bombardment. Subsequently the particles either become of equipotential with the rotor, as would a conductor, and are released, or if a dielectric material such as coal, remain attached to the rotor. All particles are also subjected to centrifugal and gravitational forces. The splitters are used to divide the stream of released material for the most effective concentrations of reject, middlings, and product.

Dry feed materials subjected to "high intensity" or a corona field of dissociated gas molecules are momentarily attracted to the rotor. This high intensity band is relatively narrow and depends on the proximity of the active electrode and the intensity of the rectified transformer current. A range of 18 kilovolts to 30 kilovolts was found adequate for particle attraction, although the unit had a range up to 40 kilovolts. Generally, fine particles separate more efficiently with higher rotor speeds and lower voltages, while larger particles give better separation at lower rotor speeds and high voltages. For these reasons the size of particulate is best kept within narrow ranges for a single pass unit. However, multipass units with provisions for sizing of reject and/or middlings at 50 mesh would give higher concentration of product than multipass units alone.

Other factors are also involved in making efficient separations, such as atmospheric humidity, moisture and fines content of the coal. Humidity affects ionization and separations are improved at a mid-range. Moisture and fines content affect the extent of balling of fines and coating of the larger particles. Neither of these factors enhances separation efficiency, and both must be controlled for efficient separation.

Grindability Aids Separation

Figure 4 demonstrates that coal is ground to 70 percent below 200 mesh in one-seventh of the time required for pyrite. While the spread is less in the early stages of Hardgrove milling (a ball and race mill), it increases rapidly as milling proceeds. Since both centrifugal and electrostatic separation remove larger particles of pyrite more efficiently than fine particles, the advantage of pulverizing in a manner that minimizes pyrite grinding is apparent. Thus, if the proper grinding process is incorporated as staged steps of the removal system, pyrite could be removed as it is released from the coal matrix.

Centrifugal Separator Performance

The capability of centrifugal separation for removing pyrite from closely sized feed material is shown in table 1 and figure 5. The portion of total pyritic sulfur concentrated in a 10-percent reject increased as the particle size decreased until nearly 60 percent was concentrated from the 270 x 400 mesh cut. The accompanying bar at each size fraction in figure 5 shows the pyritic sulfur which is available. Available pyritic sulfur is defined as pyritic sulfur in the sink portion from float-sink separation at a specific gravity of 1.6. The size and chemical analysis of the coal from which these closely sized fractions were taken is shown in table 2. It is significant that the 400 x 0 mesh fraction underwent reverse enrichment when subjected to centrifugal separation. This demonstrated the breadth of particle-size range of this fraction containing extremely fine pyrite. The amount of the fine pyrite probably resulted from grinding in an air-swept mill in which the particles are returned to the mill until fine enough to be carried out by the air sweep.

Electrostatic Separation Performance

The effectiveness of electrostatic separation for concentrating pyrite is shown by table 3. Blends consisting of 90 percent coal and 10 percent pyritic material were submitted to the electrostatic separator. Each component of the blend had been previously cleaned by float-sink

separation, i.e., the coal floated at 1.6 specific gravity while the pyritic material reported to sink at 2.89 specific gravity. With closely sized fractions of these blends, the separation was very sharp. As shown in table 3 with the 80 x 100 mesh fraction, nearly 98 percent of the pyrite was rejected while 97 percent of the coal went to the product bin. Treatment of the 270 x 400 mesh fraction placed 98 percent of the pyrite in the reject bin, 92 percent of the coal in product bin, and about 6 percent of the coal in the middling bin.

Combined Centrifugal-Electrostatic Separation Performance

The float-sink behavior of ground Pittsburgh-seam roof coal at 1.6 specific gravity is shown in figure 6. The upper curve shows the portion of these consists below 200 mesh. The results of combined centrifugal-electrostatic separation treatment of this same coal are given in table 4 and shown in figure 7. While only about 35 percent of the total pyritic sulfur was removed, this amounted to nearly 70 percent of the available pyritic sulfur. Where grinding time is shown as a variable in the process the initial size of the coal feed is 16 x 30 mesh.

Figure 8, which shows the data of table 5, demonstrates the improvement in separation efficiency when cleaning is carried out between stages of grinding. Grinding of this same Pittsburgh-seam roof coal was accomplished in three 15-minute stages followed by one 30-minute stage. As shown in figure 8, over 40 percent of the total pyritic sulfur was removed after the first stage, with an additional 12 percent removed after the remaining grinding stages. While only about 53 percent of the total pyritic sulfur was removed, this amounted to virtually all the available pyritic sulfur as shown by the upper curve of figure 8. The fact that more than 100 percent of the available pyritic sulfur was removed from the 15- and 30-minute grinds was due to considerable size reduction occurring in centrifugal separation of these relatively coarse consists.

A third coal was chosen for testing because its sulfur content was highly pyritic, much of which occurred as a larger, more available particulate. The results of combined separation tests on this coal are shown in table 6 and in figure 9. Over 50 percent of the total pyritic sulfur was removed from the 90-minute ball-mill product in a reject of about 13 percent. With staged grinding, i.e., pyrite removal steps between grinding stages, this removal could probably be increased to more than 70 percent of total pyrite. Float-sink results on this coal are not yet completed.

CONCLUSIONS

Wet cleaning methods currently in practice effectively remove available pyrite from relatively coarse coal. Removal of fine pyrite, however, requires crushing the coal to very fine size. If these fine coals are cleaned by wet methods, problems of drying and wet waste disposal are introduced.

An integrated dry process was investigated that involved grinding followed by centrifugal and electrostatic separation, using three coals that are burned for power generation in the Appalachian region. Centrifugal separation removed the light, pyrite-poor portion of the crushed coal, after which the heavy fraction was submitted to electrostatic separation that concentrated the pyrite in a relatively small reject portion.

From 35 to 55 percent of the total pyritic sulfur (amounting to 70 to 100 percent of available pyritic sulfur) was removed in rejects of 10 to 15 percent. Since both centrifugal and electrostatic separation are benefited by restricting particle-size range and by maintaining the pyrite particles as large as possible, the efficiency of pyrite removal is improved by integrating grinding with the dry process.

When integrated with the grinding operation, the dry process was equally as effective as the wet process, and because of its potential advantages may warrant further research on a larger scale.

TABLE 1. - Dry removal of pyrite from closely-sized fractions of finely ground Pittsburgh-seam coal via centrifugal separation

Feed size, U.S. sieve	Light fraction					Heavy fraction					Adjusted portion of total pyritic sulfur, pct
	Percent of feed	Sulfur, pct	Pyritic sulfur, pct	Portion of total sulfur, pct	Portion of total pyritic sulfur, pct	Percent of feed	Sulfur, pct	Pyritic sulfur, pct	Portion of total sulfur, pct	Portion of total pyritic sulfur, pct	
60-80	89.4	2.30	0.98	86.1	81.8	10.6	3.12	1.84	13.9	18.2	17.2
80-100	91.0	2.65	1.00	89.8	87.1	9.0	3.04	1.50	10.2	12.9	14.3
100-140	93.5	2.70	1.20	91.5	88.6	6.5	3.60	2.23	8.5	11.4	17.5
140-200	86.1	2.77	1.15	81.5	71.6	13.9	3.89	2.83	18.5	28.4	20.4
200-270	89.4	2.44	0.96	80.0	68.1	10.6	5.14	3.79	20.0	31.9	30.1
270-400	91.6	2.32	0.72	72.7	50.6	8.4	9.51	7.65	27.3	49.4	58.8
400-0	88.6	3.47	1.31	91.2	95.9	11.4	2.59	0.43	8.8	4.1	3.6

¹ The percent of total pyritic sulfur contained in a 10% coarse cut of same composition as the actual coarse cut.

Note: Analyses of feed fractions are given in Table 2.

TABLE 2. - Analysis of Pittsburgh-seam coal

Fraction, U. S. sieve	Portion of feed, pct	Sulfur, pct	Portion of total sulfur, pct	Pyritic sulfur, pct	Portion of total pyritic sulfur, pct	Ash, pct	Portion of total ash, pct
16 x 60	0.8	2.03	0.7	0.75	0.6	7.91	0.9
60 x 80	2.4	2.02	2.1	.65	1.7	6.27	2.2
80 x 100	3.1	2.06	2.8	.66	2.2	6.04	2.7
100 x 140	10.1	2.27	10.0	.90	9.8	5.99	8.9
140 x 200	12.6	2.34	12.9	.97	13.2	6.20	11.4
200 x 270	10.3	2.59	11.7	1.14	12.7	6.27	9.4
270 x 400	11.9	2.60	13.5	1.18	15.1	6.20	10.8
400 x 0	48.8	2.17	46.3	.85	44.7	7.53	53.7
COMPOSITE	100.0	2.35	102.6	.97	104.3	6.94	101.3

TABLE 3. - Electrostatic separation of closely-sized blends consisting of 90 percent coal, 10 percent pyritic material

Component	Distribution of each component, percent		
	Reject	Middling	Product
80 x 100 mesh blend			
Coal ¹	2.7	0.3	97.0
Pyritic material ²	97.8	0.4	1.8
270 x 400 mesh blend			
Coal ¹	1.8	6.2	92.0
Pyritic material ²	97.9	2.0	.1

¹ Coal from Kittanning seam, comprising 90% of blend, previously cleaned by removing sink @ 1.6 sp gr.

² Pyritic material from Pittsburgh seam, comprising 10% of blend, previously cleaned by removing float @ 2.89 sp gr.

TABLE 4. - Combined centrifugal-electrostatic separation of pyrite from a Pittsburgh seam roof coal

Feed		Centrifugal separation				Electrostatic separation				Product of combined separations				Reject of combined separations				
		Yield, pct of feed	Analysis of product, pct	Pct of total pyritic sulfur	Total sulfur	Yield, pct of feed	Analysis of product, pct	Pct of total pyritic sulfur	Total sulfur	Yield, pct of feed	Analysis of product, pct	Pct of total pyritic sulfur	Total sulfur	Pct of feed	Pct of total pyritic sulfur	Pct of total available pyritic sulfur		
Ball mill- ing time, min- utes	Pct of total pyritic sulfur in sink @ 1.6 sp gr	Total sul- fur	Py- ritic sul- fur			Total sul- fur	Py- ritic sul- fur			Total sul- fur	Py- ritic sul- fur							
		28.9	50.1	4.07	1.90	52.3	42.1	3.45	1.30	30.0	92.2	3.78	1.62	82.3	7.8	17.7	61.2	
15		28.9	25.8	3.84	1.68	23.6	63.4	3.49	1.34	46.5	89.2	3.59	1.44	70.1	10.8	29.9	103.5	
		45.7	30.3	3.54	1.39	22.1	60.1	3.47	1.32	42.0	90.4	3.49	1.34	64.1	9.6	35.9	78.6	
30		45.7	44.9	3.77	1.61	39.5	44.7	3.37	1.22	29.8	89.6	3.57	1.42	69.3	10.4	30.7	67.2	
		52.8	45.2	3.54	1.39	32.3	48.8	3.65	1.49	37.1	94.0	3.59	1.44	69.4	6.0	30.6	57.9	
60		52.8	24.2	3.40	1.25	15.5	61.7	3.68	1.56	49.1	85.9	3.63	1.47	64.6	14.1	35.4	67.0	
		52.8	11.4	3.27	1.13	6.6	77.8	3.48	1.33	52.8	89.2	3.45	1.30	59.4	10.8	40.6	76.9	
		52.8				90.7	3.51	1.36	62.9	90.7	3.51	1.36	62.9	9.3	37.1	70.2		

¹ All 4 runs in the 60 minute consist were made by reconstituting electrostatic separation products and adding the last cut from centrifugal separation.

² Pyrite sulfurs were calculated from total sulfur using the relation P.S. = .96 (T.S.) - 2.01. This relation was determined experimentally for this coal.

³ The percent of total pyritic sulfur reporting to sink @ 1.6 sp gr is taken as the percent of available pyritic sulfur.

TABLE 5. - Combined centrifugal-electrostatic separation of pyrite from a Pittsburgh seam roof coal utilizing staged grinding

Feed			Centrifugal separation product				Electrostatic separation reject				Cumulative product total				Cumulative reject total			
Sep'n Stage	Cumulative ball milling time, minutes	Pct of total pyritic sulfur in sink @ 1.6 sp gr	Yield, pct of feed	Analysis		Portion of feed, pct	Analysis		Total pyritic sulfur, pct	Yield, pct of feed	Analysis		Pct of total pyritic sulfur	Pct of feed	Pct of total available pyritic sulfur	Pct of total available pyritic sulfur		
				Total sulfur	Pyritic sulfur		Total sulfur	Pyritic sulfur			Total sulfur	Pyritic sulfur						
1	15	28.9	19.9	3.83	1.67	18.7	9.4	9.98	7.57	40.5	19.9	3.83	1.67	18.7	9.4	40.5	140.1	
2	30	45.7	3.3	3.33	1.19	2.2	3.2	5.61	3.38	6.1	23.2	3.76	1.60	20.9	12.6	46.6	102.0	
3	45	49.0	1.7	3.18	1.04	1.0	3.1	4.92	2.71	4.7	24.9	3.72	1.56	21.9	15.7	51.3	105.0	
4	75	55.0	5.6	3.06	0.93	3.0	1.2	4.72	2.52	1.7	30.5	3.59	1.44	24.9	16.9	53.0	96.4	
Electrostatic separation product																		
42.83																		
3.50																		
1.35																		
32.8																		

¹ Pyritic sulfurs were calculated from total sulfur using the relation P.S. = .96 (T.S.) - 2.01. This relation was determined experimentally for this coal.

² The percent of total pyritic sulfur reporting to sink @ 1.6 sp gr is taken as the percent of available pyritic sulfur.

TABLE 6. - Combined centrifugal-electrostatic separation of pyrite from Pittsburgh seam strip mine

Feed			Centrifugal separation product				Electrostatic separation product				Product of Combined Separation				Reject of combined separation			
Ball milling time	Pct of total pyritic sulfur in sink @ 1.6 sp gr	Yield, pct of feed	Analysis		Portion of feed, pct	Analysis		Total pyritic sulfur, pct	Yield, pct of feed	Analysis		Pct of total pyritic sulfur	Pct of feed	Pct of total available pyritic sulfur		Pct of total available pyritic sulfur		
			Total sulfur	Pyritic sulfur		Total sulfur	Pyritic sulfur			Total sulfur	Pyritic sulfur			Total sulfur	Pyritic sulfur			
15	51.3	7.3	2.26	1.17	4.7	80.8	2.67	1.56	68.9	88.1	2.64	1.53	73.6	11.9	26.4	51.5		
30	59.1	19.1	2.19	1.09	10.2	71.0	2.95	1.84	64.0	90.1	2.79	1.68	74.2	9.9	25.8	43.7		
60	73.2	38.7	1.98	0.88	18.5	46.1	2.54	1.44	36.2	84.8	2.28	1.18	54.7	15.2	45.3	61.9		
90	76.9	58.0	2.11	1.01	32.0	29.1	2.23	1.13	18.0	87.1	2.15	1.05	50.0	12.9	50.0	65.0		

¹ Pyritic sulfur is calculated by the relation P.S. = 0.99 (T.S.) - 1.079. This relation was determined experimentally for this coal.

² The percent of total pyritic sulfur reporting to sink @ 1.6 sp gr is referred to as the available pyritic sulfur.

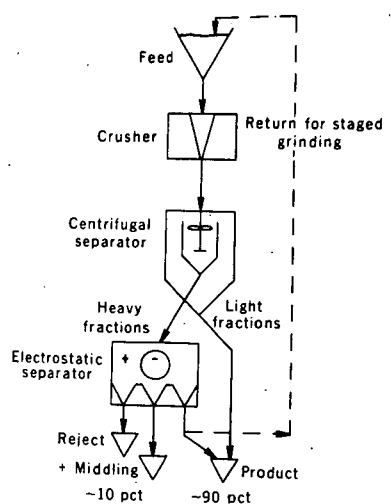


FIGURE 1. - Dry Process for Removal of Pyrite from Coal

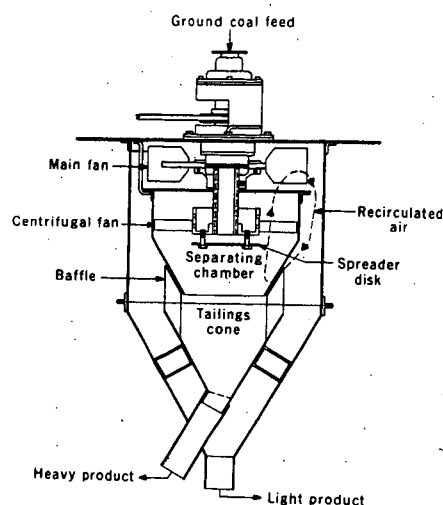


FIGURE 2. - Cross Section of Centrifugal Separator

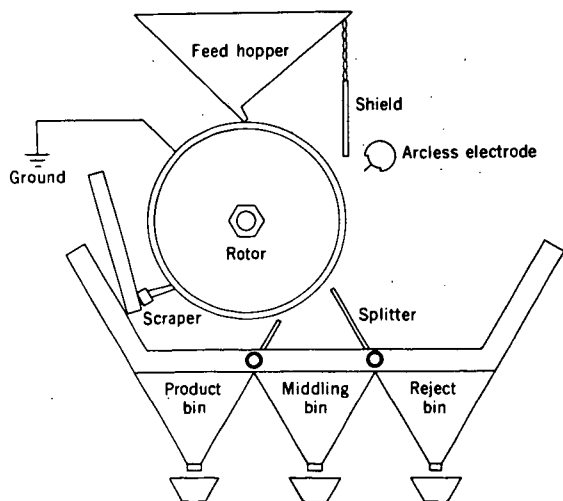


FIGURE 3. - Sketch of Electrostatic Separator

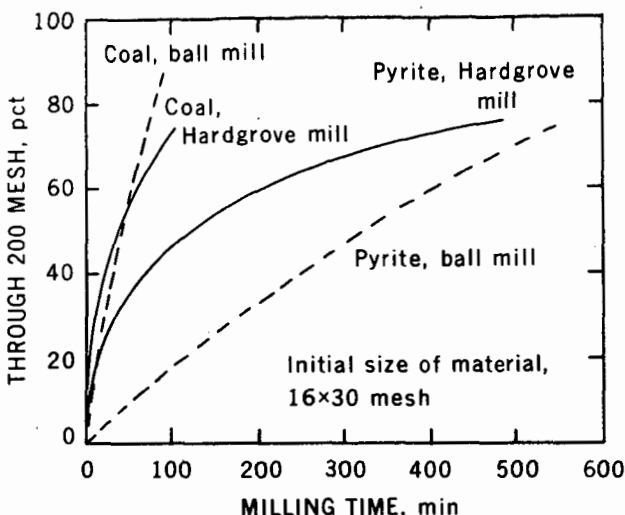


FIGURE 4. - Grindability of Pittsburgh-Seam Coal and Pyritic Material by Ball and Hardgrove Mills

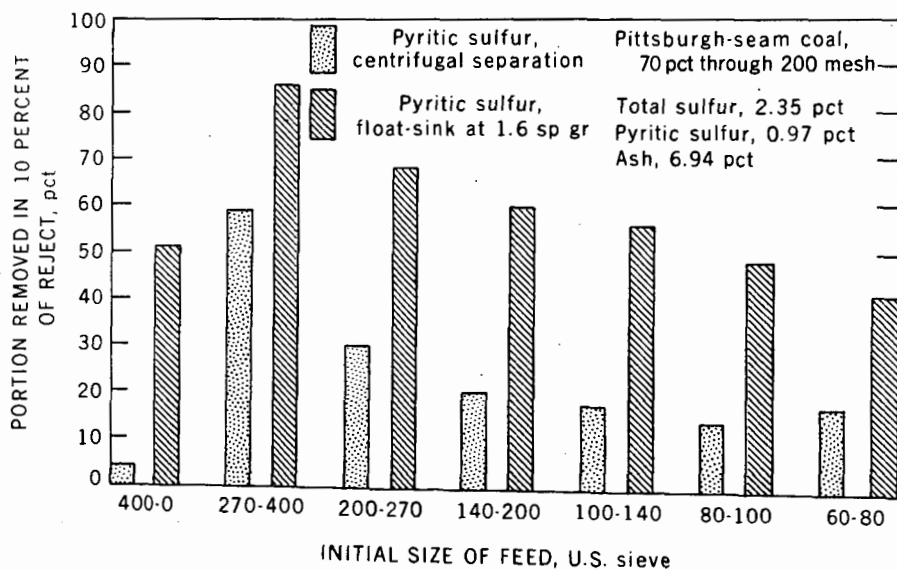


FIGURE 5. - Removal of Pyrite from Closely Sized Fractions of Finely Ground Coal by Centrifugal Separation

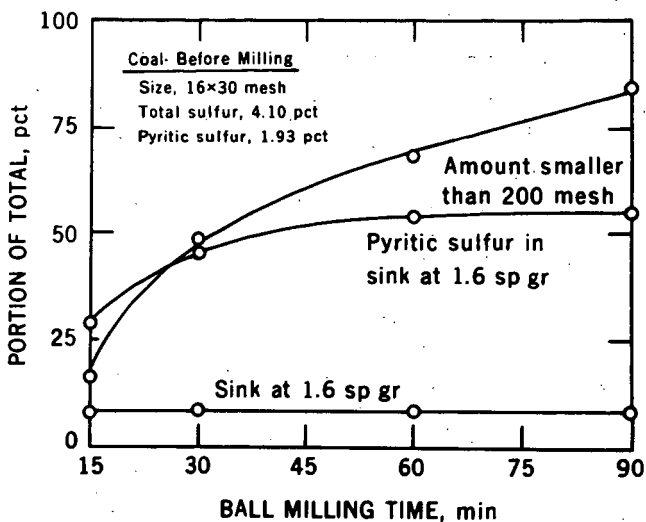


FIGURE 6. - Float-Sink Behavior of Pittsburgh-Seam Roof Coal Following Pulverization by Ball Milling

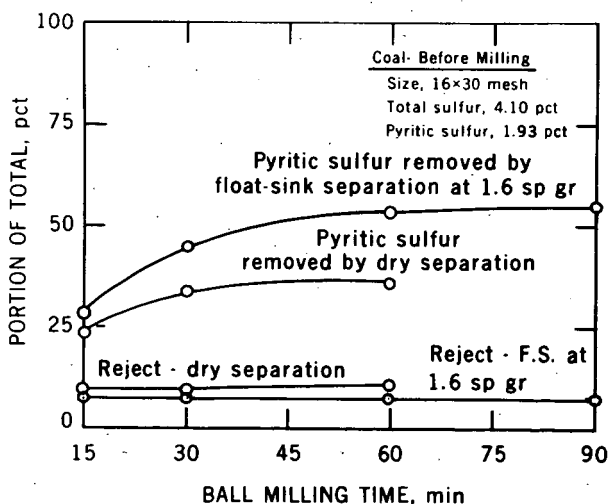


FIGURE 7. - Combined Centrifugal-Electrostatic Removal of Pyrite from a Pittsburgh-Seam Roof Coal

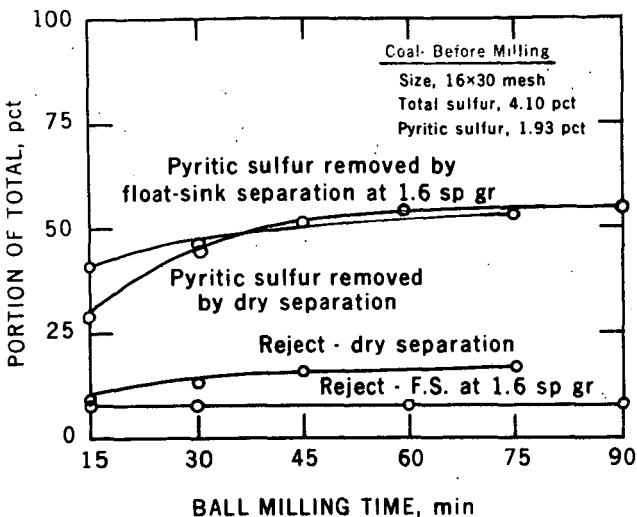


FIGURE 8. - Combined Centrifugal-Electrostatic Separation of Pyrite from a Pittsburgh-Seam Roof Coal Using Stage Grinding

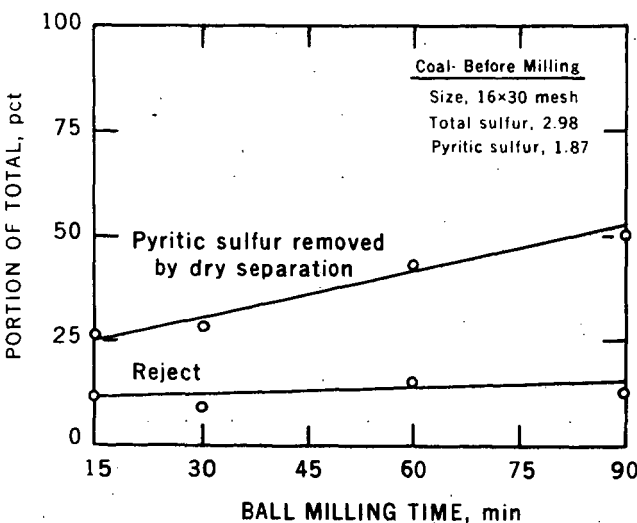


FIGURE 9. - Combined Centrifugal-Electrostatic Removal of Pyrite from a Pittsburgh-Seam Strip Coal

REDUCTION OF HYDROUS FERRIC OXIDE TO A MAGNETIC FORM WITH SODIUM DITHIONITE; IMPLICATIONS FOR COAL MINE DRAINAGE TREATMENT

R. C. Streeter,¹ D. C. McLean, and H. L. Lovell

College of Earth and Mineral Sciences
The Pennsylvania State University
University Park, Pennsylvania

INTRODUCTION

The technique of neutralization with a cheap alkali, usually hydrated lime, is still the principal approach to coal mine drainage treatment today. As the number of these lime treatment plants has increased in response to stricter legislative controls, there has been a growing awareness that sludge dewatering and disposal present a major problem in the lime treatment process.

The sludge from a typical lime treatment plant is gelatinous and slow-settling; it rarely attains a solids content of more than five percent by weight after gravity settling; it cannot be dewatered economically with conventional mechanical dewatering equipment; depending on water quality and flow rate, the sludge can represent a significant percentage of the total throughput volume; and, the costs for sludge storage or disposal can increase operating expenses appreciably. Most of these problems could be alleviated if a method could be found to substantially increase the density of the sludge, either during or subsequent to the actual treatment process.

Various approaches to the control of mine drainage sludge properties have been reviewed by Lovell. (1) One such approach which has been the subject of a more extensive study (2), has involved the chemical reduction of the major sludge component, hydrous ferric oxide, to a ferromagnetic form.

Methods for the conversion of hydrous iron oxides in aqueous suspension to the magnetic ferroferric oxide (magnetite) have been thoroughly documented in the chemical literature, although these processes are almost entirely concerned with either 1) partial oxidation of ferrous hydroxide, or 2) mixture of ferric and ferrous iron solutions in the proper stoichiometric amounts followed by the addition of alkali to precipitate the magnetic oxide. The third possible route, involving controlled partial reduction of hydrous ferric oxide, has received surprisingly little attention, possibly because the relatively strong reducing agents employed have tended to result in problems with reaction control (e.g. over-reduction of iron) as well as air-oxidation or decomposition of the reducing agent itself, leading to undesirable side reactions and reagent handling problems.

Unlike most of the reductants which reportedly yield a magnetic product on reaction with hydrous ferric oxide, sodium dithionite (sodium hydrosulfite)

¹ Present address: Bituminous Coal Research, Inc.
350 Hochberg Road
Monroeville, Pennsylvania 15146

is a commercially available, relatively inexpensive, and stable solid in dry air at room or slightly elevated temperatures. Its use in this application was first described in 1951 by Robl (3) and later mentioned by Ackermann (4), although neither of these authors reported in detail concerning the reaction stoichiometry, the effects of reaction variables such as temperature and pH, or the nature of the magnetic product. Consequently, the primary objective of this investigation was to conduct a more systematic study of the hydrous ferric oxide - sodium dithionite reaction, and to deduce whether this reaction might provide the basis for a feasible coal mine drainage treatment process. In line with this approach, the experiments were conceived to provide realistic analogies with coal mine drainage systems. For example, only sulfate salts of iron were used for the preparation of reagent solutions, and iron concentrations were maintained within representative limits.

A secondary objective of this research was to consider the effects of dissolved impurities on the reaction, since such effects are known to be of considerable significance. (5-8) Because the process envisioned involved the use of lime as an alkali, attention was focused largely on the effect of dissolved calcium.

EXPERIMENTAL

Most of the reactions were carried out using a 400-ml beaker containing 200 ml of reagent grade ferric sulfate solution. The beaker was fitted with a 1/8-inch thick Lucite cap containing four large holes to accomodate electrodes for pH and millivolt measurements. Three smaller holes were drilled in the cap through which a thermometer, nitrogen gas inlet tube, and buret (or reagent funnel) were introduced. The apparatus was mounted on a stirring hot plate, which provided temperature control to within $\pm 0.5^{\circ}\text{C}$ for experiments at elevated temperatures. Measurements of pH and electromotive force (Eh) during the reaction were accomplished using two Heath Model EUW-301 recording electrometers.

At the beginning of an experiment, stirring and nitrogen flow were commenced, and 1 N sodium hydroxide solution was added dropwise from a buret to achieve the desired pH (usually 10.0) in the system. The resulting suspension of hydrous ferric oxide was then purged continuously with nitrogen for a one-hour period to minimize decomposition of the dithionite by dissolved oxygen. The Eh of the suspension was monitored during this period, and usually reached a constant value within the last 30 minutes. Anhydrous sodium dithionite (Virginia Chemicals, Inc.; 94.3 percent purity) was then added to the deoxygenated suspension as a dry solid powder through a reagent funnel. It was found necessary to employ the dithionite in the solid form to avoid prior decomposition through hydrolysis or air oxidation.

The reaction was allowed to proceed for about six minutes, during which the pH was maintained at the desired level by further additions of 1 N sodium hydroxide. The suspension was then made up to constant volume with deionized water and aliquots were taken for iron analyses, sludge centrifugation and settling tests. Aliquots for iron analyses were filtered immediately with suction through a 30-ml fritted glass filter crucible, and filter cakes were dissolved in 2 ml of concentrated hydrochloric acid. Ferrous and total iron were determined by titration with 0.01 N potassium dichromate using sodium diphenylamine sulfonate as an internal indicator. Centrifugation tests were performed by centrifuging 15 ml aliquots of the suspension in graduated

centrifuge tubes at 3,100 rpm for 5 minutes. Settling tests were conducted using 100-ml graduated cylinders.

Magnetic properties of the reaction products were observed qualitatively with the aid of a small Alnico V horseshoe magnet.

In experiments involving the effect of dissolved calcium, weighed amounts of reagent grade calcium oxide were dissolved in the acidified ferric sulfate solution before alkalization with sodium hydroxide and subsequent addition of the dithionite. The Eh of the resulting suspension was monitored for a 1.5-hour period following dithionite addition.

RESULTS

The relationship found by these experiments between the mole percentage of Fe(III) reduced and the initial Fe(III):Na₂S₂O₄ molar ratio is shown in Figure 1. The equation of the best straight line through the experimental points was found to be

$$\log x = 2.3315 - 1.1760 \log y$$

where x = mole percentage of Fe(III) reduced

and y = Fe(III):Na₂S₂O₄ molar ratio.

If the experimental line is extrapolated, it is found that 100 percent reduction of Fe(III) occurs approximately at the point where the Fe(III):Na₂S₂O₄ molar ratio is equal to 2.0. Therefore, the theoretical reaction stoichiometry may be expressed more accurately by the relationship

$$\log x = 2.30103 - \log y$$

and this line is included in Figure 1 for comparison.

It should be noted that in the presence of excess dithionite, the reduction of hydrous ferric oxide continues beyond the point of reduction of one-third of the Fe(III) available (corresponding to the formation of magnetite). This was indicated by the appearance and magnetic properties of the reaction products. Thus, at high Fe(III):Na₂S₂O₄ molar ratios (excess Fe(III)) reaction products were more voluminous, only moderately magnetic, and brown in color, indicating the presence of unreacted Fe(OH)₃; at low Fe(III):Na₂S₂O₄ molar ratios (excess Na₂S₂O₄), reaction products were gelatinous, weakly magnetic, and blue-green in color, suggesting the presence of Fe(OH)₂. Nevertheless, it is significant that ferromagnetic properties of the product were observed in varying degrees throughout the range Fe(III):Na₂S₂O₄ = 3 to 10.

The formation of the magnetic phase near an Fe(III):Na₂S₂O₄ molar ratio of 6 is further revealed by a plot of redox potential in the system versus the amount of dithionite added. This is shown in Figure 2, which indicates a break in the curve near the point corresponding to reduction of one-third of the Fe(III) present.

Distinct variations in the settling behavior of the product solids were observed with changes in the Fe(III):Na₂S₂O₄ molar ratio. Curiously, optimum settling behavior and minimum solids volume, as measured by centrifugation tests, appeared to occur at an Fe(III):Na₂S₂O₄ molar ratio near 6.5, corresponding to about 25 mole percent Fe(III) reduction for samples prepared at 30°C and pH 10. The results of experiments at other temperatures and pH values are summarized in Tables 1 and 2, respectively. All of the experiments indicated in Table 1 yielded magnetic products. On the other hand, changes in reaction pH at constant temperature (30°C) produced changes in the nature of the reaction product, as shown in Table 2.

TABLE 1. EFFECT OF TEMPERATURE ON THE REDUCTION OF HYDROUS FERRIC OXIDE BY SODIUM DITHIONITE AT pH 10^a

Temperature, °C	Mole Percent Fe (III) Reduced	Centrifugate Volume, ml	Percent Solids Vol. after 60 minutes ^b
10	22.66	0.50	13.7
20	20.65	0.45	12.5
30	21.65	0.48	12.7
40	21.94	0.52	14.1
50	22.53	0.60	17.8
60	21.71	0.65 ^c	18.9
70	21.92	0.52	18.9
80	19.73	0.44	9.8

^aFe(III):Na₂S₂O₄ molar ratio = 6.5 in all runs

^bGravity-settled solids

^cMechanical difficulties with the centrifuge were encountered; true centrifugate volume is probably less than 0.65 ml

The effect of pH on the reaction was also investigated in a series of tests at 80°C. In terms of the mole percentage of Fe(III) reduced, the results of these tests were essentially identical with those shown in Table 2. However, in all cases centrifugate volumes decreased markedly and settling rates were two to three times greater than those observed in the tests at 30°C. In addition, a phenomenon involving a color change of the solids from the orange-brown of amorphous Fe(OH)₃ to a distinct yellow-brown was observed to occur at 80°C during the one-hour nitrogen purge period.

prior to the addition of dithionite. This color change appeared to be accompanied by a decrease in the gelatinous nature of the solids and the formation of more granular particles. In such cases, the reaction products were also more granular and showed a greater tendency toward flocculation in a magnetic field. Subsequent x-ray diffraction analyses revealed the presence of small amounts of crystalline α -FeOOH (synthetic goethite) in several of the reaction products prepared at 80°C.

TABLE 2. EFFECT OF pH ON THE REDUCTION OF HYDROUS FERRIC OXIDE BY SODIUM DITHIONITE AT 30°C^a

pH	Mole Percent Fe(III) Reduced	Centrifugate Volume, ml	Percent Solids Vol. after 60 minutes ^b	Nature of Reaction Product
8.0	26.08	1.50	72.5	dark olive-green, nonmagnetic
9.0	25.27	0.75	21.1	black, flocculent, moderately magnetic
10.0	21.65	0.48	12.7	black, strongly magnetic
11.0	19.41	0.66	18.0	black, strongly magnetic
12.0 ^c	0.37	1.38	43.0	orange, gelatinous, nonmagnetic

^aFe(III):Na₂S₂O₄ molar ratio = 6.5 in all runs

^bGravity-settled solids

^cpH electrode response was very sluggish near pH 12 and there is some question as to whether the desired pH was attained. Thus, the results of this run may be anomalous.

The effect of initial iron concentration was investigated briefly in a series of tests in which the reaction vessel was open to the air and no attempts were made to remove dissolved oxygen from the system. The results revealed that below an initial Fe(III) concentration of about 3×10^{-2} molar (ca. 1,700 mg/l) there was a gradual decrease in the apparent mole percentage of Fe(III) reduced.

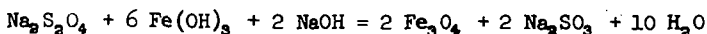
X-ray diffraction patterns of the freshly formed, magnetic reaction products corresponded to that of magnetite, and results of iron content analyses were very close to the theoretical value of 67.14 percent for $\text{Fe}_3\text{O}_4 \cdot \text{H}_2\text{O}$. On exposure to air, however, the initial reaction product was transformed to a rust-brown material with a corresponding decrease in iron content. This rust-brown material, which was still strongly ferromagnetic, was identified by x-ray diffraction analyses as $\gamma\text{-Fe}_2\text{O}_3$ (also hydrated).

The effect of calcium on the nature of the reaction product was investigated through a series of experiments in which increasing amounts of Ca^{2+} (as CaO) were introduced to the system before alkalization and reduction of the resulting solids by sodium dithionite. The Eh of the system was monitored throughout the course of the reaction, and usually reached a constant value within ± 10 millivolts about one hour after addition of the dithionite. There were no appreciable changes in the Eh, centrifugate volume, or appearance of the reaction product up to a Ca^{2+} concentration of about 1.2×10^{-2} molar. Above this concentration, however, the Eh of the system increased regularly and the reaction product became bulkier and less strongly magnetic. At a Ca^{2+} concentration of 2.4×10^{-2} molar, the reaction product was blue-green, gelatinous, and nonmagnetic, and appeared to consist largely of ferrous hydroxide. These results are summarized by Figure 3. Subsequent calculations showed that the point at which the observed changes began to occur in the system corresponded to the point at which the $(\text{Ca}^{2+})(\text{SO}_4^{2-})$ ion concentration product exceeded the solubility product of calcium sulfate dihydrate (gypsum) in the system (designated as K_{sp} in Figure 3). Also shown in Figure 3 are data from a similar study by Kakabadse et al. on the effects of Mg^{2+} . (8)

Several experiments were conducted using sludges prepared by alkalization (with NaOH, NH_4OH , or CaO) of actual coal mine drainage samples. In every instance, however, it was found impossible to effect a conversion of the sludge to a magnetic form by sodium dithionite reduction. On the other hand, if the iron was first oxidized (e.g. by H_2O_2), fractionally precipitated as $\text{Fe}(\text{OH})_3$ below pH 4, and separated from the liquid phase, conversion of the sludge to a magnetic form was readily effected and the results were essentially the same as those obtained using pure iron solutions. For those experiments where lime was used as the alkali, however, it was necessary to heat the suspension to at least 80°C to effect the desired conversion.

DISCUSSION

The experimental data indicate that the reduction process can be represented by the following overall reaction:



This reaction is similar to one proposed by Ackermann based on theoretical considerations. (4) It should be emphasized that no attempts were made in this study to isolate or identify the sulfur-containing by-product(s) of the reaction. The aqueous chemistry of dithionites is quite complex, and their oxidation can result in several species depending on reaction conditions. (9) Moreover, side reactions due to hydrolysis (10) or thermal decomposition (11) are common. In fact, loss of dithionite through such side reactions is believed to account in part for the discrepancies encountered in these studies between the theoretical and empirical stoichiometries, as reflected by Figure 1. A second factor which undoubtedly affected the results involved the oxidation of the reaction product to hydrated $\gamma\text{-Fe}_2\text{O}_3$. The available evidence indicated that this oxidation was sufficiently rapid during the first few minutes following preparation of the magnetic product to result in significant negative errors in the analytical determinations of Fe(II).

As mentioned earlier, reaction products exhibiting the maximum densities and fastest settling rates were found by experiment to have an Fe(III):Fe(II) molar ratio of about 3, corresponding to 25 percent Fe(III) reduction. Since both extraneous losses of dithionite and negative errors in the Fe(II) determination would have the effect of increasing the apparent Fe(III):Fe(II) ratio, it is possible that such reaction products did in fact correspond closely to true hydrated magnetites (Fe(III):Fe(II) = 2.0) at the actual time of preparation. However, it is interesting that Hoak and Sindlinger, during their development of a process for the recovery of ferrosoferric oxide from steel plant waste pickle liquors, observed that optimum settling rates were obtained when the Fe(III):Fe(II) molar ratio of the product was in the range of 2.5 to 3.5 (average 3.0). (12)

Variations in reaction temperature throughout the range 10 to 80°C appeared to have little effect on the reaction stoichiometry (Table 1). To the contrary, increases in the reaction pH throughout the range 8 to 12 resulted in definite decreases in the amounts of Fe(III) reduced (Table 2). This phenomenon is believed to be associated with the depressed dissociation of $\text{Fe}(\text{OH})_3$ with increasing pH, together with the supposition that the dithionite reduction proceeds through a solution mechanism involving the ferric ion. (4) It is apparent that, under the experimental conditions employed, optimum properties of the reaction product with respect to solids volume, settling rate, and magnetic response occurred at pH 10.

The results of experiments on the effect of initial iron concentration indicated that the role of dissolved oxygen in the system (i.e., through consumption of dithionite) became apparent below an Fe(III) concentration of about 3×10^{-2} molar. At an experimental Fe(III): $\text{Na}_2\text{S}_2\text{O}_4$ molar ratio of 6, the sodium dithionite concentration corresponding to this apparent limit would be about 5×10^{-3} molar, and this value is in agreement with that reported by Conley et al. in studies on the dithionite reduction of Fe^{3+} in neutral or acidic media. (13) In terms of practical application of the reaction, these results suggest that the initial Fe(III) concentration should be much greater than that of dissolved oxygen in order to prevent the latter from exerting a significant influence on the overall reaction stoichiometry.

There were indications throughout this investigation that factors affecting crystal growth are of considerable importance in the formation

and stability of the magnetic reaction product. Thus, the most strongly magnetic, densest, and fastest settling products were prepared under conditions which enhance crystal ordering, such as elevated reaction temperatures and the absence of impurities. The effect of temperature was especially apparent at or above 80 °C, and x-ray data indicated that the improved properties of the reaction product may have been largely due to the conversion of amorphous Fe(OH)_3 to crystalline $\alpha\text{-FeOOH}$ at these elevated temperatures, prior to the reaction with $\text{Na}_2\text{S}_2\text{O}_4$.

With regard to the effects of impurities in the system, it has been well established that the presence of foreign species in solution or suspension ordinarily has an adverse effect on ordering during crystal growth. (14, 15) A case in point involves the apparent adverse effects of coprecipitated gypsum on the magnetic and other properties of the reaction products prepared by dithionite reduction of Fe(OH)_3 . Of further relevance, it has been reported that interfering effects of other species (e.g. aluminum, magnesium) on the formation of magnetite in aqueous suspension are significant only within the pH ranges where these elements exist in the form of insoluble hydroxides or hydrous oxides. (6) Thus, it is quite conceivable that the mode of interference may be similar in all cases. Although some workers have implied that the mode of interference may involve cation substitution or colattice formation in the magnetic phase, the only compelling evidence for this type of mechanism has been that given by Kakabadse et al. for the case of magnesium inhibition, and even in this instance the magnesium was evidently present in the system as magnesium hydroxide. (8)

The results of Kakabadse et al. on the effects of magnesium are shown in Figure 3 for comparison. The first maximum in the redox potential curve corresponds to the consummated formation of a "magnesio-wustite" ($\text{MgO}\cdot\text{FeO}$) sublattice within the inverted spinel lattice of magnetite. This maximum was always found to occur at a $\text{Mg}^{2+}:\text{Fe}^{2+}$ molar ratio of 1.0. At higher $\text{Mg}^{2+}:\text{Fe}^{2+}$ ratios, ferrous iron was presumably replaced by Mg^{2+} with concurrent loss of magnetic properties of the precipitate, until complete substitution occurred (indicated by the second redox potential maximum). The overall process was marked by significant increases in the volume of centrifugate solids, as shown by Figure 3.

Despite certain dissimilarities in the procedures employed by these workers compared with those of the present study, the results shown by Figure 3 on the effect of calcium reveal that there were no sudden changes or significant reversals in the Eh of the system which could be correlated with some integer $\text{Ca}^{2+}:\text{Fe}^{2+}$ molar ratio. Thus, there is no evidence from the present study to indicate that the mechanism of calcium interference involves substitution by Ca^{2+} for Fe^{2+} in the magnetite crystal lattice.

In view of the findings during this investigation, it seems apparent that a conceptual coal mine drainage treatment process involving the sodium dithionite reduction of hydrous ferric oxide would require some rather significant departures from the simple mixing-aeration-settling operations common in current practice. This is exemplified by the flowsheet shown as Figure 4. The conceptual process indicated by Figure 4 includes the following major steps:

1. Oxidation and fractional precipitation of iron at $\text{pH} \leq 4$. This approach is necessary to minimize the residual dissolved iron concentration

as well as to prevent interferences due to coprecipitated aluminum hydroxide. (6, 16) Since the rate of ferrous iron oxidation with gaseous oxygen is impractically slow under these conditions, the use of catalysts or strong chemical oxidants such as hydrogen peroxide or ozone would appear to be necessary.

2. Sludge concentration and separation. Thickening of the precipitated hydrous ferric oxide and its separation from the bulk of the process flow would be necessary to reduce that volume of material requiring subsequent thermal and chemical treatment, as well as to reduce interference by dissolved oxygen.

3. Alkalization of the concentrated sludge to near pH 10 and heating of the sludge suspension to at least 80°C. The data show that optimum properties of the reaction product are obtained under these conditions. In addition, the heating step presupposes the use of lime as an alkali in the process, and is dictated by the need to overcome possible interference due to coprecipitated gypsum.

4. Addition of solid sodium dithionite to the heated, alkaline suspension. In actual practice, an amount of $\text{Na}_2\text{S}_2\text{O}_4$ in slight excess of that required by the stoichiometric ratio $\text{Fe}(\text{III}) : \text{Na}_2\text{S}_2\text{O}_4 = 6.0$ would probably be necessary to compensate for losses due to hydrolysis, air oxidation, or thermal decomposition during reaction with the heated sludge.

5. Magnetic sludge recovery. This could conceivably involve thickening and/or magnetic separation techniques, using wet drum separators of the type employed in heavy media recovery operations.

The potential advantages of the process outlined above would be the elimination of aeration facilities, holding lagoons, and sludge settling basins, as well as the possibility of higher treatment capacities and the recovery of saleable products.

On the other hand, economic considerations reveal that reagent costs would probably be excessive. For example, treatment of a coal mine water containing 800 mg/l of iron by the dithionite reduction process would involve a cost for sodium dithionite alone of nearly \$1.00 per 1,000 gallons of water treated. In pilot plant tests, a coal mine water of similar composition was treated by conventional lime neutralization at a total (capital and operating) cost varying between \$1.09 and \$1.28 per 1,000 gallons. (17)

In summary, it is doubtful whether the dithionite reduction process would be economically feasible by present-day standards, since the relatively complex flowsheet (Figure 4) indicates the likelihood of a larger capital investment and increased operating costs for chemical reagents and sludge heating. Further developmental work should be undertaken, however, before a final judgement is made.

Acknowledgments

This research was supported by funds from the Mineral Conservation Section of the College of Earth and Mineral Sciences, The Pennsylvania State University.

REFERENCES

1. Lovell, H. L., "The control and properties of sludge produced from the treatment of coal mine drainage water by neutralization processes," 3rd Symp. Coal Mine Drainage Res. Preprints, Pittsburgh, Pa., by Coal Ind. Advisory Comm. to Ohio River Valley Water Sanit. Comm., 1970. pp. 1-11.
2. Streeter, R. C., "Reduction of hydrous ferric oxide to a magnetic form with sodium dithionite; implications for coal mine drainage treatment," Ph.D. Thesis, The Pennsylvania State University, 1971.
3. Robl, R., "Magnetizable ferric oxides," Ger. Patent 801,723, 1951; Chem. Abstr. 45, P4009b (1951).
4. Ackermann, G., "Magnetic recording media. V. Reduction of iron(III) hydroxide with formamidinesulfonic acid," J. prakt. Chem. 5 (4), 298-309 (1958).
5. Kakabadse, G. J. and P. Whinfrey, "Sodium silicate - ferrous hydroxide system," Nature 189, 829 (1961).
6. Kakabadse, G. J. and P. Whinfrey, "The effect of certain ions on the formation of magnetite from aqueous solution," Ind. Chim. Belge 29 (2), 109-12 (1964).
7. Riddoch, J., "The hydrolytic and redox properties of ferric iron, with special reference to the effect of magnesium ions above pH 10," Ph.D. Thesis, Victoria University, Manchester, England, 1964.
8. Kakabadse, G. J., J. Riddoch, and D. St. P. Bunbury, "The effect of magnesia on the formation of magnetite from aqueous solution," J. Chem. Soc. (A), 1967, 576-9.
9. Rinker, R. G., T. P. Gordon, D. M. Mason, R. R. Sakaida, and W. H. Corcoran, "Kinetics and mechanism of the air oxidation of the dithionite ion ($S_2O_4^{2-}$) in aqueous solution," J. Phys. Chem. 64, 573-81 (1960).
10. Spencer, M. S., "Chemistry of sodium dithionite," Trans. Farad. Soc. 63 (10), 2510-15 (1967).
11. Rinker, R. G., S. Lynn, D. M. Mason, and W. H. Corcoran, "Kinetics and mechanism of the thermal decomposition of sodium dithionite in aqueous solution," Ind. Eng. Chem., Fundamentals 4 (3), 282-8 (1965).
12. Hoak, R. D. and C. J. Sindlinger, "New technique for waste pickle liquor neutralization," Ind. Eng. Chem. 41, 65-70 (1949).
13. Conley, R. F., H. J. Golding, and M. W. Taranto, "Improvement of iron bleaching in clays through potentiometric control of sodium dithionite addition," Ind. & Eng. Chem., Process Des. Develop. 3 (4), 183-8 (1964).
14. Buckley, H. E., "Crystal Growth," John Wiley & Sons, Inc., New York, N. Y., 1951. Chapter 10, "Crystal habit modification by impurities."

15. Harbury, L., "Solubility and melting point as functions of particle size. II. The induction period of crystallization," J. Phys. Chem. 51, 382-91 (1947).
16. Stauffer, T. E. and H. L. Lovell, "The oxygenation of iron(II) - relationship to coal mine drainage treatment," Special Research Report SR-69 to the Pennsylvania Coal Research Board, The Pennsylvania State University, 1968.
17. "Operation Yellowboy," report submitted to the Pennsylvania Coal Research Board by Dorr-Oliver, Inc., Stamford, Connecticut, June, 1966.

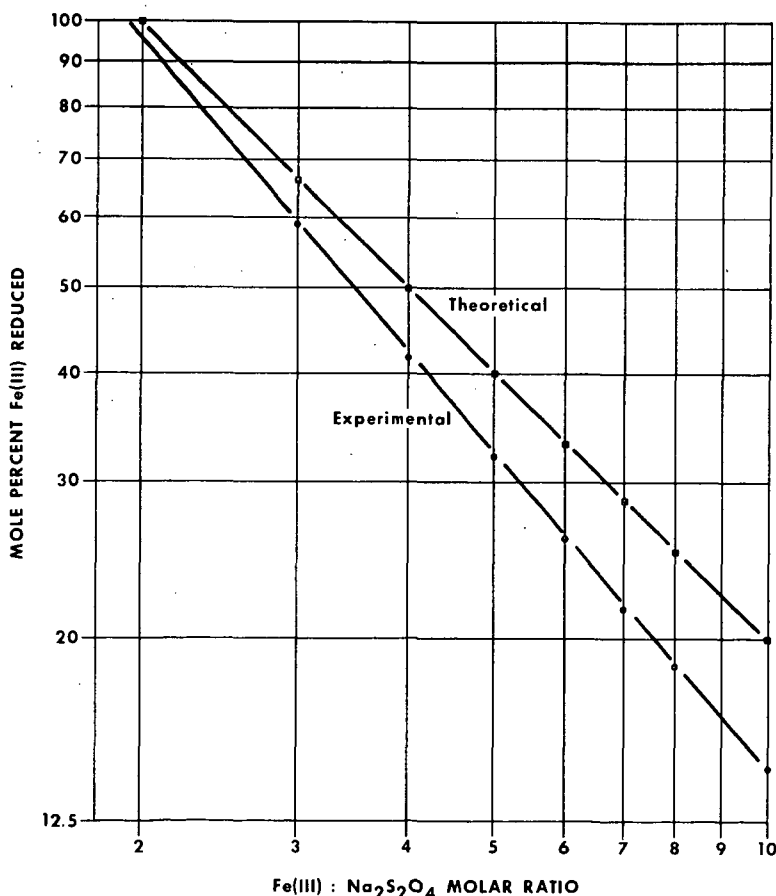


Figure 1. Mole Percent Iron (III) Reduced as a Function of Fe(III):Na₂S₂O₄ Molar Ratio at pH 10 and 30°C

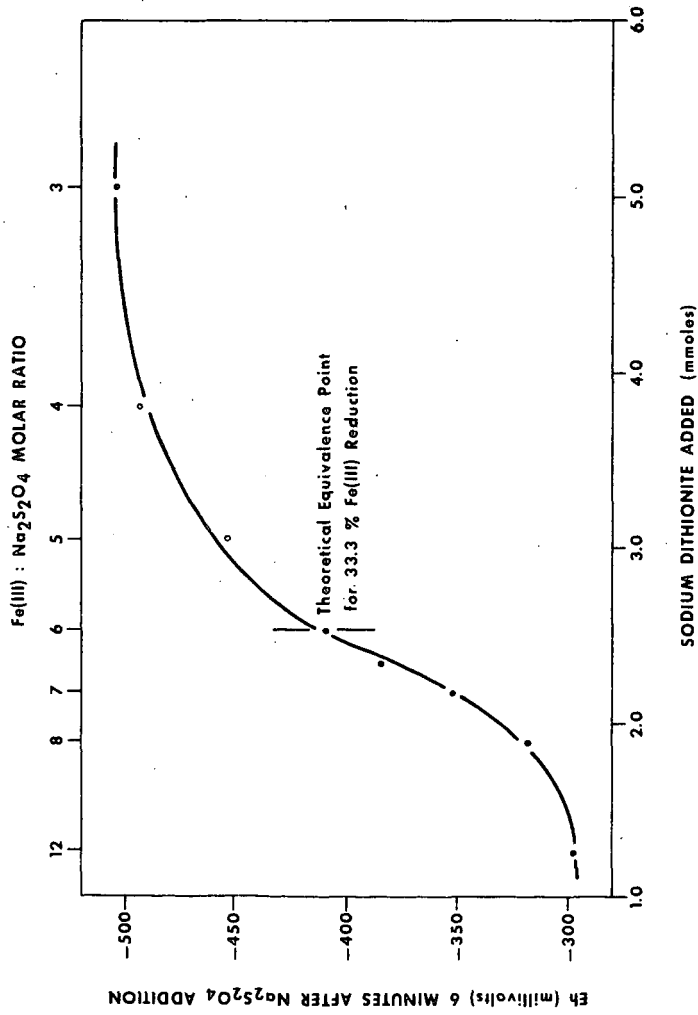


Figure 2. Change in Redox Potential During the Reduction of 15.19 mmoles of Hydrous Ferric Oxide at pH 10 and 30°C with Increasing Amounts of Sodium Dithionite

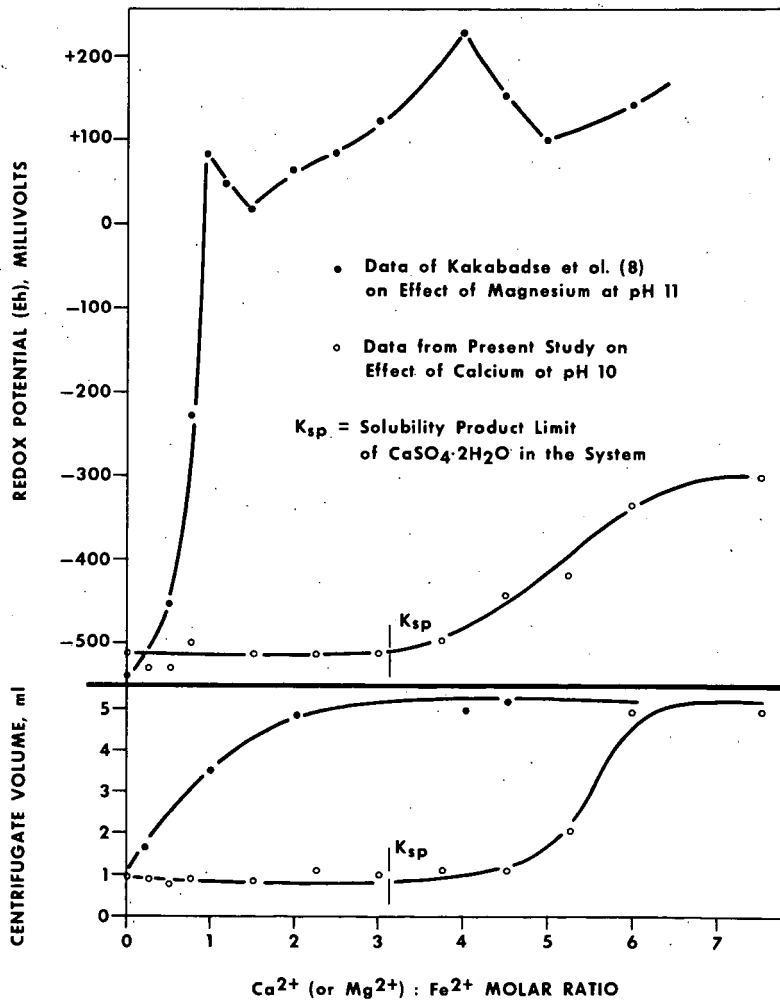


Figure 3. Variation of Redox Potential and Centrifugate Volume with Increasing Ca^{2+} (or Mg^{2+}) : Fe^{2+} Molar Ratio

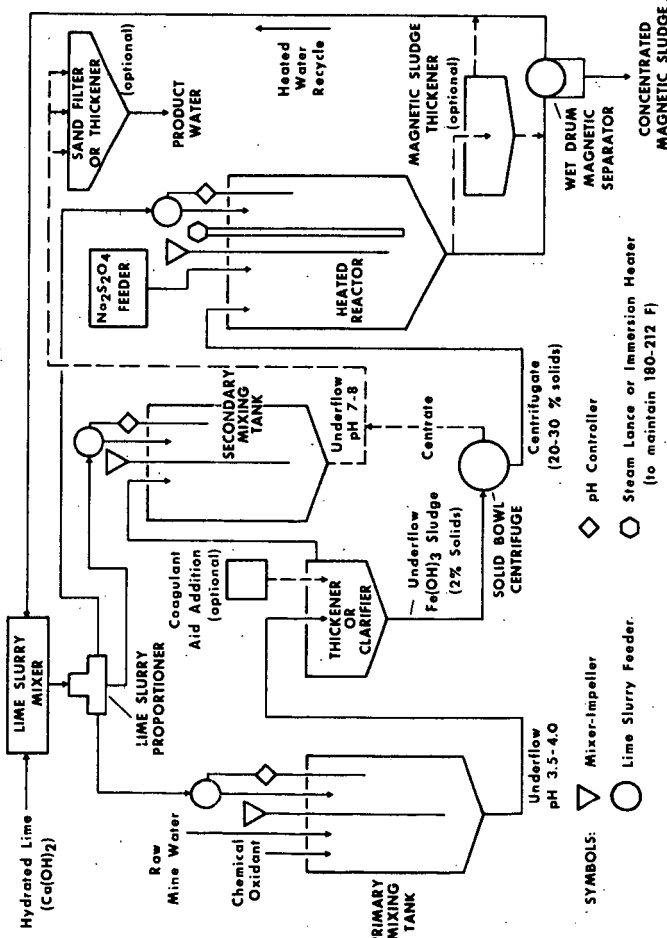


Figure 4. Conceptual Design of Coal Mine Drainage Treatment Process for the Recovery of Magnetic Sludge by Sodium Dithionite Reduction of Fractionally Precipitated Hydrous Ferric Oxide

RECLAMATION OF COAL MINE WASTES AND STRIP SPOIL
WITH FLY ASH

By

John P. Capp and Lester M. Adams
Bureau of Mines, U. S. Department of the Interior
P. O. Box 880, Morgantown, West Virginia

ABSTRACT

Strip mine scars, coal refuse piles and fly ash dumps are solid wastes resulting from the mining and combustion of coal. The total unclaimed area resulting from these wastes is over 2 million acres. Disposition of these wastes is obviously a monumental problem. Large-scale field experiments in the reclamation of acid surface-mined coal lands and refuse piles with raw fly ash from bituminous-coal-fired powerplants were conducted at several sites in Northern West Virginia. Plots were treated with varying tonnages of fly ash from area powerplants and were planted with a variety of grasses, legumes, trees and shrubs. Greatest potential for growth and survival under harsh soil conditions was shown by Kentucky 31 fescue, rye and red top grasses and by birdsfoot trefoil, a legume. Application of fly ash to the acid materials increased the pH to a range tolerable to plant growth, improved the texture of the soil, increased the water-holding capacity of the resulting mixture, and added trace nutrients to the soil.

INTRODUCTION

Solid wastes from the mining and combustion of coal are serious environmental problems of vital concern to the producers and users of coal as well as the general public. Establishment of vegetative cover on each of these areas through reclamation procedures is essential to maintain effective control over erosion and stream pollution.

Vegetation of areas where adverse conditions (steep slopes, highly acid soil material, etc.) prevail is not always possible. In such cases, it may be necessary to modify the sites with a soil amendment such as lime, mulch, additional nutrients in the form of fertilizer and even waste materials such as composted garbage, processed sewage, and bark may be employed. If fly ash can be used as a soil amendment on acid spoil and refuse, it might be possible to achieve a good balance of physical, chemical and biological factors essential to the success of the reclamation effort. An additional benefit is the disposal of large quantities of fly ash in a manner that is useful to the environment in coal mining areas.

Researchers at the Bureau's Morgantown (W. Va.) Energy Research Center are investigating the technical feasibility of utilizing power-plant fly ash to reclaim coal mine refuse and surface mine spoils.¹

SCOPE OF FLY ASH DISPOSAL PROBLEM

Within 10 to 15 years, coal-fired power generating stations will be producing about 40 million tons of ash annually in the United States, and this could double if lime or limestone injection becomes widely used to control sulfur oxide emissions. Most of this ash will be entrained in the stack gases and trapped as fly ash. Although uses for about 10 percent of the fly ash have been developed, mainly in the construction industry, the bulk of it is transported either in slurry or dry form to disposal areas at considerable cost to the power companies and therefore to the public. The accompanying economic loss in terms of unused raw materials and displaced land is not as obvious but is just as significant.

SCOPE OF SURFACE MINE RECLAMATION PROBLEM

Another environmental problem of considerable magnitude in the United States and one that is closely related to the surface mining of coal is the reclamation of the disturbed spoil materials that remain after the mineral is recovered. According to D. M. Whitt², table 1, every state in the United States has land disturbed by strip mining of one kind or another.

The total area requiring reclamation (over 2 million acres) is almost as large as Yellowstone National Park. Whitt reviews a study³ by several cooperating Federal agencies that reveals the following facts:

1. About 91 percent of the affected acreage is in private ownership, and nearly half of that is in small scattered ownerships.
2. More than 80 percent of the mined land surveyed was a mile or more from towns of 200 or more people. About 40 percent of the mined land was more than 5 miles from towns of this size. In other words, most disturbed land is in rural areas.

¹ Adams, L. M., J. P. Capp and E. Eisentrot. Reclamation of Acidic Coal-Mine Spoil with Fly Ash, BuMines Rept. of Inv. 7504, April 1971, 29 pp.

² Whitt, D. M. Surface-mined land. Soil Conservation, v. 33, No. 6, January 1968, pp. 123-125.

³ Udall, Stewart L. Study of strip and surface mining in Appalachia. An interim report of the Secretary of the Interior to the Appalachian Regional Commission, June 30, 1966, 78 pp.

3. About one-third of the land disturbed by surface mining has been rehabilitated. Some of this was restored by natural seedings, but more than half was treated through the efforts of private owners.
4. Restored surface-mined land can serve several useful purposes. A survey in 1966 by the Soil Conservation Service in 14 states showed that the greatest potential uses were woodland production and wildlife habitat.

The study recommended that the appropriate Federal agencies demonstrate leadership with technical and financial aid working through local conservation districts and that "research studies, and field demonstrations be expanded."

More than 50 minerals are produced by surface mining in the United States. About 95 percent of the acreage disturbed by 1965 was for seven commodities, as shown in figure 1.

SCOPE OF THE COAL REFUSE PROBLEM

For many years, burning coal refuse banks have blighted coal-producing areas of this country, posing a health hazard to local populations, producing local defoliation of vegetation and causing other losses in property damage. Further, there are hundreds of non-burning refuse piles which are potentially dangerous; moreover, additional annual accumulation of coal refuse amounts to approximately 70 million tons.

Recently much attention has been focused on this situation. Renewed efforts have been made by the coal industry, by state controlling agencies and by research organizations to prevent the spontaneous heating, ignition and burning of refuse banks, and even find uses for the high quantities of refuse material.

Currently, active dumps are leveled, covered with soil, and planted with grass and/or trees with varying degrees of success.

EXPERIMENTAL PROCEDURE

The surface mine reclamation field experiments were started by the Morgantown Energy Research Center in 1965 and have continued through 1971 on so-called orphaned strip mines that fall into the category of areas that require considerable treatment in order to support vegetation. Table 2 summarizes the Bureau's program and shows treatment at the various sites.

The coal refuse bank or "gob pile" reclamation effort was done on a leveled refuse dump that was owned by a large coal company. Both types of material (i.e., spoil and gob) were acidic due to the presence of pyritic minerals associated with the coal and the overburden with soil pH values mostly in the range of 2.5 to 3.5.

All the sites were droughty⁴ and generally devoid of plant cover and nutrients. Routine soil textural classifications indicated that the materials were loams, sandy loams or clay loams. However, the surfaces of these areas were covered with scattered pieces of rock, shale or coal, ranging in size from pebbles to boulders. A chemical analysis of the spoil materials is given in table 3.

Although the fly ash for these experiments was obtained from several local powerplants, the largest tonnage used came from the Fort Martin power station because of the easy availability, the large daily production, and consistent quality. A typical analysis of this ash is given in table 4. This fly ash has a pH of 12 and an alkaline soil reaction when mixed with acid soils. Since limestone normally is used to neutralize acid soils, a comparison of the limestone requirement for a particular strip spoil and the fly ash to give the same effect shows that approximately 10 times more fly ash may be required.

The application rate of fly ash actually used in the field was determined in the laboratory by measuring the pH of equilibrated soil-water mixtures on a 1:1 by weight basis. The ratio of fly ash to spoil was adjusted empirically to obtain a near neutral condition. The ratio was then used to calculate the fly ash application rate based on a 6-inch plow layer depth of soil material. These applications varied between 150 and 800 tons per acre depending upon the fly ash used, the type of spoil and its buffering capacity, and the depth of mixing anticipated.

The type of machinery used for spreading and mixing fly ash with the spoil or refuse depended primarily upon the relative roughness of the surface. Conventional farm equipment was used at some sites while large earthmoving machines were required at others. After the area was prepared, fertilizer and seed were applied at the desired rates.

One typical seed mixture was used, as shown in table 5, at the rate of 43-47 lbs/acre. Kentucky 31 fescue was almost always included in the mixture because of the high degree of success experienced with this grass.

⁴ Gravimetric moisture determinations of spoil and refuse indicated that moisture content was generally at or near wilt point. See discussion of Chemical and Physical Benefits of fly ash, last paragraph.

Fertilizer (granular, 10-10-10-analysis) was applied at 1,000 lbs per acre in most cases but higher rates were occasionally employed for special purposes.

The Morgantown Energy Research Center presently has two large-scale demonstration sites under treatment. One is a surface mine spoil area (Strip Site No. 4) consisting of about 65 acres, half of which has been treated with fly ash. Approximately 12 acres have a vegetative cover consisting mostly of Kentucky 31 fescue and rye grass. Several varieties of trees, shrubs, various grasses and legumes have also been planted experimentally on small plots for survival and growth studies.

The other site is a one-acre area (Coal Mine Refuse Site No. 1) that was laid out in the middle of a level coal refuse dump. A successful grass cover has been established that consists of the first four grasses shown in the mixture in table 5.

Most of the data discussed in the next section was obtained at strip sites 1, 2 and 3, and represents accumulated experience since the start of the work in 1965. The collection and analysis of data at these sites is continuing and it is expected that similar information will be forthcoming from the two large-scale demonstration sites presently being reclaimed with fly ash.

RESULTS AND DISCUSSION

Dry Matter Yields

Dry matter (hay) yields are indicative of the beneficial effects of fly ash treatment. At site No. 1 an average yield of 1.09 tons/acre was obtained from the fly ash-treated areas; a limestone-treated control plot at the same site produced only 0.54 ton/acre. At site No. 2 the yields ranged from 1.6 to 2.3 tons per acre, as shown in table 6. Similar yields were obtained at site No. 3.

During the third year at site No. 2, fertilizer (N, P and K) rates were increased. Since nitrogen is the most easily lost by leaching, it was applied in equal portions of 70 pounds per acre as urea in the spring and after the first two cuttings. Spring applications of P and K were 90 pounds per acre of P (as P_2O_5) and 180 pounds of K (as K_2O) from 0-15-30 analysis granulated fertilizer. This treatment increased yields and permitted three cuttings instead of the usual one or two per year. Average dry matter yields from all the plots for each cutting are given in table 6. The overall average yields for the three cuttings are 44, 34 and 22 percent of the season total, which is comparable with those obtained at the West Virginia University Agronomy Farm, Reedsville, W. Va., in high-fertilization-rate experiments. Furthermore, the total average yield of about 4 tons per acre for the third year at site 2 was typical of the yields obtained during West Virginia University's pasture experiments with these same perennial tall grasses.

Chemical and Physical Benefits from Fly Ash

Periodic pH determinations were made for three consecutive years at two of the experimental sites and plotted to show long-range changes, figure 2. The untreated controls in both cases show a slight increase, but it would require many years before conditions would become favorable for plant survival. Fly ash-treated plots on the other hand show slight decreases indicating the need for additional fly ash application or the application of small quantities of lime periodically to maintain acceptable soil pH levels for long-range use.

Mixing large quantities of fly ash with spoil also produced physical changes that enhanced plant survival and growth. Bulk density of the mixtures was decreased by the large additions of the light-weight amendment. Decreased bulk density values resulted in greater pore volume, greater moisture availability, and higher air capacity, and hence better conditions for root penetration and growth.

Soils consist of sand, clay and silt-sized mineral fractions and the relative proportion of these various fractions defines a specific soil texture classification. For example, the plow layer (6 inches deep and weighing 1,000 tons per acre) of a typical clay loam has the following analysis per acre: Clay, 350 tons; sand, 350 tons; and silt, 300 tons. A typical silt loam has the following per acre analysis: Clay, 150 tons; sand, 200 tons; silt, 650 tons. (Obviously considerable changes in these amounts would be required to change from one classification to another.)

Although soil scientists consider alteration of texture virtually impossible under ordinary circumstances, this study showed that adding fly ash to surface mine spoil changed the textural classification. (See figure 3.)

Spoil texture influences the amount of moisture available for plant growth. In general, spoil composed largely of sand has good aeration but is apt to be droughty. Clay banks compact easily and crust over during dry periods. Loams and silty shales usually have enough fine material to hold moisture.

Figure 4, which compares the wilt point and field capacity of different textured soils, further illustrates this point. The capacity of the soil to hold water is related to surface area, pore-space volume, and continuity of the pore space. Water-holding capacity is therefore related to structure as well as to texture. It can be seen in figure 4 that fine-textured soils have the maximum total water holding capacity, but that maximum available water is held in medium-textured soils. Research has shown that available water in many soils is closely correlated with the content of silt and very fine sand.

Fly ash, which is mostly in the silt size range, was applied at rates of 150 to 800 tons per acre. This proved to be a sufficient quantity of ash (particularly at the higher rates) to produce a textural change by shifting the analysis toward the silt side of the textural triangle.⁵

Further evidence of the beneficial effect that the use of fly ash has on the water capacity of the spoil and the availability of this moisture is indicated by figure 5. This figure gives quantitative moisture values for the undisturbed control plot and a plot treated with 800 tons/acre of fly ash at strip site No. 2. Field capacity and wilt point values for these plots, indicated in the figure by dashed lines, show how the available water range corresponds to the actual moisture content under field conditions. Heavy spring rains built up a significant reservoir of moisture in the fly ash-treated plot and continued to be available even during the summer dry period, as the bar graph indicates. On the other hand, the control plot retained little moisture from the spring rains and during the dry period moisture was not in the available range for plants for several weeks. Since the actual moisture content of the control spoil remains at or near the wilt point value, most of the water that fell on this area as rain probably ran off and was not absorbed.

SUMMARY

These experiments demonstrate the feasibility of disposing of large quantities of power plant fly ash on acid surface mine spoil and coal refuse dumps. The benefits that result are:

- 1) Acid materials are partially neutralized and soil conditions improved to a tolerant level for some grasses and legumes.
- 2) The grasses and legumes establish an immediate cover that resists erosion and hence reduces stream pollution potential.
- 3) Soil texture changes increase moisture holding capacity, increase pore space and improve root growth conditions.
- 4) Yields of forage and hay from reclaimed lands are comparable to yields from undisturbed pastures and meadows as reported by the West Virginia Cooperative Crop Reporting Service.⁶

⁵ Textural changes discussed in this text refer to the "plow layer" or top 6 inches of material.

⁶ West Virginia Department of Agriculture, Div. of Statistics, Charleston, W. Va., July 12, 1968, Monthly Farm Report.

Although reclamation of strip spoil with fly ash appears technically feasible, practical application and widespread acceptance depend on a number of other considerations. Economic justification will be a major factor, and esthetics and strip mining laws will also play important roles. Surface mining doubtless will continue to be a major factor in recovering minerals vital to the nation's economy, hence there is continued incentive to evolve better reclamation techniques and develop methods of recovering minerals with minimum damage to surface areas and streams.

ACKNOWLEDGEMENTS

The authors gratefully acknowledge the various staff members of the West Virginia University Agronomy Department, Virginia Polytechnic Institute and State University Agronomy Department, representatives of the U. S. D. A. Soil Conservation Service, the U. S. Forest Service and the West Virginia Department of Natural Resources Division of Reclamation, Consolidation Coal Company and the Monongahela Power Company for assistance, advice and support in contributing to the success of these experiments.

TABLE 1. - Condition of surface-mined land,
by state, January 1, 1965

[In thousands of acres]

State	Land needing treatment ¹	Land not needing treatment ¹	Total land disturbed ²
Alabama	83.0	50.9	133.9
Alaska	6.9	4.2	11.1
Arizona	4.7	27.7	32.4
Arkansas	16.6	5.8	22.4
California	107.9	66.1	174.0
Colorado	40.2	14.8	55.0
Connecticut	10.1	6.2	16.3
Delaware	3.5	2.2	5.7
Florida	143.5	45.3	188.8
Georgia	13.5	8.2	21.7
Hawaii ³			
Idaho	30.7	10.3	41.0
Illinois	88.7	54.4	143.1
Indiana	27.6	97.7	125.3
Iowa	35.5	8.9	44.4
Kansas	50.0	9.5	59.5
Kentucky	79.2	48.5	127.7
Louisiana	17.2	13.6	30.8
Maine	21.6	13.2	34.8
Maryland	18.1	7.1	25.2
Massachusetts	25.0	15.3	40.3
Michigan	26.6	10.3	36.9
Minnesota	71.5	43.9	115.4
Mississippi	23.7	5.9	29.6
Missouri	43.7	15.4	59.1
Montana	19.6	7.3	26.9
Nebraska	16.8	12.1	28.9
Nevada	20.4	12.5	32.9
New Hampshire	5.1	3.2	8.3
New Jersey	21.0	12.8	33.8
New Mexico	2.0	4.5	6.5
New York	50.2	7.5	57.7
North Carolina	22.8	14.0	36.8
North Dakota	22.9	14.0	36.9
Ohio	171.6	105.1	276.7
Oklahoma	22.2	5.2	27.4
Oregon	5.8	3.6	9.4
Pennsylvania	229.5	140.7	370.2
Rhode Island	2.2	1.4	3.6
South Carolina	19.3	13.4	32.7
South Dakota	25.3	8.9	34.2
Tennessee	62.5	38.4	100.9
Texas	136.4	29.9	166.3
Utah	3.4	2.1	5.5
Vermont	4.2	2.5	6.7
Virginia	37.7	23.1	60.8
Washington	5.5	3.3	8.8
West Virginia	111.4	84.1	195.5
Wisconsin	27.4	8.2	35.6
Wyoming	6.4	4.0	10.4
Total	2,040.6	1,147.2	3,187.8

¹ Compiled from data supplied by Soil Conservation Service, U.S. Department of Agriculture.

² Compiled from data supplied by U.S. Department of the Interior; from Soil Conservation Service; and from study-group estimates.

³ Less than 100 acres.

* Does not include 108,000 acres of National Forest land needing treatment.

TABLE 2. - Description of surface mine spoil sites
treated with fly ash

Site No., name, year treated	Bituminous coal seam mined	Area, acres	Original pH	Fly ash rate, tons/ acre	pH after treatment
1, Westover 1965	Sewickley	½	3.5	55-600	4-6
2, Albright 1966	Bakerstown	1	2.6-3.3	200-800	6-8
3, Fort Martin 1968	Sewickley	5	3.1-4.7	150	6-7
4, Stewartstown 1970	Pittsburgh	65	3.0	150	7-8

TABLE 3. - Chemical analysis of surface
mine spoil at sites 1, 2 and 3¹

Constituent	Weight-Percent		
	Site 1	Site 2	Site 3
Al ₂ O ₃	18.0	24.0	21.4
SiO ₂	69.3	59.7	62.1
Fe ₂ O ₃	7.9	9.2	7.7
P ₂ O ₅	.1	.1	.1
TiO ₂	.7	.7	.8
CaO	.2	1.0	.5
MgO	.2	.5	.8
K ₂ O	2.4	3.5	3.1
Na ₂ O	.7	.5	.5
S	.3	.6	.1
H ₂	.8	1.0	--
C	1.7	5.0	2.9
Bulk density, g/cc	1.4	1.6	--

¹ Sample cores were taken to depth of 6 inches and composited for analysis.

TABLE 4. - Typical analysis of Fort Martin fly ash

<u>Constituent</u>	<u>Wt pct (ppm)</u>
<u>Major elements</u>	
SiO ₂	47.7
Al ₂ O ₃	23.6
Fe ₂ O ₃	15.6
CaO	3.5
MgO	1.5
Na ₂ O	1.9
K ₂ O	2.2
TiO ₂	2.7
P ₂ O ₅	.6
N.D.	.7
LOI	3.6
<u>Trace elements</u>	
B	450 ppm
Cu	40 ppm
Mn	200 ppm
Mo	20 ppm
Zn	90 ppm
Bulk density g/cc	1.15

TABLE 5. - Typical seed mixture of various grasses applied to fly ash-spoil or refuse areas

<u>Seed mixture</u>	<u>Wt pct</u>
Kentucky 31 fescue (Festuca arundinacea shrebe)	35
Red top grass (Agrostis alba)	14
Orchard grass (Dactylis glomerata)	18
Rye grass (Lolium perenne)	28
Birdsfoot trefoil (Lotus corniculatus)	5
	100

TABLE 6. - Average dry matter yields, site 2

Year	Dry weight, tons/acre						
	1st Cutting		2nd Cutting		3rd Cutting		Total
	Date	Yield	Date	Yield	Date	Yield	Yield
First (1967)	June 1	1.6	--	None	--	None	1.6
Second (1968)	June 5	1.4	Sept. 5	.9	--	None	2.3
Third (1969)	June 2	1.7	July 29	1.2	Sept. 30	.9	3.8

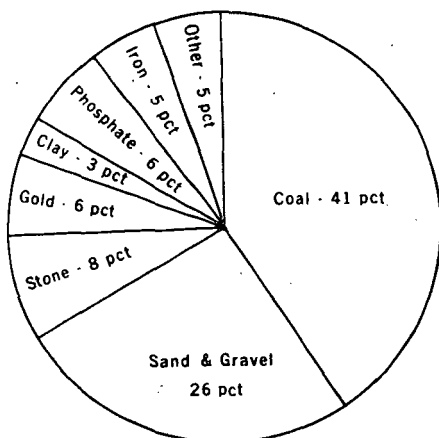


FIGURE 1. - Surface mining in USA by mineral

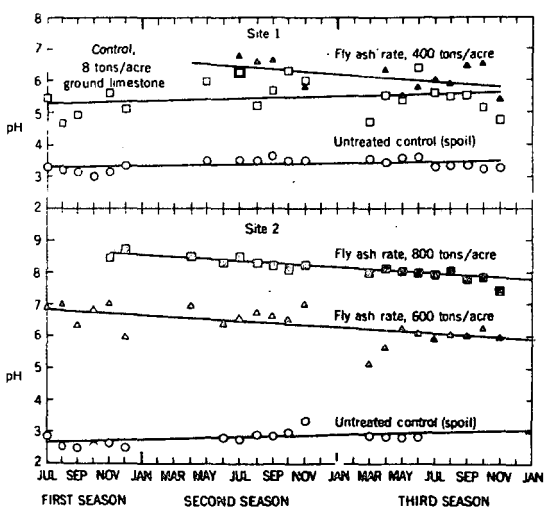


FIGURE 2. - Untreated spoil remains acidic, pH of spoil-fly ash mixtures remain sufficiently high to maintain plant life

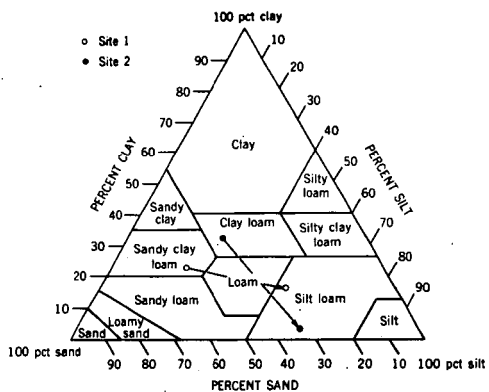


FIGURE 3. - Fly ash changes spoil to silt loam classification

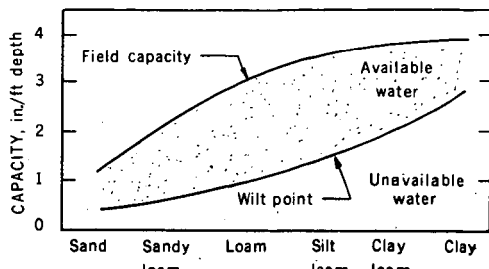
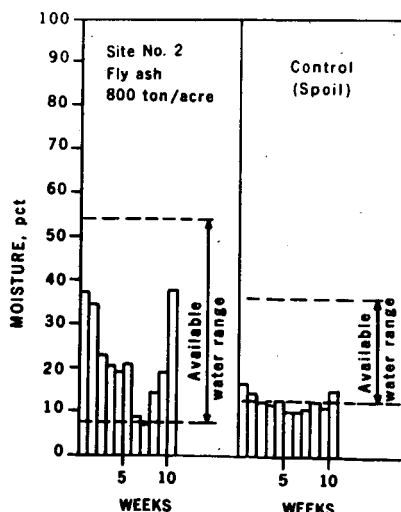


FIGURE 4. - Water-holding capacities of different textured soils

FIGURE 5. - Moisture availability of fly ash-modified soil



PRODUCTION OF ASHLESS, LOW-SULFUR
BOILER FUELS FROM COAL

B. K. Schmid and W. C. Bull

The Pittsburg & Midway Coal Mining Co.
Kansas City, Mo.

SUMMARY

Current and impending restrictions on emission of sulfur dioxide to the atmosphere have brought out the fact that a shortage of low-sulfur fuels exists for power plant and industrial use. This situation has prompted considerable research work on removal of sulfur dioxide during or after combustion (i.e. the so called stack gas treatment processes). Because they have had considerable research emphasis throughout the industry, much of the publicity discussing methods of alleviating sulfur dioxide pollution has been concentrated on stack gas treating processes.

Coal conversion processes have generally been overlooked in this field, since most of them have historically been directed toward conversion of coal to light distillate fuels, and hence have been fairly costly. A much less costly process is now under development, however, which is capable of producing an ash-free, low-sulfur fuel for power plant and industrial use. The process, known as the Pittsburg & Midway Solvent Refined Coal Process, is being developed under the sponsorship of the Office of Coal Research. The process appears to be potentially more attractive than other methods of alleviating sulfur dioxide pollution.

The Solvent Refined Coal Process can produce a low-sulfur, ashless fuel to sell at a considerably lower price than most other low-sulfur fuels. Furthermore, the use of Solvent Refined Coal has a number of potential advantages over stack gas treating processes even at about the same basic overall cost. It appears that the Solvent Refined Coal Process will ultimately play a key role in providing a low-sulfur fuel to meet the requirements of utilities operating under air pollution control laws and at the same time make possible the utilization of current reserves of high-sulfur coal.

INTRODUCTION

The past few years have seen a much greater concern in this country regarding atmospheric pollution, and this has led to increased legislation restricting the discharge of many substances to the atmosphere. Two of the major targets of such legislation have been sulfur dioxide and particulate matter. While restrictions on particulate matter are not new, they are becoming more stringent all the time. Restrictions on sulfur dioxide are more recent, however, and promise to have a much greater impact on the national energy picture. Many of the major cities of the United States now have limitations on the sulfur dioxide content of stack gases and it appears that such limitations will become both more widespread and more stringent. Even in remote areas such as the Black Mesa region of Arizona there is great concern about atmospheric pollution (1). Eventually restrictions on sulfur dioxide emissions will probably be applied to the entire country. On the basis of present trends it appears that these restrictions will limit fuels to a

sulfur content of less than 1% and in many densely populated areas the limits will be less than 0.5%.

Many articles and publications in the past several years have discussed various means of alleviating the air pollution problem resulting from emission of sulfur dioxide to the atmosphere. Most of the research work being done and therefore most of the publications have emphasized only one method of reducing sulfur dioxide emissions; namely, the treatment of stack gases following combustion of high-sulfur fuels. A number of processes have been announced for desulfurization of petroleum residual fuels, but comparatively little has been said publicly about removing sulfur from coal prior to combustion. Even when sulfur removal prior to combustion has been discussed it has generally dealt only with mechanical removal of pyritic materials from the coal. While this can be done in some cases for a moderate reduction of sulfur content, it is not practical for attaining the extent of sulfur removal required for most high-sulfur coals.

When coal conversion processes are discussed in connection with sulfur removal, they are usually dismissed with the contention that they are too expensive. This conception has undoubtedly resulted from the background on the work on coal conversion processes in the past. Research work on direct hydrogenation of coal dates back to the work by Bergius as early as 1913. Most of the early work was directed toward production of gasoline and distillate fuel oils from coal. The early workers very quickly discovered that they could not produce significant quantities of distillate materials by direct hydrogenation without the use of catalysts. Almost from the earliest days, therefore, catalytic processing was used in the direct hydrogenation of coal. For the same reason catalytic processes were also emphasized in the hydrogenation of coal tars produced by the carbonization of coal.

Research work in hydrogenation of both coal and coal tars derived from carbonization of coal has continued intermittently since that time. Even the latest processes developed have not as yet proved to be economically attractive, however, in spite of the improved technology and improved catalysts developed since the early days. All of the research work carried out from 1913 to the present time, primarily using catalytic conversion, undoubtedly forms the basis for conclusions by many observers that sulfur removal by direct conversion is not economical.

SULFUR REMOVAL BY COAL CONVERSION

1. Solvent Refined Coal Process

A coal conversion process is currently being developed which is not nearly as costly as earlier processes. The coal is converted not to distillates but to a low-sulfur, ashless fuel resembling pitch in its outward appearance. There are a number of factors which make this process much less expensive than prior coal conversion processes. These factors are (1) a much lower hydrogen consumption (about 1-2% by weight of coal compared to about 6-8% for conversion to distillates); (2) less costly equipment and lower operating costs resulting from the use of less severe operating conditions; and (3) no catalyst is required.

The process is being developed by The Pittsburg & Midway Coal Mining Co. under the sponsorship of the Office of Coal Research, U. S. Department of the Interior. It has been designated as the Pittsburg & Midway Solvent Refined Coal Process.

A schematic flow diagram of the Solvent Refined Coal Process is given in Figure 1. Raw coal is pulverized and mixed with a coal-derived solvent boiling in the general range 550-800°F. The coal-solvent slurry is pumped, together with hydrogen, through a preheater to a reaction zone, or dissolver. The dissolver is operated at a temperature of about 800°F. and a pressure of 1000 psig. At these conditions about 95% of the MAF coal is dissolved. After separation of excess hydrogen, the dissolver effluent consists of the coal solution plus the undissolved inorganic material from the coal. This slurry goes to the filtration section of the plant where the undissolved coal solids are separated. The filtrate is sent to a vacuum flash distillation step for removal of the solvent for recycle. The bottoms fraction from the vacuum flash tower is a hot liquid with a solidification point of about 300°F. This is the major product of the process, and is known as Solvent Refined Coal. This material can either be sent as a hot molten liquid to an adjacent power plant or solidified for shipment to another location.

The Solvent Refined Coal has a heating value of about 16,000 BTU per pound and is surprisingly uniform in its analysis regardless of the type of coal fed to the process. For example, Solvent Refined Coal products derived from both lignite and bituminous coals, when vacuum flashed to the same melting point, have the same carbon-hydrogen ratio, heating value and oxygen content even though the coals from which they were derived differ widely in these characteristics.

There is some variation in sulfur content, however, for Solvent Refined Coal produced from widely different coals. In general all of the pyritic sulfur and over 60% of the organic sulfur is removed during the process. This means that in processing a coal containing 2% pyritic sulfur and 2% organic sulfur (total sulfur content of 4%) the Solvent Refined Coal product would contain considerably less than 1% sulfur. This represents a substantial reduction in potential sulfur dioxide emission. Where the ratio of pyritic sulfur to organic sulfur is higher than 1 to 1, as it is in most cases, the extent of sulfur reduction would be even greater. A total sulfur removal of 85% is not uncommon for the process. Since the heating value of the Solvent Refined Coal is much greater than that of raw coal the effective sulfur content is even lower than it would first appear. For example, Solvent Refined Coal having a sulfur content of 0.8% would be equivalent in sulfur dioxide emission to a Western coal containing 0.4% sulfur and having a heating value of 8000 BTU per pound.

The hydrogen requirement of the Solvent Refined Coal Process is about 1-2% by weight of the coal treated. The hydrogen can be readily obtained by steam reforming of the by-product gas from the process. There is sufficient gas produced to supply all of the hydrogen requirements if process fuel can be obtained from another source. In most cases it is expected that a part of the Solvent Refined Coal produced would be used as process fuel. This would eliminate any requirement for natural gas. In view of the impending shortage

of gas in most areas having large coal deposits, this is a very real advantage.

In addition to the Solvent Refined Coal, a light liquid is also produced in the process. This liquid has a boiling range of about 100-450°F. and is usually about 10-15% by weight of the original coal charged. This product would be suitable as feed stock to a petroleum refinery and should be a very valuable blending component.

The liquid product is considerably higher in nitrogen than petroleum fractions of the same boiling range, but nitrogen removal processes have been and are still being developed in connection with catalytic hydrocracking processes. It is anticipated that the heavier fraction of this product would be processed by catalytic hydrocracking followed by catalytic reforming, while the light liquids would be processed by hydrotreating plus reforming. The high cyclic content of the coal-derived material should provide excellent reformer charge stocks in either case. The reformate would thus have a high concentration of benzene, toluene and xylene. These materials are valuable either as chemical by-products or to provide the aromatic compounds which will be needed in greater quantities for non-leaded gasolines of the future. The light liquid also contains large quantities of phenol and cresylic acids (about 15-20% by weight) which could be separated and sold as by-products. The results of work in other laboratories on similar coal-derived liquids generally support the above observations⁽²⁾.

The solids from the filtration section are dried to remove excess solvent, then burned in a fluidized combustion zone. The solids contain considerable undissolved carbon (35-55% by weight) and it is desirable to recover this for its heating value. In addition to carbon, the solids also contain about 5-8% sulfur. This makes the sulfur dioxide content of the combustion gases quite high, high enough so that it is feasible to combine this sulfur dioxide with hydrogen sulfide from the solution step in a modified Claus process. The fluidized combustion zone would be a Pope, Evans and Robbins fluidized bed boiler. It has recently been shown that sulfur dioxide from such a boiler can be concentrated in a small part of the total combustion gas. The concentration in this gas stream is over 30 times that obtained in normal combustion⁽³⁾. Such concentrations should make it even more practical to use the sulfur dioxide in a Claus type reaction. This scheme permits the recovery of essentially all of the sulfur from the process as elemental sulfur.

The steam generated from combustion of the mineral residue plus that from process waste heat can be readily converted to electrical power. The power generated is sufficient not only to supply the coal mine and the processing plant, but would also provide excess power. If the processing plant is located close enough, additional savings could probably be attained by sending the steam directly to the main power plant.

2. Other Processing Methods

While the Solvent Refined Coal Process was for some time the only publicly announced process for producing low-sulfur fuels from coal, at least one other coal conversion process for production of low-sulfur fuels has recently been announced⁽⁴⁾. This is the H-Coal Process, also sponsored in part by the Office of Coal Research. The major difference between the H-Coal Process

and the Solvent Refined Coal Process is that the H-Coal Process uses a petroleum type desulfurization catalyst in an ebullated bed reaction zone. The ebullated bed is maintained by liquid phase fluidization of the catalyst and this requires a very high rate of internal liquid recycle. Both the catalyst and the high internal recycle increase the cost of the process over the Solvent Refined Coal Process. In general it appears that the Solvent Refined Coal Process will be more economical where the required sulfur levels can be reached without the use of a catalyst. The use of a catalytic process may be desirable when sulfur requirements are in the order of 0.1 to 0.2%, although even in such cases it may still be more efficient to use the Solvent Refined Coal Process as the first stage of a two-stage scheme. The second stage would be a catalytic step in which the feed stock would contain much fewer contaminants than the raw coal.

The Solvent Refined Coal Process has been referred to as "non-catalytic", primarily because a commercial catalyst is not used. There is considerable experimental evidence, however, that the inorganic mineral matter in the coal has a significant catalytic effect in the Solvent Refined Coal Process. While the catalytic effect is certainly not as great as that obtained from a fresh commercial hydrodesulfurization catalyst, the difference is probably not nearly as great after normal deactivation of the commercial catalyst. The extent of the expected difference has not yet been established, but it is this difference which will ultimately determine the feasibility of using a catalytic process for direct hydrogenation of coal.

3. New Process Developments

Additional laboratory work has revealed that the use of carbon monoxide and steam to replace part of the hydrogen promises to result in further process improvement. Although this idea had been tried many years ago, it is only recently that advantageous results have clearly been shown for the use of carbon monoxide and steam in processing of coal. This recent work was originated by scientists at the U. S. Bureau of Mines⁽⁵⁾⁽⁶⁾⁽⁷⁾. As a result of these promising disclosures, laboratory work was undertaken by Pittsburg & Midway to apply the principle to the Solvent Refined Coal Process. It was found by P&M that the use of carbon monoxide and steam was more effective than hydrogen alone for processing of lignite and subbituminous coals. The results were very promising also for bituminous coal, although the improvements were not as pronounced as with lignites or subbituminous coals. In addition, mixtures of carbon monoxide and hydrogen with steam have been found to be about as effective as carbon monoxide and steam alone.

These results strongly suggest that synthesis gas could be used in place of hydrogen in the Solvent Refined Coal Process. The use of synthesis gas should also have an economic benefit since some of the steps normally used to convert synthesis gas to hydrogen could be eliminated. Another advantage is that the reaction of carbon monoxide and steam in the dissolver forms hydrogen in excess of that used in the solution process, with a consequent enrichment of hydrogen in the recycle gas system. Removal of part of this hydrogen could make it cheaply available as a pure gas for later use in catalytic hydrogenation step. This would not adversely affect the composition of the recycle gas and might, in fact, be beneficial. Other potential advantages are that the coal would not require a drying step and phenolic waste

water could be recycled to provide part of the water for the process. This would also eliminate the necessity for treatment of phenolic waste water.

The potential use of synthesis gas or carbon monoxide and steam in the Solvent Refined Coal Process is a relatively new development and is being further studied at the present time. It is anticipated that the work will ultimately make the process even more economically attractive.

4. Economics of Solvent Refined Coal Process

An economic study has recently been made to determine the price at which the Solvent Refined Coal would have to be sold to attain a 10% discounted cash flow rate of return on investment(8). The price of Solvent Refined Coal is very dependent on credits allowed for by-products of the process. A summary of the effect of by-products on the price of Solvent Refined Coal is given in Table I. If the light liquids, sulfur and electrical power are considered as by-products, the price of Solvent Refined Coal would be about 40¢/MM BTU (Case I). The light liquids are valued at \$3.50 per barrel, sulfur at \$10 per long ton and the excess electrical power at 0.4¢ per KWH.

If the Solvent Refined Coal plant were located in an area where it is impractical to market the light liquid as a by-product, the cost of the Solvent Refined Coal would increase to about 45¢/MM BTU (Case II). In this case the light liquid would be included in the Solvent Refined Coal and would lower its melting point to some extent. If it is also not possible to sell sulfur and electrical power as by-products, the cost of the Solvent Refined Coal would further increase to about 47¢/MM BTU (Case III).

The above prices are based on the assumption that the Solvent Refined Coal plant would be located adjacent to a power plant in the Illinois-Kentucky area. This means that the Solvent Refined Coal would be pumped as a liquid directly to the power plant. If the power plant were located at some distance from the processing plant, about 2¢/MM BTU would have to be added for product solidification, in addition to any transportation costs.

The price range of 40 to 50¢/MM BTU for the Solvent Refined Coal product appears very reasonable in comparison with current prices for competitive low sulfur fuels. For example, the recent price quoted for 1% sulfur No. 6 fuel oil was \$4.10 per barrel (about 65¢/MM BTU in New York Harbor) and \$4.62 per barrel (about 73¢/MM BTU) in the Chicago area(9). Furthermore, even at these prices the quantity of No. 6 fuel oil containing less than 1% sulfur is definitely limited.

Some power plants in the Illinois area have turned to shipping low-sulfur coal from the Western states in an effort to meet the restrictions on sulfur content. While such coal is available at the mine site for a low price, the cost of shipping it for 1000-1500 miles is very high. For example, the total cost of Wyoming low-sulfur coal delivered to the Chicago area is about 55-60¢/MM BTU(10). Although lower negotiated freight rates may bring this down to the range of 45-50¢/MM BTU(10), this is at least as high as the price for Solvent Refined Coal. Because it is virtually free and would not require an electrostatic precipitator, the Solvent Refined Coal is much more advantageous for a power plant even at the same price.

OTHER METHODS OF SULFUR DIOXIDE CONTROL

1. Stack Gas Treating Processes

In most reviews of the general problem of air pollution abatement, stack gas treating processes have been discussed as if they were the only practical methods for control of sulfur dioxide emission. Various groups calling for more research on sulfur dioxide control nearly always specifically mention stack gas treatment processes. Considerable research efforts have already been directed toward removal of sulfur dioxide from combustion gases. These efforts have resulted in the emergence of no less than 21 different stack gas treating processes in various states of development.

Probably the most advanced of such processes are the dry limestone process and Combustion Engineering Corporation's dolomite injection wet scrubbing process. Both of these processes adsorb sulfur dioxide on the dolomite or limestone. No attempt is made to recover the sulfur dioxide and as a result no significant by-products are available for sale.

Another of the more advanced stack gas processes is the Monsanto catalytic oxidation process. This process is much more costly than the other two, but recovers sulfuric acid as a by-product. The value of sulfuric acid as a by-product has diminished somewhat in recent months, however, since the price of sulfur has decreased sharply.

All three of these processes have been installed on a test basis in a few power plants throughout the country. The results of these tests have indicated that actual costs of all of these stack gas treating processes will be far in excess of the generally published cost estimates. The increases are apparently so great that it has been said that costs published even six months ago are now obsolete⁽¹¹⁾. In addition, the effectiveness of these processes for sulfur removal has generally been less than originally anticipated.

For these reasons no attempt will be made to directly compare stack gas treating costs with the costs of producing a low-sulfur fuel from coal. Information obtained from private sources indicates that the actual cost of stack gas treating processes will be in the same general range as the costs of decreasing the sulfur content of the fuel. It is still far too early to attempt any actual cost comparisons at this time, however, and it appears that experimental work should probably be continued in both types of pollution control methods.

In connection with the relative merits of stack gas treating vs. desulfurization of coal it is of interest to consider certain aspects which would not be directly accounted for in most economic comparisons. In this regard there are certain benefits which would tend to favor the coal desulfurization route if the obvious costs of pollution control were about the same in both cases.

(a) By-products - The potential by-products available from stack gas treating processes are generally limited to sulfur or sulfuric acid. A coal conversion process, however, has the potential for production of many

more by-products than can reasonably be considered in an initial economic evaluation. Ultimate utilization of such by-products through further research and development holds the promise of making the Solvent Refined Coal Process considerably cheaper than stack gas treating processes.

In addition, it seems that the power companies generally prefer not to diversify into the chemical business as they would be forced to do by the installation of any stack gas treating process requiring recovery of by-products such as sulfur or sulfuric acid. At the same ultimate cost it is much more convenient for them to simply buy a low-sulfur fuel.

(b) Uniform Boiler Design - Because of the uniformity of the Solvent Refined Coal regardless of coal source its widespread use for power generation could lead to a uniform off-the-shelf design for power plant boilers. At the present time boilers must be designed for a particular type of coal and when a different type of coal is used, severe operating problems can result. This has happened in the substitution of low-sulfur Western coals in boilers designed for Illinois coals⁽¹²⁾. It is almost certain that the use of uniform boilers would lead to cost savings for the power companies, since the cost of producing such boilers should be less than if many different designs were required.

(c) The use of a low-sulfur fuel is a positive guarantee that sulfur dioxide pollution would be controlled at all times. Any down-time in the coal processing plant could be handled by appropriate stock-piling of low-sulfur fuel. With stack gas cleaning processes, however, any interruption in the operability of the process would result in excessive emission of sulfur dioxide to the atmosphere. Thus, the use of a low-sulfur fuel is a more reliable and positive method of pollution control.

(d) Integration with other processes - Even though the economics of a Solvent Refined Coal plant standing alone are attractive, additional economic benefits can be attained by integrating it with other processes in a multi-process complex. For example, the Solvent Refined Coal product can be simply a first stage in an overall process to produce distillate fuels and pipeline gas, as well as a low-sulfur power plant fuel.

An especially attractive combination process scheme is now under study by P&M through a subcontract with Chem Systems, Inc. In this scheme the Solvent Refined Coal is hydrocracked and hydrotreated in two catalytic hydrogenation steps to produce a distillate material suitable for use as feed stock to a petroleum refinery. A coal gasification process is used to produce hydrogen for the three hydrogenation steps in the complex. Methane for pipeline gas is produced in both the gasification and hydrogenation steps. The mineral residue from the Solvent Refined Coal Process is charged to the gasification process to utilize the undissolved carbon.

Preliminary results of this study indicate that all of these processes complement each other effectively so as to make a very promising scheme. A conceptual design and economic study of this scheme is being made by Chem Systems, Inc., the first phase of which is soon to be published by the Office of Coal Research.

2. Methane

Probably the ultimate pollution-free fuel is natural gas, and its use by power plants would eliminate sulfur dioxide emissions. This is not a very practical solution to the problem, however, since there simply is not enough gas to supply fuel requirements even for existing power plants, not to mention the large quantity of new power plants which will be required in the future. In fact, it is questionable how long many of the power plants now using natural gas will be able to continue burning this fuel.

A number of processes are now being developed to convert coal to synthetic gas. The costs for producing synthetic gas from coal, however, are almost certain to be higher than the costs of producing a heavier liquid material such as Solvent Refined Coal. These higher costs result from greater requirements in terms of both hydrogen consumption and the process steps necessary for conversion. The conversion of coal to gas will almost certainly become a commercial reality as gasification processes are developed, but it is likely that such gas will be used primarily as a premium fuel where its cost can be more easily justified than in a power plant. Similarly, liquified natural gas imported into this country is so costly that it is very unlikely to be used to a significant extent for power generation. To satisfy the requirements for a low-sulfur power plant fuel, it is much more realistic to use a less costly fuel such as Solvent Refined Coal.

3. Nuclear Power

Among the other methods which have been suggested for sulfur dioxide emission control is the use of nuclear power. This is also not a realistic solution since the anticipated demand for electrical power is so great that even with the most optimistic advances in nuclear power generation, fossil fuels will be required for many years into the future. Furthermore, nuclear power has its own peculiar type of environmental problems to be solved.

CONCLUSIONS

The problem of sulfur dioxide and particulate emissions to the atmosphere can best be solved by removing the ash and sulfur from coal prior to combustion. From a practical standpoint, this can be accomplished by the Pittsburg & Midway Solvent Refined Coal Process, now being developed under the sponsorship of the Office of Coal Research. This process appears to be potentially more attractive than other methods of alleviating the present problem of sulfur dioxide and particulate pollution from power plants. In addition, the Solvent Refined Coal Process can help to relieve the current shortage of low-sulfur fuels and at the same time provide a means of utilizing the high-sulfur coal reserves of the nation.

TABLE I

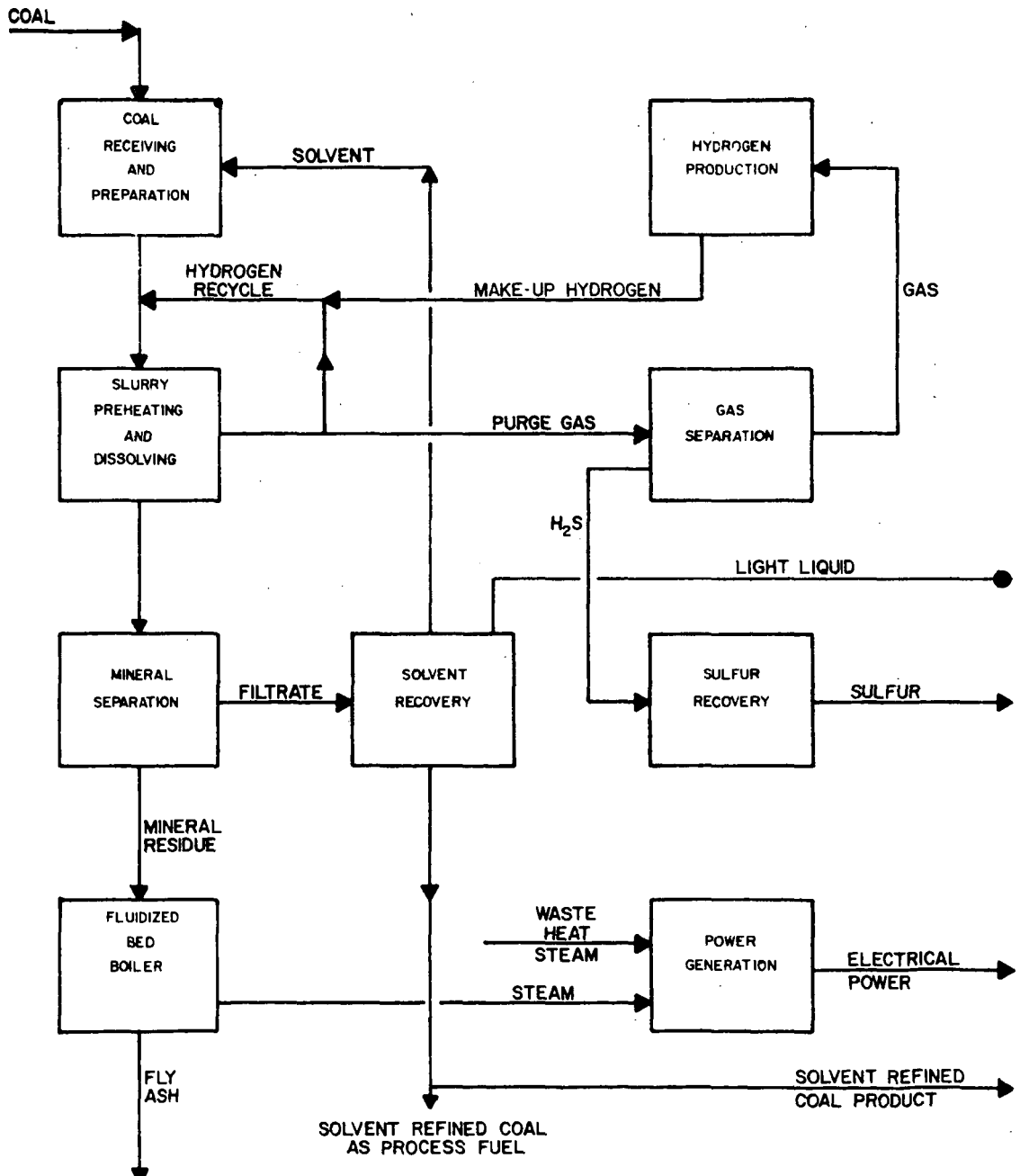
REQUIRED PRICE FOR P&M SOLVENT REFINED COAL

	Selling Price, Including 10% DCF <u>Return on Investment</u> (Cents per Million BTU)
Case I - Light liquid product sold as refinery feed stock. Sulfur and electrical power sold as by-products.	40.7
Case II - Light liquid combined with Solvent Refined Coal for sale as power plant fuel. Sulfur and electrical power sold as by-products.	45.0
Case III - Light liquid combined with Solvent Refined Coal for sale as power plant fuel. No by-products sold.	47.4

REFERENCES

- (1) Wall Street Journal, April 13, 1971.
- (2) Pennington, R. E., and Souby, A. M. "Aromatics from Coal", presented at the National Meeting of American Chemical Society, Los Angeles, California March 28 to April 2, 1971.
- (3) Annual Report of the Office of Coal Research, pp. 38-41 (1971).
- (4) Johnson, C. A., Hellwig, K. C., Johanson, E. S., Stotler, H. H., "Production of Low-Sulfur Fuel Oil from Coal", presented at meeting of American Chemical Society, September 13-18, 1970.
- (5) Appell, H. R. and Wender, I., PREPRINTS, Division of Fuel Chemistry, ACS, 12, No. 3, 220-222, (1968).
- (6) Appell, H. R., Wender, I., and Miller, R. D., PREPRINTS, Division of Fuel Chemistry, ACS, 13, No. 4, 39-44, (1969).
- (7) Appell, H. R., Wender, I., and Miller, R. D., Chem. and Ind. (London), No. 47, 1703, (Nov. 22, 1969).
- (8) "Economic Evaluation of a Process to Produce Ashless, Low-Sulfur Fuel From Coal", R&D Report No. 53, Interim Report No. 1, prepared for Office of Coal Research under Contract No. 14-01-0001-496 (issued June, 1970).
- (9) Oil & Gas Journal, 69, No. 22, 98 (May 31, 1971).
- (10) Electrical World Week, August 10, 1970.
- (11) Harrington, R. E., "Nitrogen Oxides, Sulfur Oxides and Particulates Control Technology for Fossil Fuel Combustion", presented at the Lignite Symposium, Bismarck, North Dakota, May 12-13, 1971.
- (12) Coal Mining & Processing, 7, 13 (February, 1970).

FIGURE I
SOLVENT REFINED COAL PROCESS



A NOVEL AND FAST TECHNIQUE FOR THE DIFFERENTIATION OF
CARBON AND CARBON COMPOUNDS IN COAL

Abund O. Wist, Ph.D.

Department of Occupational Health, University of Pittsburgh
130 De Soto Street, Pittsburgh, Pa. 15213

Introduction:

The different types of coal are normally classified with the help of thermal methods. One of the main aims of such methods is to determine the amount of carbon not bound to any other elements in the coal, called "fixed" carbon here which is probably equivalent to the term "free" or even "elemental" carbon in other investigations. A short tentative method was suggested by Swain⁽¹⁾ using Differential Thermal Analyses requiring standards with known amounts of chemically determined carbon in which the carbon has to be a very similar form to that of the sample. This is very inconvenient considering the many different forms of carbon alone in one coal. The standard test for the classification of coal is published by the Bureau of Mines⁽²⁾. It does not need any Standards and the precision of the carbon determination is very high. But this method needs specially built equipment, is time consuming and needs several samples of the same coal.

Recent improvements in the design and reliability of automatic Thermoanalyses instrumentation makes it desirable to reinvestigate this technique for the determination of "fixed" carbon in coal to see if it would be possible to adapt the Bureau of Mines carbon test to one of the automatic Thermoanalyses techniques with the smallest amount of change.

The Bureau of Mines test is made in the following way. The first sample of the coal is used to determine the moisture in coal by the weight difference of bedfresh coal and air dried and heated (105°C) coal. The ash content of the coal is measured in a second sample by heating it in an aerated oven for 1 1/2 hrs. at 750°C and weighing the remaining ash. The volatile matter is determined by heating a third sample to 950°C in an enclosed container for 7 minutes and measuring the weight difference occurred on the sample during the heating. The fixed carbon content is derived by deducting the weight of water, ash and volatile matter from the original weight of the coal.

From the several Thermoanalysis techniques Thermogravimetry seems to be especially suited to use for the fixed carbon test as it can measure the weight change of the sample in different atmospheres as function of the temperature as required by the Bureau of Mines test.

The fixed carbon test could be made with the help of Thermogravimetry in the following way. First the sample is heated in an inert gas atmosphere (nitrogen, helium) to 950°C linearly with temperature. Then the sample is automatically cooled to about 350°C and reheated up with the same heating rate in an oxidizing atmosphere (air or helium oxygen mixture) to about 800°C . The weight loss of the coal recorded in the oxidizing atmosphere is the amount of fixed carbon in the sample. Water and all volatile matter were removed in the run in the inert atmosphere, and as only ash is left after the run in the oxydizing atmosphere, the weightloss in this atmosphere indicates the amount of fixed carbon.

If one assumes a heating rate of $15^{\circ}\text{C}/\text{min.}$, which is usually used in thermogravimetry the test will take about two and a half hours. Increase in the heating rate to about $25^{\circ}\text{C}/\text{min.}$ should have little effect on the reproducibility (1 - 3%) of Thermobalances. The advantage of measuring fixed carbon with the help of thermogravimetry is that the test can be done in a very similar way as the manual test but a shorter time, on a single sample, fully automatically on standard instrumentation and the fixed amount of carbon is recorded permanently on a graph paper or a print out. At the same time a record is made of the amount of water, of the volatile matter and the ash.

The disadvantage of thermographic equipment against other thermoanalysis instrumentation is that it is delicate to handle, vibration sensitive, relatively expensive and any off-coming gases are difficult to measure.

If one is more interested in measuring the amount of fixed carbon and would like to do this on a more rugged, smaller and less expensive instrument which might be hand portable, Evolved Gas Analysis seems to be the better choice. In Evolved Gas Analysis instead of weight changes the gases evolving from the sample are measured. Therefore, instead of a delicate and expensive balance mechanism, a sturdy, small and sensitive all gas detector like the Thermoconductivity detector can be used. For special gases even higher sensitivity gas detectors can be used, for hydrocarbons, f.e. flame ionsation detectors capable of detecting 10^{-6} grams. And as a weight change can only occur when gases evolve, Evolved Gas Analysis gives principally the same information as Thermogravimetry.

To detect the amount of fixed carbon in coal the sample can be run very similarly as in Thermogravimetry by heating it up first in an inert carrier gas stream (helium, nitrogen) to 950°C ; then cooled down to about 350°C and reheated to about 800°C in an oxydizing atmosphere. The fixed carbon which was left over from the inert gas run is converted to carbon dioxide in the oxydizing atmosphere and indicated by the thermoconductivity detector. The area under the carbon dioxide peak is measured and with the help of a calibration run of ultrapure carbon converted to milligrams

of carbon. If a calibration is made for water and the remaining ash in the crucible is weighted, then also Evolved Gas Analysis, short EGA, can measure the content of water, volatile matter (by difference), fixed carbon and ash in coal. The advantage of the EGA method over the other methods lies mainly in its ruggedness, smaller size and low cost. The precision of the fixed carbon determination should be similar to the Thermogravimetric method. If it can be verified that for all existing coal the carbon peak can be recognized in the oxidizing atmosphere without removing the volatile gases as it could be done in the samples which were run in this investigation, then the EGA test for the fixed carbon would be much simpler than any of the other mentioned tests.

EGA systems have been designed by the author in the past and applied among other fields with another investigator to the determination of carbon in the airborne particulate.⁽⁵⁾ The question arose how well this method is suited for determination of fixed carbon in coal. In the following the feasibility of such an approach is being studied and reported results seem to encourage further investigation of this approach.

Method:

In the following an improved EGA system is described based on earlier work of the author⁽³⁾.

Figure 1 shows the basic EGA design used in this investigation. The weighted sample is filled into a quartz cuvette, which is held in place by a sample holder. A thermocouple measures in the middle of an average size sample the temperature. A platinum shield protects and enhances the output of the thermocouple. Through a small hole at the tip of the thermocouple passes pre-warmed carrier gas into sample taking with it any evolving gases to the detector. The shown portion of the EGA head is heated by a surrounding oven linearly with temperature.

To achieve high sensitivity and reproducibility by creating a very similar chemical and physical environment for each sample and to be adaptable to many different samples, the EGA design has the following characteristics:

- (1) Uniformity of temperature at the sample (1°C)
- (2) The free space in the sample chamber and the connecting tubing to the detector area as small as possible to allow least dilution, highest sensitivity and fastest response.
- (3) The carrier gas is preheated to the sample temperature.
- (4) The carrier gas flows through the sample powder.

- (5) The sample temperature is measured in the sample.
- (6) Any cold spots are avoided.
- (7) The pressure can be changed from 10^{-6} mm Hg to 500 psi.
- (8) The temperature range is from -100°C to 1200°C .
- (9) Differential Thermal Analysis set up is also available in the EGA head.
- (10) The unit is made from chemically inert Inconel 600.

The complete schematic of the EGA system is shown in Figure 2.

The carrier gas is supplied by high purity gas tanks (impurities 2 ppm) and is pressure regulated and if necessary, mixed in a special tee with oxygen, before it enters the reference side of the thermoconductivity cell, from where it flows into the EGA head, where it is first prewarmed in the forechamber to the sample temperature. From there, the carrier gas flows through the sample, where it takes any offcoming gas from the sample through a small annular space between the forechamber and the sealing tube to the sample side of the thermoconductivity detector, where any unbalance in the sensing bridge created by the evolved gases is indicated by a recorder, which also indicates with a second pen the sample temperature and with the help of a disc integrator the area under the gas peak.

As the thermoconductivity detector does not alter in any way the offcoming gases, they can be injected for further study with a gas sample valve into a gas chromatograph, where the offcoming peaks can be separated and identified. Further identification can be made by mass spectrometry or other detectors for specific gases.

The EGA-head is located in a furnace which is heated linearly with temperature by a temperature programmer. The thermoconductivity detector is located on the top of the furnace next to the EGA head to avoid cold spots and allow immediate detection of offcoming gases.

In order to calibrate the system, first baselines in different atmospheres and heating rates with no sample in the EGA head were obtained. No significant deviation could be observed ($\pm 2\%$) in the ranges used for the coal samples. The bimetallic temperature controller for the Thermoconductivity cell creates a small just visible sinuous deviation of the baseline. Over 800°C the very hot offcoming carrier gas is in the heat exchanger coil not more properly cooled down to the T/C temperature range and creates a downward imbalance in the thermoconductivity cell. A

longer and better temperature stabilized coal would extend considerably the useful range of the temperature.

To measure the amount of carbon in the coal samples 2 mgr of ultrapure spectrographic grade carbon (0.0001%) was filled into the quartz cuvette of the EGA head and the area under the peak determined as figure #3 shows. This run was as the following runs obtained under the following conditions: Heating rate $10^{\circ}\text{C}/\text{min.}$, paper advance 6"/hour, helium gas flow 20cc/min., oxygen gas flow 10cc/min., Thermoconductivity detector 140 mA, 150°C , sensitivity 4, fullscale on recorder 2 mV. The blue line across the diagram indicates the sample temperature, the red line the offcoming gas and the disc integrator trace the area under the peak. One can see that the CO_2 comes off around 760°C and that the area underneath the peak corresponds to 94 squares per milligram carbon.

In another investigation⁽⁴⁾ it was found that the temperature of the carbon peak depends strongly on the presence of certain catalysts, some of which occur like iron, in its many forms, in relative large concentrations in coal. These catalysts may cause downward shifts of the carbon peak in the order 300 to 400°C . Therefore, the carbon peak in coal may be expected in the temperature range of 450 and 600°C .

The next three figures show typical EGA diagrams of coal powder. In figure 4, 5 milligrams of coal powder from the Mary Lee seam in Alabama was run in a helium oxygen atmosphere from room temperature to 900°C . First a negative peak occurs at 270°C followed by a shoulder at 400°C and a sharp peak at 470°C , which seems to be located on a lower broader peak as indicated by the dashed line. This peak can be identified as coming from the carbon of the coal by the following method which also allows to measure the area under the peak. First the volatile matter of the coal sample (broad peak) is removed by heating the sample in a pure helium atmosphere as seen in the next Figure 5. The evolved gas trace shows a shoulder at 200°C a peak around 500°C a shoulder at 725 and a peak at 770°C without returning to zero at the end of the run (900°C). The peak around 500°C is most probably due to carbon with the oxygen derived from decomposing material. The area of this peak indicates a smaller amount of carbon than a similar area in the last figure as the carrier gas flow is reduced in this run by the amount of oxygen present in the earlier run and all evolved gases appear therefore in higher concentration (66%).

In Figure #6 the remaining sample from the run shown in Figure #5 is reheated in a helium-oxygen atmosphere. The diagram shows a declining baseline between 300°C and 600°C and a single peak at 490°C . As the offcoming gas for this peak and all the other peaks around 500°C is CO_2 , they are due to the carbon in the coal. If one compares the areas of the carbon peaks in these three

runs one finds that the area of the carbon peak in this run (Figure #6) and the corrected area of the carbon peak in the run before result in the area of the carbon peak in the first run (Figure #4). Using the calibration run with ultrapure carbon (Figure #3) one can now find the weight of the fixed carbon in the coal sample and calculate the percentage of carbon in coal.

To check the above calculations each sample was before and after each run weighted in a Cahn Micro balance. In this way according to the standard method, the amount of fixed carbon could be determined by subtracting the weight of the volatile matter (including the water) and the weight of the ash from the original weight of coal.

The results from four different samples are shown in the last Figure (#7).

In this table the amount of fixed carbon in the four samples is shown first as determined by the EGA method and then by the standard method using weight difference. One can see that the results of these two methods are very close in spite of quite varying fixed carbon content in the coal. Also, on the diagram is the amount of volatile matter and ash indicated. One can see here on the other hand that the areas determined by EGA corresponding to the volatile matter do not compare well to their measured weight loss. This is easy to understand because the thermoconductivity of each of the offcoming gases is different and causes wide variations in the weight of the volatile area calculated from the area.

The capital letters H_e, O, H_e+O, indicate that the run was made correspondingly in Helium alone, in Helium Oxygen after the Helium run, in Helium Oxygen with a fresh sample.

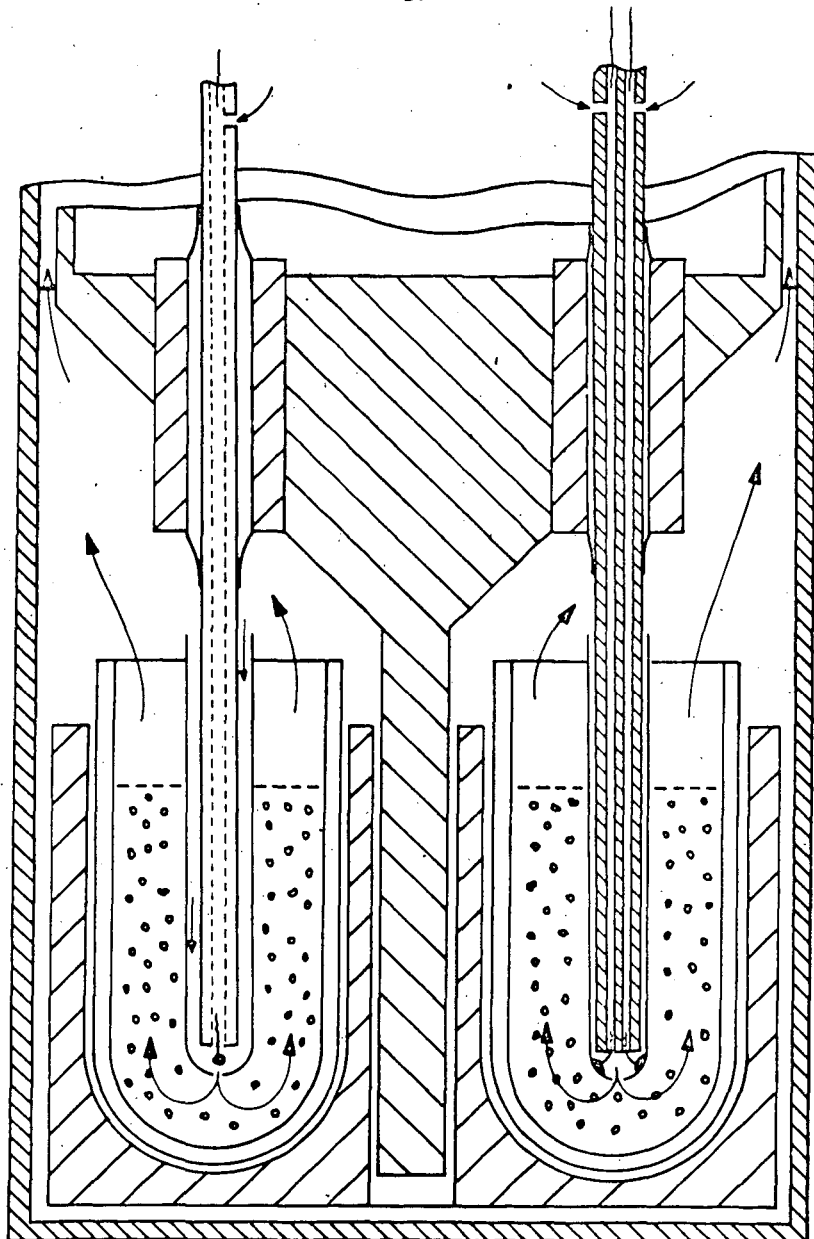
In summary the present investigation indicates that the EGA method(as measured on four actual samples) compares favorably with the standard manual weight difference method as published by the Bureau of Mines in measuring the amount of fixed carbon in coal. As the EGA method is much faster, requires only one very small sample (larger samples can be easily handled) is fully full automatic (no attendance), the whole instrument probably can be made hand portable and the strong possibility exists that only one run is necessary; therefore, further study of this approach on a much larger scale is suggested.

Acknowledgement:

"This investigation was supported by research grant AP 00908, Air Pollution Control Office, Environmental Protection Agency."

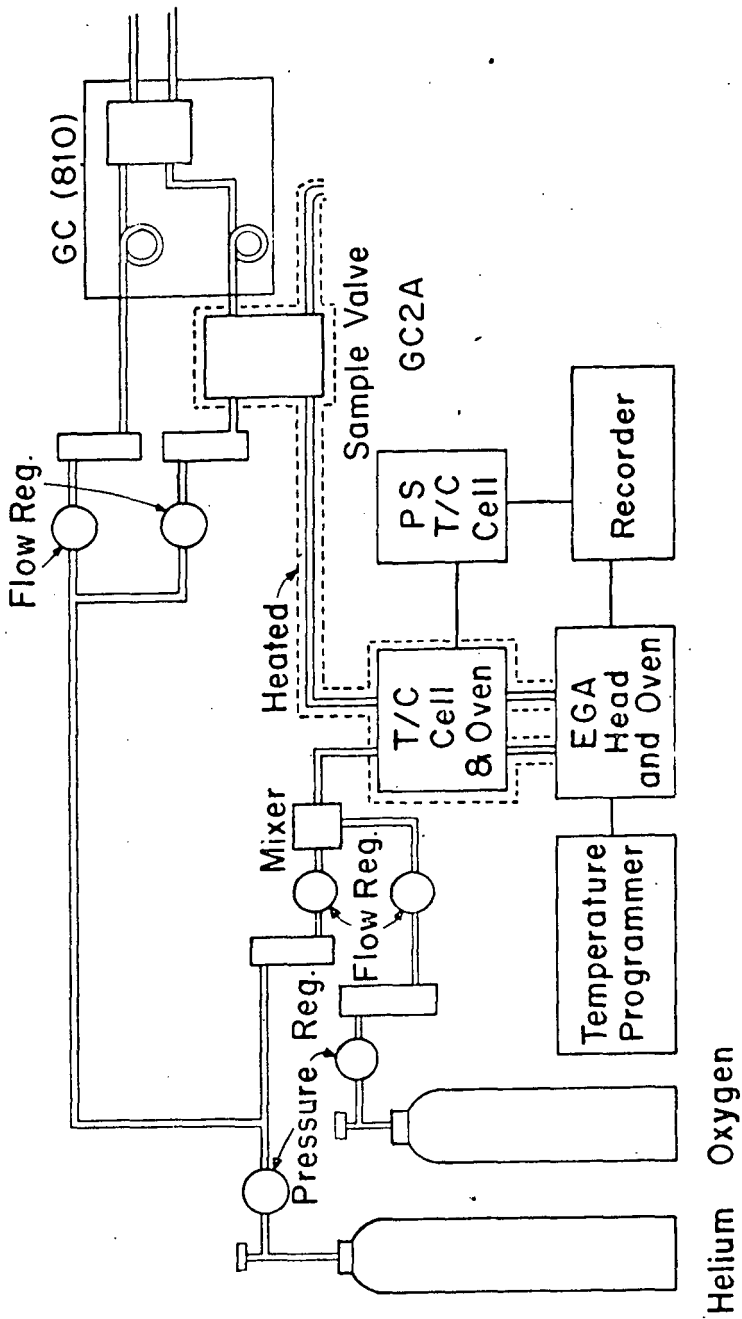
Literature Cited:

- (1) D. J. Swaine, "The Identification and Estimation of Carboneous Materials," Thermal Analysis II, Ed. Schwenk, Garn, Academic Press, New York, 1969.
- (2) "Methods of Analyzing and Testing of Coal and Coke," Bulletin 638, Bureau of Mines, United States Department of the Interior, 1967.
- (3) Abund O. Wist, "Temperature Controlled Pyrolysis Applied to Cortical Bone," J. of Gas Chrom, 157, March 1967.
- (4) Abund O. Wist, "A New Fast Method for Measuring the Speed of Chemical Reactions," Pittsburgh Conference, Cleveland, 1971.
- (5) Abund O. Wist and J. O. Frohliger, "Effluent Gas Analysis for the Chemical Determination of Airborne Particulate Matter," Proceedings of the 2nd International Clean Air Congress, Academic Press, New York, 1971.



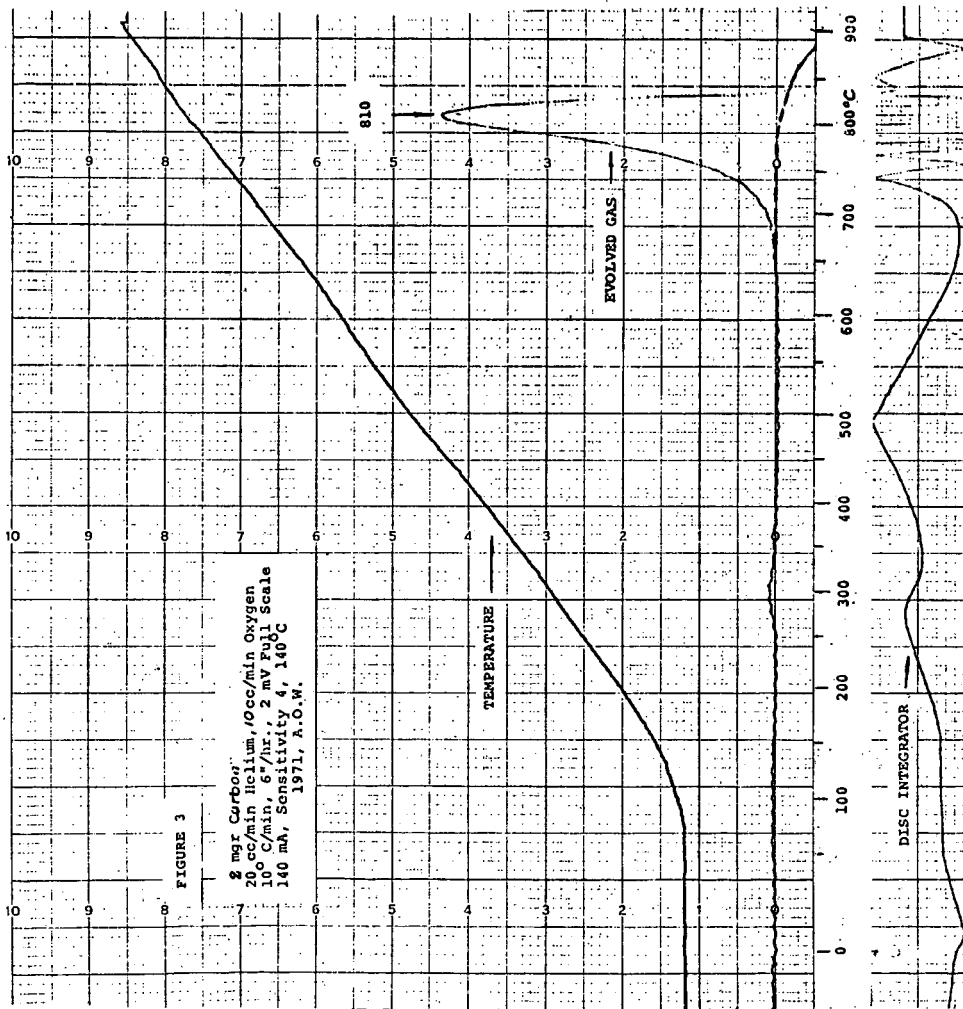
EGA Samplechamber 1970

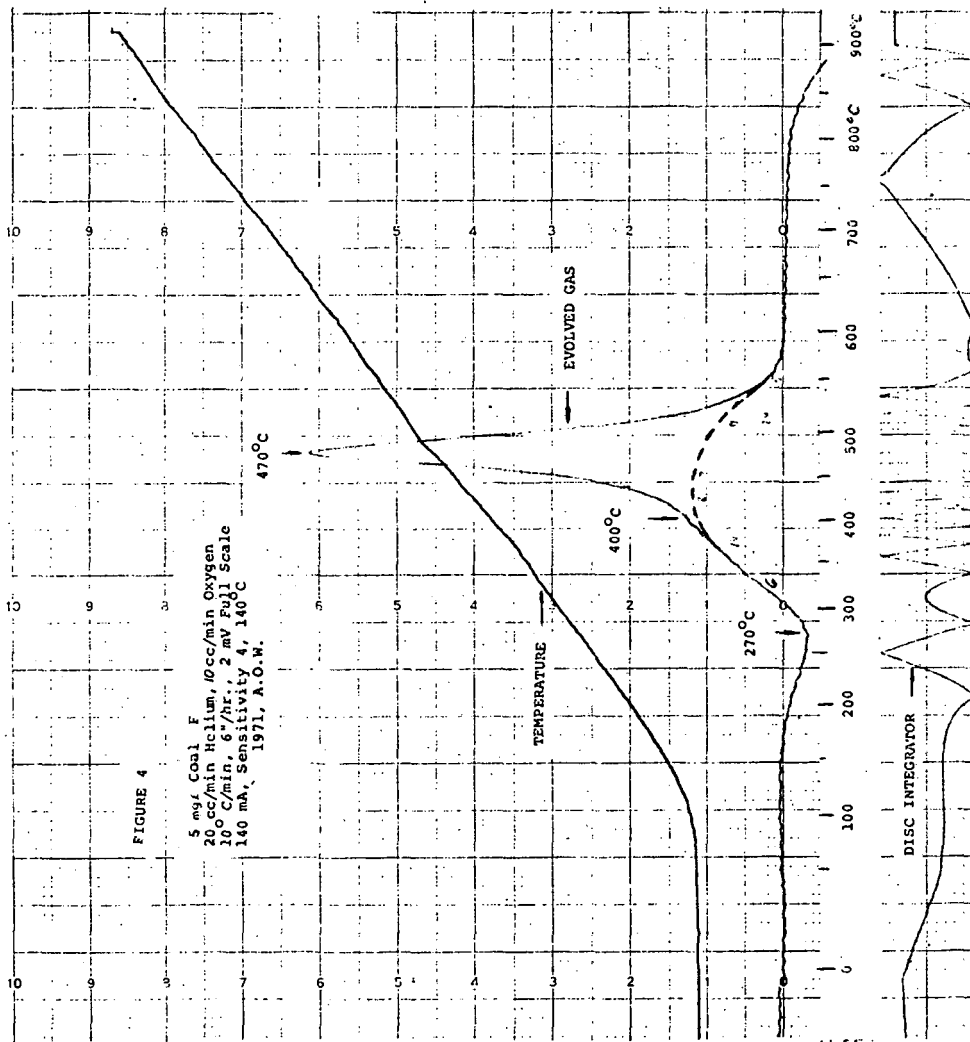
FIGURE 1

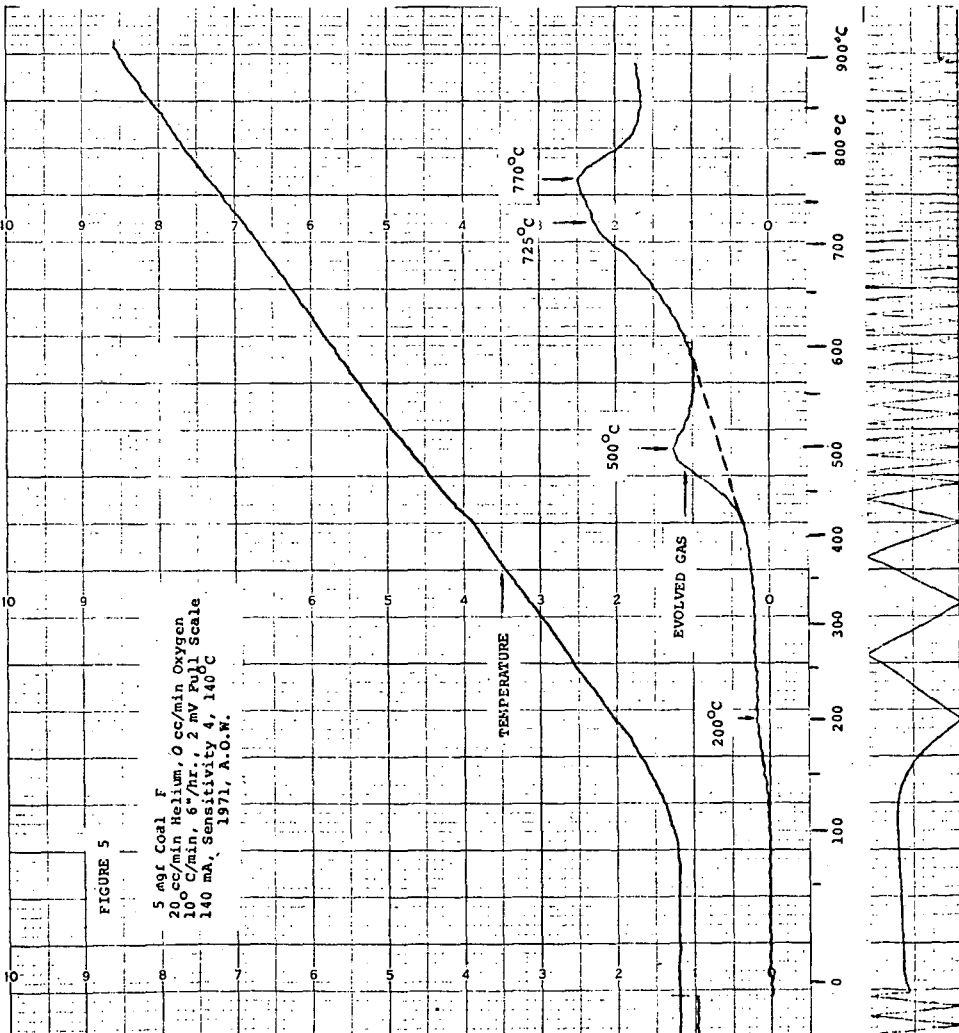


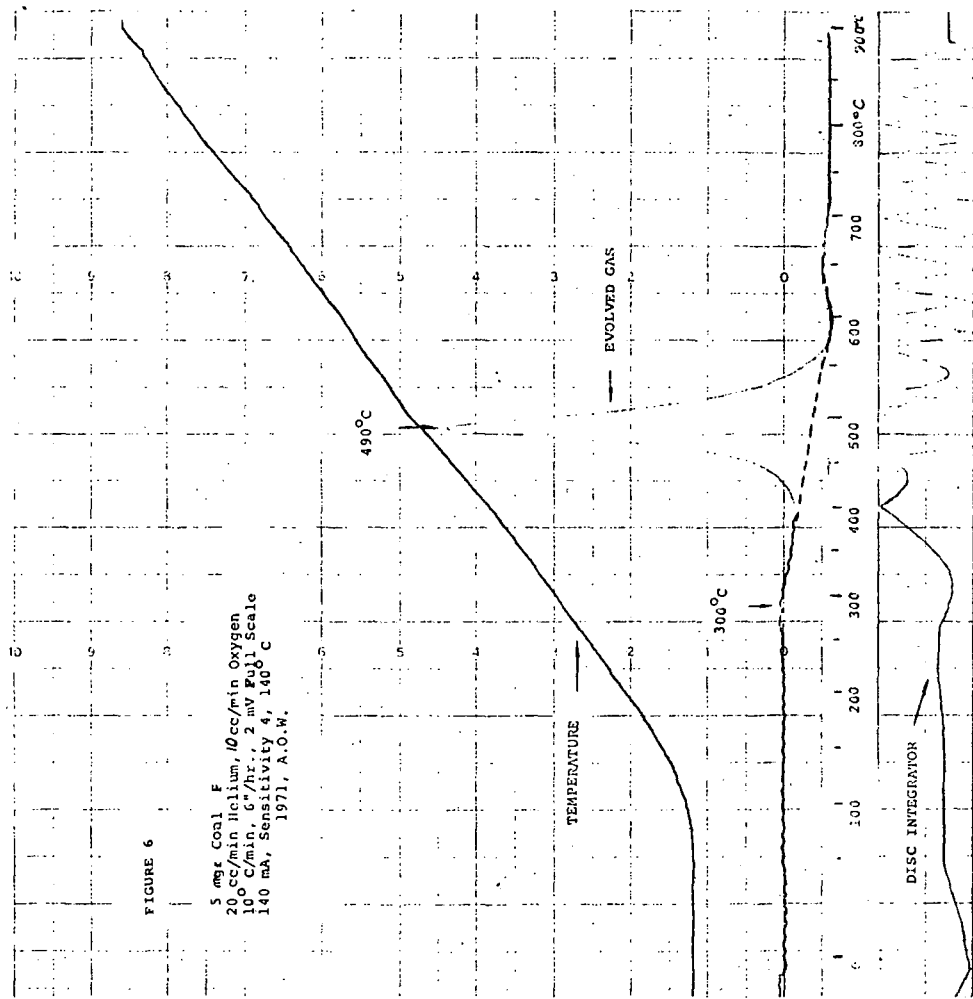
Schematic for EGA Determinations 1970

FIGURE 2









COAL	Sample Weight	FIXED CARBON				VOLATILE MATTER				ASH
		EGA Area Sqrs.	Wt. mgr.	Wt. mgr.	Weight %	EGA Area Sqrs.	Wt. mgr.	Weight %	mgr.	
A	Mathies Pa. (Pittsburgh)	He	33	0.35	7		696			
	5 mgr.	0	206	2.2	44	2.49	50.0	232	1.85	0.65
	H + O	228	2.42	48.5				37		12.5
B	Rubena, Pa. (Pittsburgh)	He	40	0.42	8.5		677			0.35
	5 mgr.	0	226	2.40	48.0					7
	H + O	251	2.67	53.5	2.65	53	236	2.00	40	
E	Olga, W.Va. (Pocahontas #4)	He	15	0.16	3.2		664			
	5 mgr.	0	335	3.49	70.0	3.66	73.2			0.277
	H + O	351	3.66	73.4			186	1.063	21.3	5.5
F	Segco #1, Ala. (Mary Lee)	H	25	0.26	5.3		752			
	5 mgr.	0	202	2.15	43	2.375	47.5			0.75
	H + O	226	2.4	48			218	1.875	37.5	15

FIGURE 7
Comparison of EGA Versus Weight Method

USE OF LIMESTONE - WET SCRUBBING FOR REDUCTION OF SULFUR OXIDE EMISSION
FROM POWER PLANTS- FACILITIES AND PROGRAM FOR PROTOTYPE-SCALE TESTING

By

H. W. Elder
Tennessee Valley Authority
Muscle Shoals, Alabama

E. L. Plyler
Environmental Protection Agency
Durham, North Carolina

Increasing worldwide concern about the quality of our environment has spurred research and development activity on all phases of pollution control. Much interest has been generated in improving the quality of air by reducing the amount of dust and objectionable gases emitted from industries that discharge gaseous effluents and particulates. The utility industry is one of the major areas where attention to the problem is being accelerated.

At present, most of the electricity generated in this country is based on combustion of fossil fuels. Power production in hydro plants is ideal from an air quality point of view, but, unfortunately, the available sites for this type plant have been nearly exhausted. Production of power from nuclear generation plants seems likely to increase at a rapid rate in the immediate future. However, the increasing demand for electricity will require continued use of fossil coal-and oil-fired plants for the foreseeable future.

In the natural process that converts organic matter into materials suitable for use as fuel, sulfur-bearing compounds are formed along with the carbonaceous material. Combustion of the fuel results in formation of sulfur oxides; reduction of sulfur oxide emission from combustion sources is one of the major objectives of the pollution control effort. Removal of sulfur prior to combustion would be ideal because the fuel could be processed in high volume before distribution. However, with the exception of natural gas, which can be desulfurized by proven methods, reduction of sulfur in fuels to acceptable levels does not appear to be economically feasible at present. Development of technology for removal of sulfur from stack gases seems to be the most expedient approach to control of sulfur dioxide emission.

Many different processes for recovery of sulfur dioxide have been proposed and development work is being carried out on a variety of types. The process that has attracted the greatest interest, because of its relative simplicity, is absorption by limestone in a slurry scrubbing process. This process does not depend on marketing a byproduct; the low-value absorbent can be discarded.

Limestone - wet scrubbing can be used in two ways, either by injecting limestone into the power plant boiler and collecting the calcined lime in the scrubber or by introducing limestone directly into the scrubber circuit. In an EPA-funded project, TVA is carrying out full-scale studies of dry sulfur dioxide sorption by limestone injection into a coal-fired 140-mw unit at the Shawnee station. This program is being expanded to include a study of the wet scrubbing method.

The Bechtel Corporation prepared a preliminary engineering study of a test facility for lime-limestone scrubbing under a contract with EPA. As a continuation of this effort, Bechtel is participating in the program to fully characterize the limestone - wet scrubbing process. EPA is funding the project and providing technical and administrative direction, Bechtel has primary technical responsibility for design of the facility and the test program, and TVA is constructing and will operate the test facility. The test program will be directed by a technical team comprised of representatives from each group.

Design is complete and construction is scheduled for completion by January 1972. The overall project cost will approach \$10 million.

Program Goals

The purpose of the project is to evaluate the feasibility, effectiveness, and economics of limestone - wet scrubbing. The test program has as its primary objective the development and demonstration of a closed-loop limestone scrubbing process. Both injection into the boiler and addition directly to the scrubber circuit will be evaluated. Following are the major goals of the study:

1. Investigate process chemistry and kinetics. The test program will be developed and conducted to provide for determination of the chemistry and kinetics of the various process steps. This is needed to both explain and solve operating problems and to allow safe extrapolation of process behavior beyond actual test conditions. Differences in process chemistry due to changes such as variations in operating conditions and reactant composition will be investigated.
2. Develop information for process optimization and scale-up. The test program will provide for development of reliable process models which describe the form and magnitude of responses to all important variables. This model should predict optimum process designs for different process sizes, modes of operation, and site restraints.
3. Investigate and solve mechanical design and operating problems. Scaling, gas distribution, corrosion, erosion, and other factors that are related to mechanical design will be evaluated.

4. Study waste disposal. The quantity and quality of liquid and solid wastes produced by the process will be determined. Treatment or disposal methods to avoid excessive water pollution will be identified.
5. Determine plume reheat requirement. The required degree of plume reheat to ensure localized air quality will be studied.
6. Define economics. The test program will provide suitable operating cost data and estimates of capital requirement to quantify economics for various size and site restraints.
7. Conduct long-term operation. The reliability of the process will be demonstrated by a period of long-term operation under normal operating conditions.

Process Description

TVA, under an agreement with EPA, conducted a conceptual design study of the limestone scrubbing process; the report of this work (1) summarized the status of process developments.

The use of limestone or lime as an absorbent for sulfur oxides has been studied over an extended period. Most of the work has been small-scale, but some pilot plant and plant tests have been made. Introduction of the absorbent directly into the scrubber system dates back to the early 1930's when research programs were carried out in England; a closed-loop system utilizing lime or chalk as the reactant was operated commercially. The two steps of the injection-scrubbing method were first studied in a combined process by Combustion Engineering, Inc. This work led to installation of scrubbing systems on two full-scale generating units. The conclusion indicated by the prior work is that limestone scrubbing is a feasible method for controlling sulfur dioxide emission from power plants. However, several major process and operating problems were identified that must be resolved to establish efficiency and reliability.

In the Shawnee program, three parallel scrubbers will be tested simultaneously to expedite evaluation of various scrubber types. A flow-sheet for one of the systems is shown in Figure 1. Gas will be withdrawn from the boiler ahead of the particulate removal equipment so that the entrained dust, including lime during injection-scrubbing tests, can be introduced into the scrubber. Analysis of the gas for sulfur dioxide, oxygen, and carbon dioxide will be made continuously by instrumental methods. Dust loading will be determined intermittently. Gas flow rate to each scrubber will be measured by venturi flow tubes and controlled by dampers on induced-draft fans. The concentration of sulfur dioxide in the outlet gas will be determined continuously. The efficiency of the process for removal of nitrogen oxides also will be determined by periodic checks of inlet and outlet concentration.

Quench sprays will be installed at the inlet of each scrubber to cool the gas prior to contact with the scrubbing slurry. Soot blowers will be installed to minimize solids deposition at each scrubber inlet. Experimental work by TVA has indicated that gas cooling may be necessary to prevent stripping of absorbed but unreacted sulfur dioxide from the slurry.

Variables that affect the rate of gas-liquid mass transfer and particulate removal efficiency in the scrubber will be studied so that optimization of the dual function can be established. The efficient removal of sulfur dioxide at a practical recirculation rate depends on an adequate limestone dissolution rate in the scrubber; factors that effect dissolution (slurry holdup, limestone particle size, stoichiometry, slurry solids content) will be evaluated. Mist elimination to prevent excessive solids carryover by slurry entrainment will be studied. Also, the reheat requirement is affected by water entrainment.

The system will be equipped with oil-fired reheaters to increase the temperature of the exit gas. In the scrubber, the gas will be cooled to its wet-bulb temperature and reheat therefore will be necessary to restore plume buoyancy for good dispersion. The Air Quality Branch (Division of Environmental Research and Development) of TVA, which has done extensive work in plume dispersion modeling (2), will assist with evaluation of the extent of reheat required. The exhaust gas from each scrubber system will be discharged through a separate stack.

Although limestone scrubbing is a relatively simple process, the process chemistry is complicated by soluble compounds from the coal ash, by low solubility of the absorbent and reaction products, and by supersaturation tendency of the calcium-sulfur compounds. The Radian Corporation has developed a computer program to predict the composition of liquid and solid phases in the system at equilibrium conditions; this work has been useful in predicting boundary conditions. However, the actual steady-state conditions depend on rates, and kinetic data are scarce. Experimental results have shown that the slurry discharged from the scrubber has not reached equilibrium. Therefore, it is necessary to provide residence time outside the scrubber in order for absorbed sulfur dioxide to react with calcium, which must be brought into solution, and to precipitate supersaturated calcium salts formed in the scrubber. The system is highly sensitive to pH and the method of absorbent addition is important. A hold tank will be provided in which the residence time can be varied. A major portion of the slurry will be recirculated to provide a source of calcium for reaction in the scrubber and to furnish seed crystals for dissipation of supersaturation. A heat exchanger will be provided in the slurry system so that the effect of slurry temperature on sulfur dioxide absorption efficiency can be studied; river water will be the cooling medium. A sidestream will be withdrawn for separation of reaction products.

The method for separating product solids from the recirculating slurry in large-scale application of the process will depend largely on the real estate available and proximity of disposal areas to the power plant. The test facility will be provided with thickeners to concentrate the solids either for further dewatering in a filter or centrifuge or for transport to the pond. A filter and a centrifuge will be installed to study solids-liquid separation problems. In some potential applications of the process, solids disposal may have to be accomplished by transport of dewatered solids to relatively remote locations by truck, rail, or barge shipment. As an alternative, the solids may be discarded by discharge of the sidestream from the slurry effluent hold tank directly to a pond where settling will occur (hopefully). Pilot plant studies by TVA have indicated that settling may be hindered by formation of plate-like crystals of calcium sulfite.

In all modes, the liquid phase will be returned to the scrubber so that closed-loop operation will be effected. The solids content of the scrubber recycle stream will be controlled by blending of process streams; a radiation-type density measuring device will be utilized.

The quality of water associated with solids discharged to the pond will be evaluated to assess potential degradation in water quality as a result of seepage or overflow.

Equipment Selection

The existing facilities installed to study the dry injection method include:

1. Limestone-receiving hopper.
2. Belt conveyor and surge tank.
3. Oil-fired rotary dryer.
4. Dry ball mill.
5. Mechanical classifier.
6. Pulverized-stone storage silo.
7. Feed tank on load cells.
8. Pneumatic transfer and injection system.

This equipment will be used during tests of injection-scrubbing. The receiving and grinding facilities will be used to supply pulverized absorbent for direct addition to the scrubber circuit.

The equipment selected for wet scrubbing was sized for minimum cost consistent with ability to extrapolate results to commercial units; 30,000 acf per scrubber train was judged to meet these requirements.

The equipment arrangement for the test facility is shown in Figure 2. For resistance to corrosion, particularly during upset conditions, it was decided that equipment should be rubber-lined mild steel. In the following discussion, it may be assumed that rubber lining is used except where noted.

The selection of scrubbers to be tested was one of the basic criteria for demonstration of the process; these devices should remove both particulates and sulfur dioxide with high efficiency. Particulate removal should be on the order of +99% (it is assumed that particulate must be removed to a level of 0.02 grain/ft³ or lower to give a clear stack) and sulfur dioxide removal should be better than 85%. The scrubber should also effectively dissolve calcium oxide or calcium carbonate. Basic scrubber characteristics were considered in selection of types, but lack of available experimental data prevented a quantitative evaluation of predicted performance. One of the primary functions of the test program will be the development of such data. Expected mechanical performance of the scrubbers was also a factor in the choice; two major areas of concern are the buildup of solids on surfaces where hot gas first contacts the scrubbing solution and the plugging of gas-liquid contact zones. Other factors considered were pressure drop, turndown capability, ability to operate with slurry, ease of control estimated maintenance requirement, and compactness of design. A comparison of the various types considered is shown in Table I. It was concluded that the following scrubbers are the best candidates:

1. Venturi followed by an absorption section.
2. Turbulent-contact scrubber (mobile ping pong ball type).
3. Flooded-bed scrubber (marble bed type).

Gas ducts (40 in. diameter) between the boiler takeoff and the scrubber are mild steel, insulated to prevent condensation. Flue gas analysis, except for sulfur dioxide, will be made with gas chromatographs; an ultraviolet photometric analyzer will be used to monitor sulfur dioxide before and after each scrubber. Provision is made for addition of sulfur dioxide during selected tests to control the sulfur dioxide concentration. Methods for measuring particulates and nitrogen oxides are presently being evaluated. The venturi flow tubes (20-in. throat diameter by 9 ft high) are constructed of stainless steel and are mounted in a vertical run of straight duct in accordance with good engineering practice.

The venturi scrubber (Chemico) has a variable throat section fabricated from stainless steel. The overall dimensions are 6 ft 4 in. diameter and 11 ft high with a 3-ft-diameter throat. The gas velocity through the throat is controlled by a mechanically actuated conical plug.

Gas flow is downward through the scrubber and exits through a side outlet near the bottom into a companion absorber. The venturi should give good performance on particulate removal but the gas residence time may be too short for good absorption. Therefore, an absorption section was added in series. The absorber shell (8-ft diameter by 38 ft high) is designed to accommodate either packed or sieve tray internals.

The turbulent contact absorber (UOP) is designed for two scrubbing stages with provision for a liquid trapout tray or a third scrubbing stage. The vessel is 5 ft 7 in. square by 38 ft 8 in. high; internals are stainless steel.

The flooded-bed scrubber (Combustion Engineering) has a single stage of marble mobile packing. The vessel is 7 ft square and 17 ft 6 in. high. All of the scrubbers will accommodate either a chevron or fixed vane-type mist eliminator.

The reheater for each train is oil fired and has a maximum capacity of 5,800,000 Btu/hr. The induced-draft fans are constructed of stainless steel and are equipped with 400-hp motors.

All piping in the system is either rubber lined (2-1/2 inch and larger) or stainless steel (less than 2-1/2 in.). The scrubber hold tank for each scrubbing system is cylindrical (20-ft diameter and 21 ft high) with a flat bottom. They are sized for 1-hr retention time at 600 gpm; liquid levels will be adjustable so that residence time can be varied. The tanks are equipped with agitators and have overflow weirs to minimize loss of unreacted absorbent to the thickeners. Each system will have a thickener with rake and scraper discharge designed for 2 hr settling time. Two are 20 ft in diameter and 15 ft high. Because of higher recirculation rates in the TCA scrubber, the third thickener will be 30 ft in diameter.

Thickener underflow may be discharged to a pond area provided for waste solids disposal or to a further dewatering step. The pond is separate from the plant ash disposal area and is equipped with a reclaim sump for return of the clarified overflow; all scrubber systems will discharge to a common pond. However, compartmented areas are provided for storage of solids from markedly different reactants. The filter is a drum type with flexibility to operate with precoat. The centrifuge is a continuous type with a variable speed drive.

Control of the scrubbing systems will be carried out from a central graphic panelboard equipped with an electronic data acquisition system. The system is hard wired for data output in engineering units directly on magnetic tape. Onsite display of selected information will be available. Also, important process control variables will be continuously recorded and trend recorders will be provided for periodic

Test Program

The initial phase of testing will involve startup to check out equipment, piping, wiring, and controls, followed by a period of calibration and performance testing prior to start of planned experiments.

The first set of experiments will consist of screening tests designed to identify the principal independent variables that affect process performance or operating reliability. These tests will also establish the range of interest for the important variables. A statistical design of experiments will be used to obtain the required data at a reasonable significance level with a minimum number of runs. The correlation of effects will be based on process models which have been developed by Bechtel for each system. The models were derived through application of chemical engineering theory to produce a series of equations relating independent and dependent process variables. The variables are related by a series of coefficients; the numerical value of these coefficients will be determined from the experimental data by regression analysis.

Following the screening experiments, a set of primary experiments will be conducted to permit a detailed investigation of performance characteristics under optimized conditions. These data are required for application of the experimental results to design of commercial systems. During this phase, periods of extended operation under uniform conditions are planned to provide information of operating reliability.

Mechanical design development will be carried out concurrently with the process-oriented tests. Many of the potential operational problems such as scaling, plugging, mist carryover, corrosion, erosion, and solids-liquid separation are directly influenced by process variables. It is important that feasible operating modes be established early in the program.

Systematic procedures for evaluating the effect of effluents on air and water quality are being developed.

In order to make maximum use of the facility, testing will be carried out on a continuous basis; the only planned delays between tests will be to allow the system to reach steady-state after a change in conditions. The analytical support required for the test program is formidable. It has been estimated that up to 420 chemical determinations per test will be needed. Instrumental procedures are being developed to minimize the cost of this work. Atomic absorption, X-ray diffraction, X-ray fluorescence, and conductivity methods are being evaluated.

The overall length of the test program has not been well defined. A test period of 2 yr has been assumed for budgeting purposes, but the actual time will depend on the many factors that tend to confound a comprehensive test program. The number of different types of limestone to be tested will have a major influence on the total program length. Also, it might be desirable to test improvements in the method that are likely to develop from pilot programs in progress around the world.

References

1. Tennessee Valley Authority. "Sulfur Oxide Removal from Power Plant Stack Gas: Use of Limestone in Wet-Scrubbing Process" (1969). Report No. PB 183-908, Clearinghouse for Scientific and Technical Information, 5285 Port Royal Road, Springfield, Virginia 22151
2. Thomas, F. W., Carpenter, S.B., and Colbaugh, W. C. J. Air Pollut. Contr. Assn. 20 (3), 170-177 (March 1970).

TABLE I
SCRUBBER PERFORMANCE SUMMARY

Type of Scrubber	Estimated SO ₂ Removal Efficiency (%)	Estimated Particulate Removal Efficiency, Np	Est. Scrub. Ldg. Req. Gal/1000 ft ³ of inlet gas	Pressure Drop* (Inches H ₂ O)	Resistance to Solids Plugging in Contact Area	Compactness	Normal Gas Velocity ft/min	Turndown** Capability (%)
Venturi	85+ (with absorption section)	4.0+	11 - 17**	6 - 15	good	good	10000 - 15000 (throat)	50+
Flooded Bed	90+	4.0+	8 - 11	6 - 10	good	good	500 (shell)	35
Turbulent Contact (2 stages)	85+	4.0+	15 - 30	6 - 10	good	good	850+ (shell)	25 - 35
Impingement Plate (2 stages)	85+	4.0	8 - 20	7 - 9	good if proper design is used	good	500 (shell)	30
Cyclone	70	2+	4 - 10	2 - 5	poor because of nozzle plugging	poor	2000 - 4000 (inlet)	15
Packed Bed	90+	3.5+	15 - 30	3+	poor	fair	200 - 450 (shell)	30
Nozzle	70	4.0	--	6+	good	good	--	15
Spray Tower	60	1.7	2 - 5	2+	poor because of nozzle plugging	poor	200 (shell)	15
Cross Flow	80	2.0+	6 - 12	4+	poor	good	200 (shell)	15

* From scrubber inlet to mist eliminator outlet

** Includes absorption section

*** For a single unit with no partitions

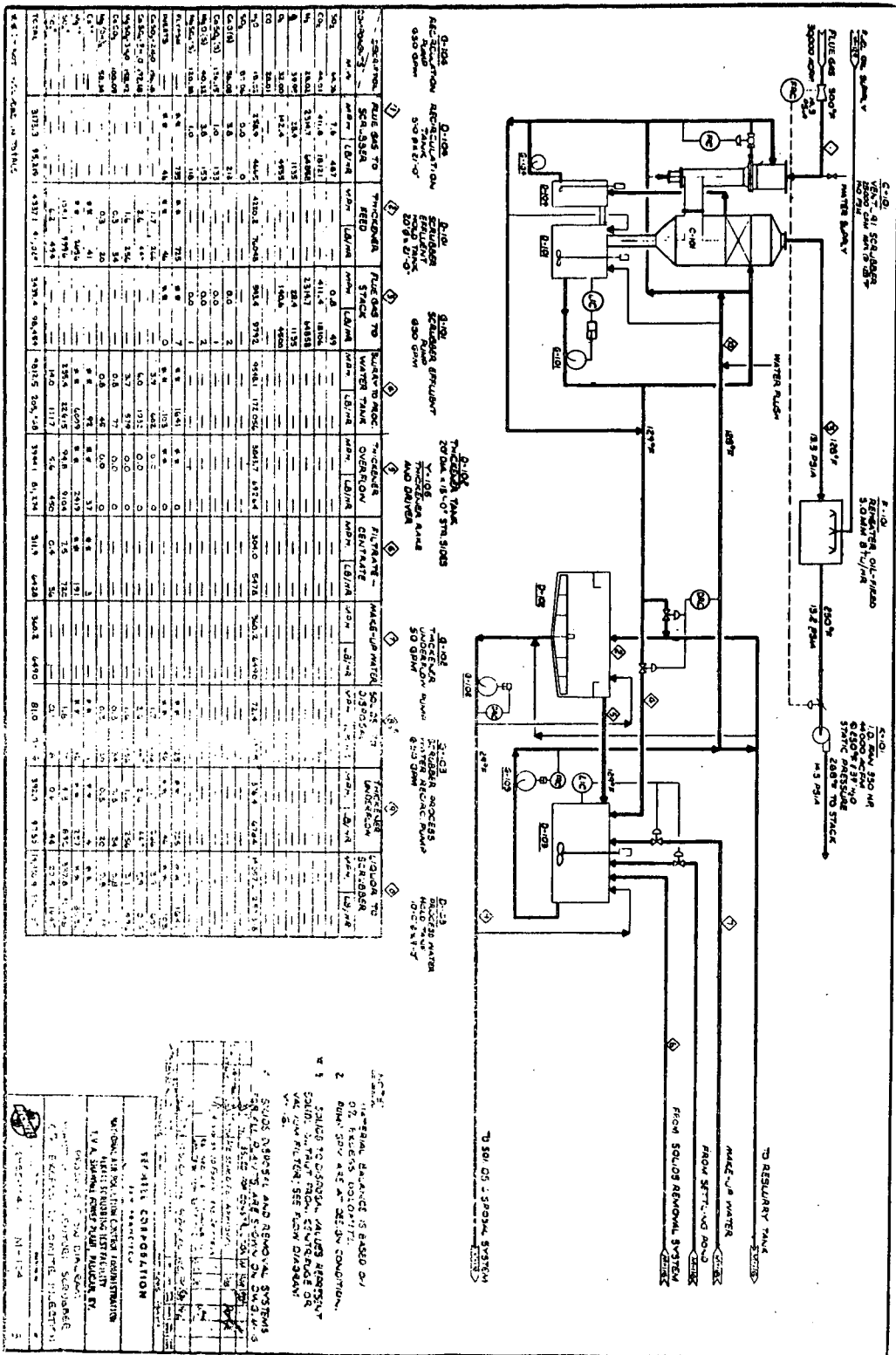
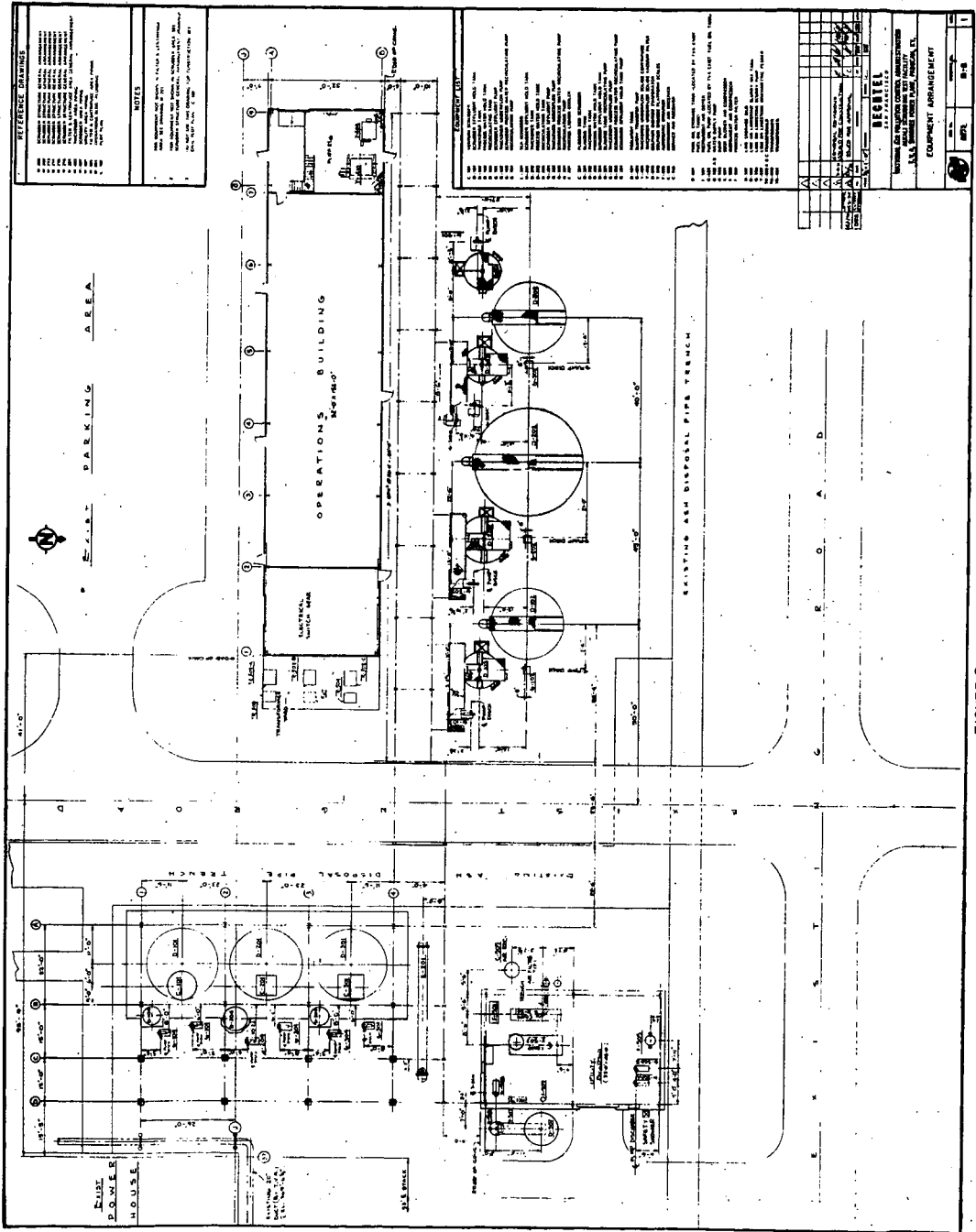


FIGURE 1

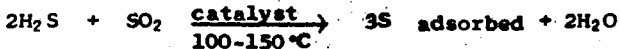


THE RECOVERY OF SULPHUR FROM SULPHIDE ORE
SMELTER WASTE GASES, CONTAINING LOW CONCENTRATIONS OF SO₂

R.G.W. Laughlin, F. J. Hopton and V.B. Sefton

ABSTRACT

A low temperature (100-120°C) Claus reaction is suggested as the basis of a recovery process to obtain sulphur from waste gases, containing low concentrations of sulphur dioxide, emitted during sulphide ore smelting. The catalyst for the reaction acts as an adsorbent for the sulphur produced.



A hot reducing gas passed through the loaded catalyst strips off the sulphur and also regenerates the catalyst for further reaction and adsorption. After condensation, two thirds of the sulphur is used to produce hydrogen sulphide for the Claus reaction and the remainder may be sold to defray expenses. Several methods for hydrogen sulphide production have been examined and the reactions between natural gas and producer gas with sulphur or sulphur dioxide are discussed. Tests of the process on site at a smelter indicate that the process would work successfully to desulphurize gases containing 1-2% sulphur dioxide by volume. Two major process flow schemes are considered, one suitable for a smelter where a strong 10-15% sulphur dioxide stream is available for hydrogen sulphide production, the other where no such stream exists. Preliminary process economics are discussed.

1. INTRODUCTION

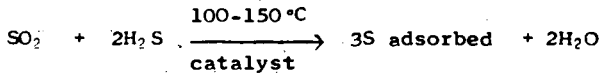
Sulphur dioxide is now universally recognized as a harmful air pollutant. The use of tall stacks, and the existence of reasonable weather patterns, have generally minimized the effect of SO₂ on people, buildings, and plants. Unusual geographic and weather conditions have lead to several catastrophes attributable to SO₂, e.g. Donora, Pennsylvania (1948)(1); and London, England (1952).

Two major sources of SO₂ pollution are coal and residual oil fired thermal electric generating stations and sulphide ore smelting operations. These sources account for 50% of the 15-20 million tons of sulphur(2) emitted to the atmosphere in North America each year. The concentrations of SO₂ in the effluent gases from these operations are 0.1-0.3% by volume SO₂ from generating plants and 1.0-15.0% from smelters. In Ontario 150,000-200,000 tons per year of sulphur are emitted from generating stations, and 1.5-2 millions tons/year from smelting operations.

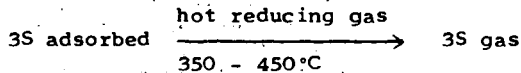
In late 1966, the Ontario Research Foundation initiated an investigation into an SO₂ removal scheme, which would be applicable to both generating plants and sulphide ore smelters. The process was aimed at both air pollution abatement and resource conservation. It was considered essential to recover sulphur in the elemental form, since this incurs minimum transportation costs per unit weight of sulphur. Ontario is already well supplied with sulphuric acid manufactured from high strength SO₂ streams being emitted from the Sudbury complex of nickel smelters. Any further sulphur recovered in Ontario would, therefore, have to be transported away from the province, thus the minimum transportation cost is essential.

The O.R.F. process(3,4) is based on a low temperature Claus reaction(5). The SO₂ in the effluent is catalytically reduced to sulphur with H₂S; a portion of the sulphur is retained as product and the balance is converted to H₂S and recycled. Fig. 1 shows a simple flow sheet for the process. The chemistry of the process is summarized in the reactions given below:

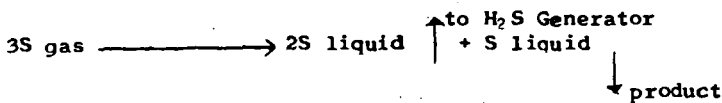
i) Reduction and Adsorption



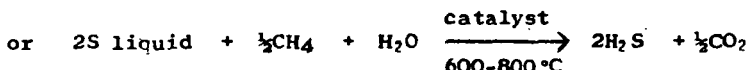
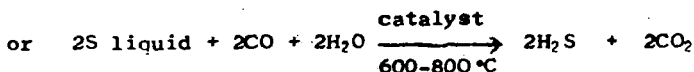
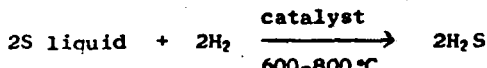
ii) Catalyst Regeneration



iii) Sulphur Condensation and Splitting



iv) H₂S Production



2. CATALYST SELECTION

The properties required for a successful catalyst/adsorbent in this process are:-

- i) High catalytic efficiency for the H₂S/SO₂ reaction in the presence of both oxygen and water.
- ii) High adsorptive capacity for sulphur.
- iii) Long active catalytic life.
- iv) High mechanical strength, low attrition loss potential.
- v) Low cost.

Tests in the laboratory were carried out using a 1% SO₂ and 2% H₂S stream passing over 10 grams of some 30 different catalysts with a gas contact time of 0.3 seconds. The results showed that the three following catalysts exhibited the best potential for fulfilling the first two required properties. Activated aluminas (Kaiser Chemicals KA-201 and Alcoa F-1) and a treated Bauxite (Engelhard Porocel SRC). All three catalyzed the reaction of H₂S with SO₂ preferentially to the reaction between H₂S and oxygen at low temperatures (<150 °C). At higher temperatures the oxidation of H₂S to water and SO₂ was favored as would be expected.

Subsequent tests showed that Kaiser KA-201 activated alumina was the best catalyst for sulphur loading, mechanical strength, and maintenance of catalytic activity, over several loading and regenerating cycles. The efficiencies of the three catalysts for the H₂S-SO₂ reaction at increasing sulphur loadings are shown in Fig. 2.

Analyses of the gas streams in the laboratory tests were made using a Perkin Elmer 154L gas chromatograph with a polypropylene glycol on chromosorb W column. This instrument was also used in the subsequent field tests.

3. FIELD TESTS

Having shown the feasibility of the reduction step in the laboratory, and having defined the optimum range of operating conditions, it was decided that some field tests should be carried out.

Two series of tests were arranged, one at an Ontario Hydro Generating Station, the other at a nickel/copper smelter in Ontario

3.1 Tests at the Generating Station

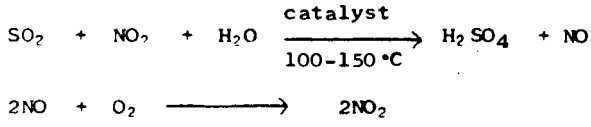
A small reactor containing KA-201 catalyst was set up and gas pulled through it by a pump at a controlled rate from a duct downstream of the electrostatic precipitators used in this station. The composition of this gas stream was:

SO ₂	1400-1500 ppm
NO _x	150-300 ppm
P ₂	3%
H ₂ O	10%
CO ₂	12-13%
N ₂	Balance

H₂S from a gas cylinder was bled into the gas stream upstream of the reactor to give a concentration of 2800-3000 ppm.

The results of these tests were extremely poor. Very low efficiency for SO₂ removal was found and very low sulphur loadings obtained. Several different catalysts were tried, but with no improvement of results.

A tentative explanation for this failure is offered. It is suggested that the NO_x in the gas stream causes poisoning of the catalyst by oxidizing SO₂ to SO₃ on the catalyst surface in the presence of moisture.



It is speculated that the H₂SO₄ on the surface inhibits the reaction between H₂S and SO₂. The extent of the inhibition was so great that further work on the application of the process to generating stations was terminated. The identification of NO_x as the cause of reaction inhibition was made by carrying out tests in the laboratory with and without 100 ppm to NO_x in the gas stream. Results of these laboratory tests were similar to those obtained during the field tests.

3.2 Tests at the Smelter

With the higher sulphur dixoide concentrations (>1.0%) expected in the smelter gases and much lower NO_x concentrations, it was thought that the poisoning process would be less likely to inhibit the H₂S-SO₂ reaction.

The composition of the gas streams tested at the smelter were as follows:-

	<u>From the Converters</u>	<u>From the Roasters</u>
SO ₂	0.2 - 2.2% mainly 0.8-1.1% mean 0.9%	0.9 - 1.4% - 1.2%
NO ₂	< 20 ppm	< 20 ppm
SO ₃	~150 ppm	~150 ppm
O ₂	~17%	17%
H ₂ O	~1%	2%
Nitrogen	Balance	Balance

A 50 gram catalyst bed of Kaiser KA-201 was used to test the effectiveness of SO₂ reduction and sulphur adsorption. The results agreed well with those found in the laboratory with simulated gas mixtures. The catalyst was regenerated using a reducing gas mixture of hydrogen and nitrogen. The catalytic activity was completely restored, and the catalyst was reloaded. This adsorption-regeneration cycle was repeated 10 times with no apparent loss in catalytic activity.

A problem encountered working with the smelter stream was the extreme variability in SO₂ concentration. In order to ensure that H₂S is not released into the atmosphere it will probably be necessary to run the process with a deficiency of H₂S. One set of loading-regeneration runs was carried out using approximately 60% of the theoretical H₂S required. No drop in efficiency was observed. It should, therefore, be quite possible to run the process with 90 or 95% of the theoretical H₂S requirement. Fig. 3 shows the variation of the SO₂ concentration with time in the gas stream from the converters. H₂S injection into the gas stream in the plant would have to be controlled by an SO₂ detector upstream of the catalytic reactor.

4. PRODUCTION OF H₂S

All the laboratory and field tests of the reduction step used pure H₂S from a gas cylinder.

H_2S could be produced in many ways for this process. A number of plausible reactions were examined experimentally in the laboratory.

4.1 Production of H_2S in the Catalyst Regeneration Step

This method of H_2S production does not fit into the general flow sheet shown in Fig. 1. It is shown diagrammatically in Fig. 4. A hot gas stream containing CO , H_2 and steam, such as might be produced from the partial oxidation of natural gas, is passed through the sulphur laden catalyst bed, heating the catalyst to about $400^\circ C$. Part of the sulphur is converted to H_2S and COS . The stream is then passed over a second catalyst bed of Harshaw Fe-0301 sulphided iron on alumina catalyst, at $350^\circ C$. The remaining sulphur, CO , H_2 and steam react together to give hydrogen sulphide and traces of carbonyl sulphide. The quantities of reducing gases used to regenerate the catalyst would be sufficient to reduce only two-thirds of the sulphur on the catalyst. Thus, one-third of the sulphur is stripped from the catalyst unreacted. This is condensed to give a marketable liquid or solid sulphur product.

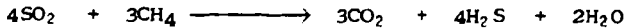
4.2 Production of H_2S by Direct Reaction of Sulphur with Methane



Tests were made using several catalysts. Kaiser KA-201 and Harshaw H-151 activated aluminas gave the best conversion. Fig. 5 shows the relationship between temperature and contact time for complete reaction of methane and sulphur. Also shown is the effect of a 10% excess of sulphur on the required contact time. As can be seen, a substantial reduction in temperature, for complete reaction of methane is achieved by using a greater than stoichiometric quantity of sulphur. It may be more economical to operate the H_2S production unit in this manner, constantly recycling the small excess of sulphur.

4.3 Production of H_2S by Reaction of SO_2 with Methane

H_2S may be synthesized by the direct reduction of SO_2 with methane⁽⁶⁾ i.e.



This reaction requires a suitable catalyst to occur at reasonable temperatures, i.e. about $700^\circ C$.

Our investigations showed that nickel sulphide supported on Harshaw H.151 Alumina was a suitable catalyst for this reaction. Complete reaction of methane was achieved at $720^\circ C$ with a methane to SO_2 ratio of 0.75 and a gas contact time of 0.56 sec.

The Texas Gulf Sulphur Co. have a patent⁽⁷⁾ on the reaction of sulphur dioxide with methane. This examines the reaction with a methane to SO_2 ratio of 0.5.



This reaction was found to be only 60-70% complete at 800°C over an alumina catalyst.

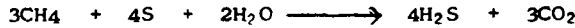
The reason for examining the possibility of producing H₂S directly from SO₂ is because some of the waste streams in the smelter contain 10-15% SO₂ with very little oxygen. If this stream can be directly reduced by methane, savings are realized on two counts.

1) The reaction:



is exothermic ($\Delta H^{700^\circ\text{C}} = -15,500 \text{ B.T.U./16 mole H}_2\text{S produced}$)

while the reaction:



is endothermic ($\Delta H^{700^\circ\text{C}} = +31,000 \text{ B.T.U./16 mole H}_2\text{S produced}$)

Thus, the additional heat produced in the CH₄ - SO₂ reaction may be utilized to raise the temperature of catalyst and gases towards the necessary reaction temperature of 700°C. For the CH₄-S reaction, additional methane would have to be combusted to provide this heat.

While it appears from the equations that the CH₄-S reaction requires one-third as much methane to produce the same amount of H₂S, it must be remembered that two-thirds of the contained sulphur is recycled. Hence the amount of methane per unit of product sulphur is the same for both reactions.

2) Use of the CH₄-SO₂ reaction to produce H₂S decreases the heat requirement per unit of sulphur product, for heating the catalyst and stripping the sulphur in the regeneration step, since all of this sulphur is product sulphur. Also, the amount of catalyst recycled per unit of sulphur product is reduced to one-third, thus decreasing catalyst loss due to attrition and deactivation.

4.4 Production of H₂S by Reaction of Methane with a Mixture of Sulphur and SO₂

In a practical situation part of the required H₂S may be produced by direct reduction of SO₂, but it may be necessary to supplement this by H₂S from sulphur. An experiment was run using a mixture of SO₂ and sulphur (SO₂, 44% of total sulphur) over Kaiser KA-201 catalyst. Fig. 6 shows that higher temperatures were required for this mixed reaction. No explanation of the inhibition phenomena which must exist is offered at this time. The results suggest that it would be preferable to run the two reactions separately.

5. PROCESS FLOW SHEETS AND PRELIMINARY ECONOMICS

The flow sheets shown in Figs. 7 and 8 are based on the concentrations, flow rates, and gas temperatures of streams from an Ontario smelter.

The waste gas flows from this smelter are as follows:

Converters - 1,770,000 a.c.f.m. at 256°F total gas flow
1.12% SO₂
36.4 tons/hour sulphur

Fluid bed roasters - 190,000 a.c.f.m. at 256°F total gas flow
13% SO₂
45.6 tons/hour sulphur

Total annual sulphur production 700,000 tons

Flowsheet "A" considers combining these two streams and treating them both in the reactor. H₂S is then manufactured from two-thirds of the sulphur condensed from the regenerator.

Flowsheet "B" considers using the 12% SO₂ stream from the fluid bed roasters to produce H₂S by direct reduction with natural gas; savings in heat requirement, catalyst circulation, and reactor size are realized.

Detailed capital cost estimation is difficult at this stage, before a comprehensive pilot plant study has been completed.

A brief discussion of each of the major plant items is given below:

i) The Reactor

It is envisaged that a fluidized bed reactor will be used. Because of the huge volumes of gas to be handled, a series of fluid bed reactors will be used in parallel. For the combined stream using a flow velocity of 3 ft/sec., a total reactor area of 12,500 ft² is needed; this would be equivalent to 6 or 7 50' diameter reactors. The minimum bed depth required at this flow rate would be 1.2 feet, based on experimental data for 100% H₂S removal at a 60 grams sulphur per 100 grams catalyst loading. This would involve a pressure drop of 10-12 inches of water across the bed.

Water sprays would be incorporated into the bed for temperature control. The H₂S/SO₂ reaction is exothermic, and if the temperature is allowed to rise too far, oxidization of H₂S by air begins.

Cyclone separators would be used to remove fines entrained in the exit gas.

ii) The Regenerator

Much smaller volumes of gas are involved in the regeneration step. Either fluidized or fixed bed operation could be considered for this operation. It is probable that a fluidized bed will be preferred for temperature control, and a lower pressure drop across the bed.

iii) The H₂S Producer

Again, a fluidized bed comparable in size to the regenerator will be used. A fairly deep bed will be required to achieve the contact time needed for complete reaction. This vessel will require ceramic lining to withstand the high temperatures and corrosive conditions encountered in this step.

5.1 Costs

The capital costs for the 700,000 tons of sulphur per year application discussed above, has been estimated from the data presently available to be of the order of \$25,000,000 - \$30,000,000. Our best estimate of costs per ton of sulphur produced is given in Fig. 9; processes based on both Flow Sheet A and Flow Sheet B are considered. Scheme B shows markedly better economics than scheme A.

Another way of reducing costs would be an upgrading of the gas stream from 1% SO₂ to 4 or 5% SO₂, thus reducing the volume of gas and cutting down the size of reactor required to a quarter or a fifth of what is needed now. This upgrading could probably be achieved by better hooding and control of dilution air.

The costs of \$20 - \$28 per ton of sulphur produced looked most encouraging, when this work was started, since the price of sulphur at that time was \$30 - \$40/ton. The present \$8 - \$10 per ton for sulphur makes the process economics much less attractive, but it compares very favourably with other proposed processes for treating dilute SO₂ streams.

6. MAJOR CONCLUSIONS AND THE STATUS OF THE PROCESS

6.1 Conclusions

Small scale field and laboratory tests have shown that:

- a) SO₂ from an actual smelter gas containing ~1% SO₂ by volume can be reduced to sulphur and adsorbed on a catalyst bed at 100 - 150°F, by adding H₂S to the gas stream.
- b) The sulphur can be removed from the catalyst and condensed to give a liquid or solid sulphur product.

- c) The catalyst can be completely regenerated for reuse in the reduction-adsorption step at 350-450°C.
- d) Hydrogen sulphide for the reduction step, can be produced by the catalytic reaction of methane with sulphur or with a fairly concentrated (>10% by volume) SO₂ stream at 650-800°C.
- e) The information available from the small scale tests is sufficient to begin the design and building of a pilot plant.

7. ACKNOWLEDGEMENT

The authors gratefully acknowledge that the work described above was supported in part by Canadian Industries Ltd.

8. REFERENCES

1. Schrenk, H.H., et al. Public Health Bulletin No. 306, Federal Security Agency, Washington, D. C. (1949).
2. U. S. Public Health Service, "Pollutant Emissions 1966", reported in Stanford Research Institute Air Pollution Control Report No. 353, August (1968).
3. Canadian Patent 846697, July (1970).
4. Canadian Patent 838599, April (1970).
5. Claus, C.F., British Patent 3603 (1882); 5070, 5928, 5929, 5960 (1883).
6. Walker, S.W., I & B.C., 38, 906 (1946).
7. U. S. 3,199,955, Aug. (1965)

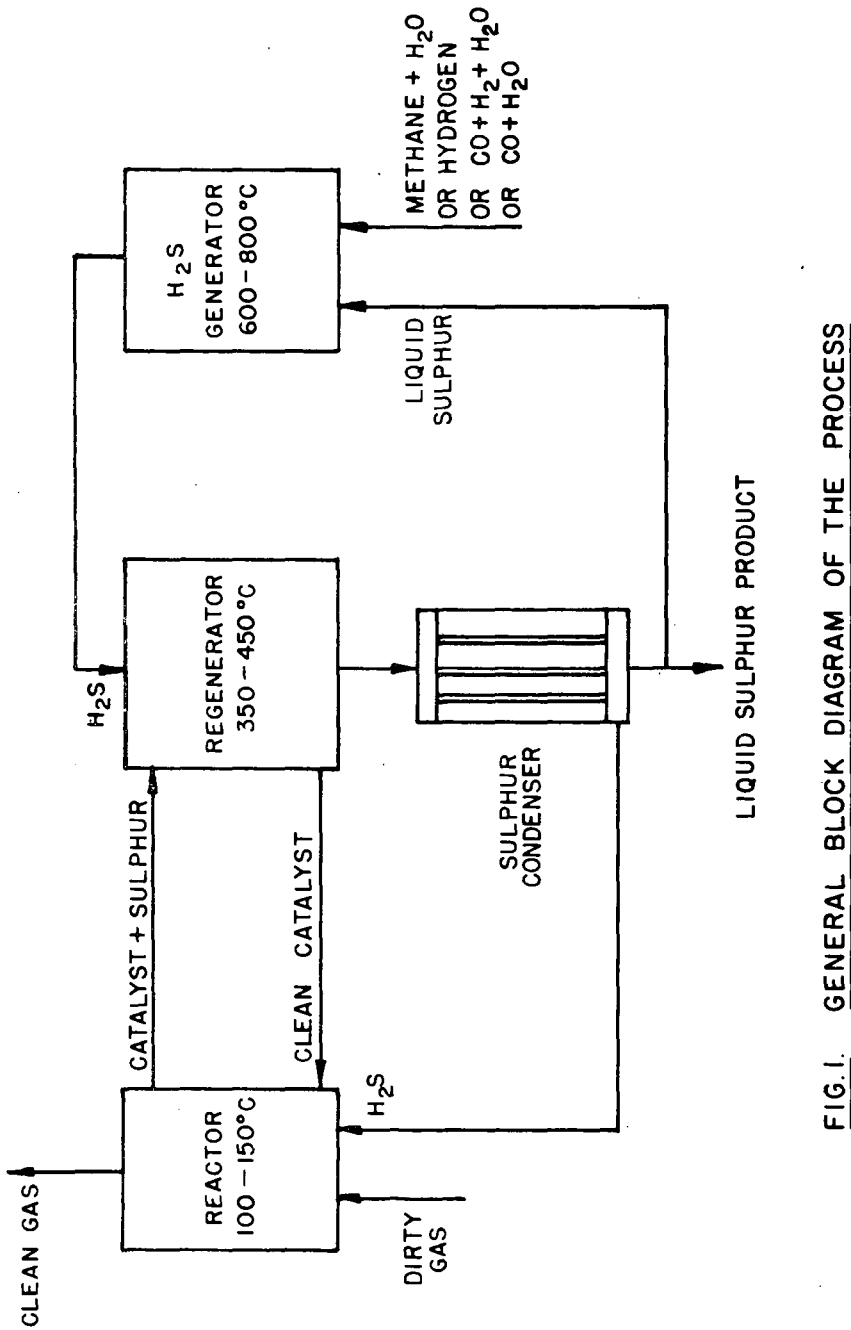


FIG. I. GENERAL BLOCK DIAGRAM OF THE PROCESS

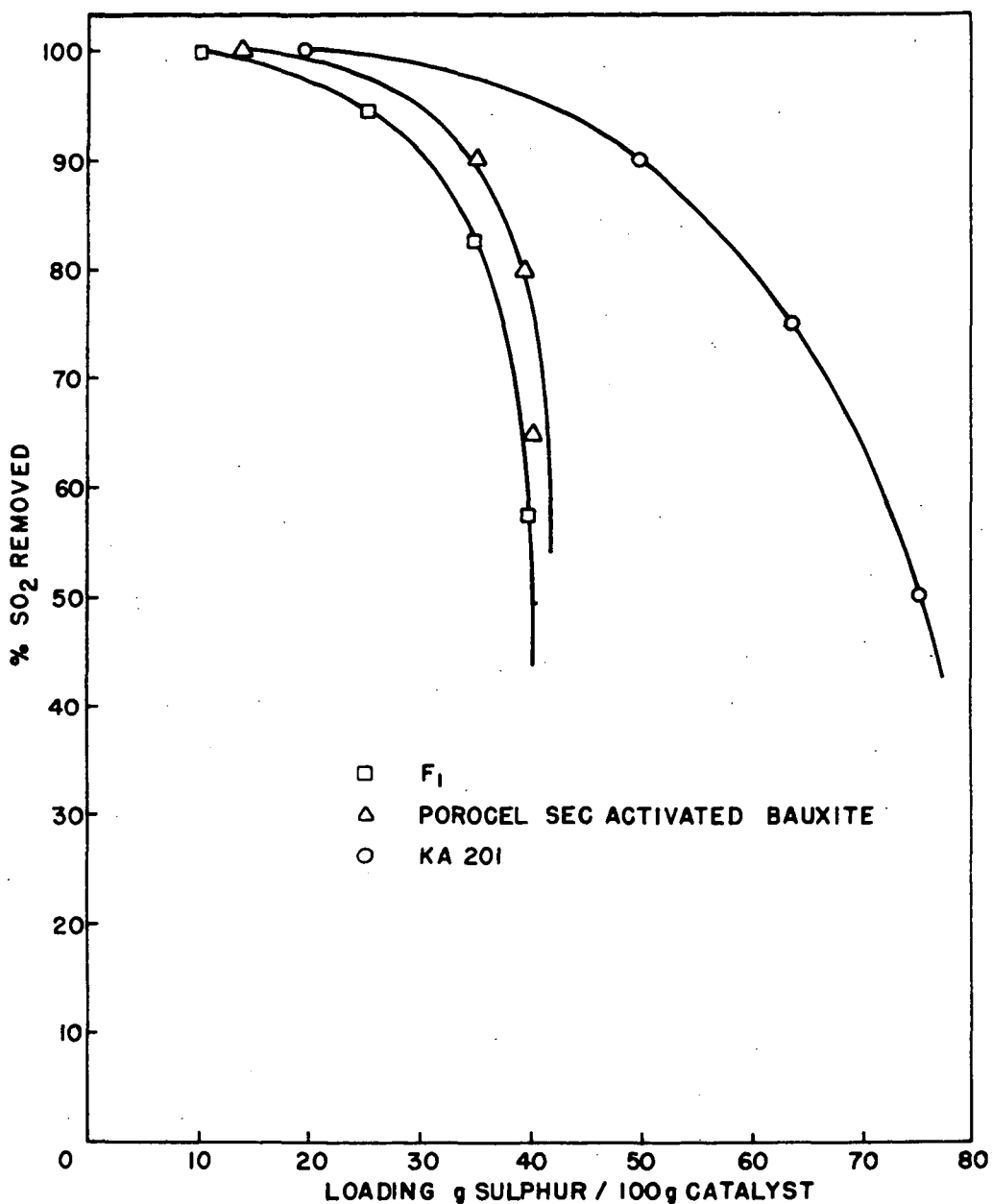


FIG. 2

THE EFFECT OF SULPHUR DEPOSITION ON CATALYTIC
EFFICIENCY
REACTION TEMP. 120°C. GAS CONTACT TIME 0.3 SECS

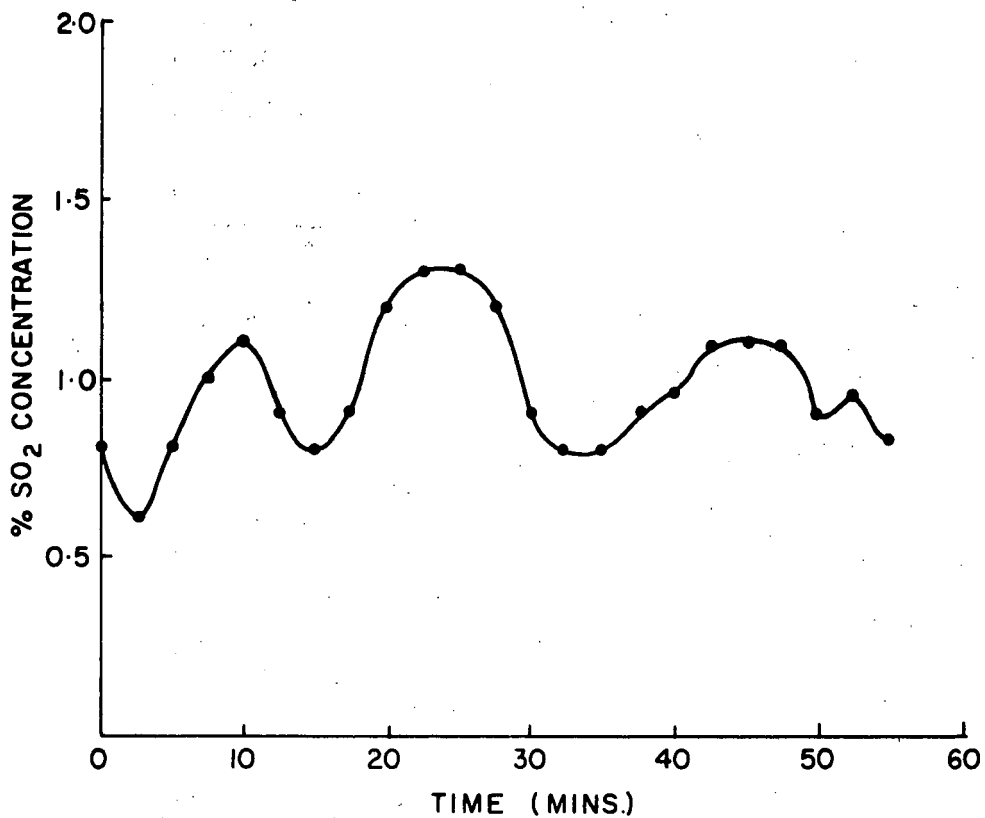


FIG. 3.

TYPICAL VARIATION OF SO₂ CONCENTRATION IN THE WASTE
GASES FROM THE CONVERTERS

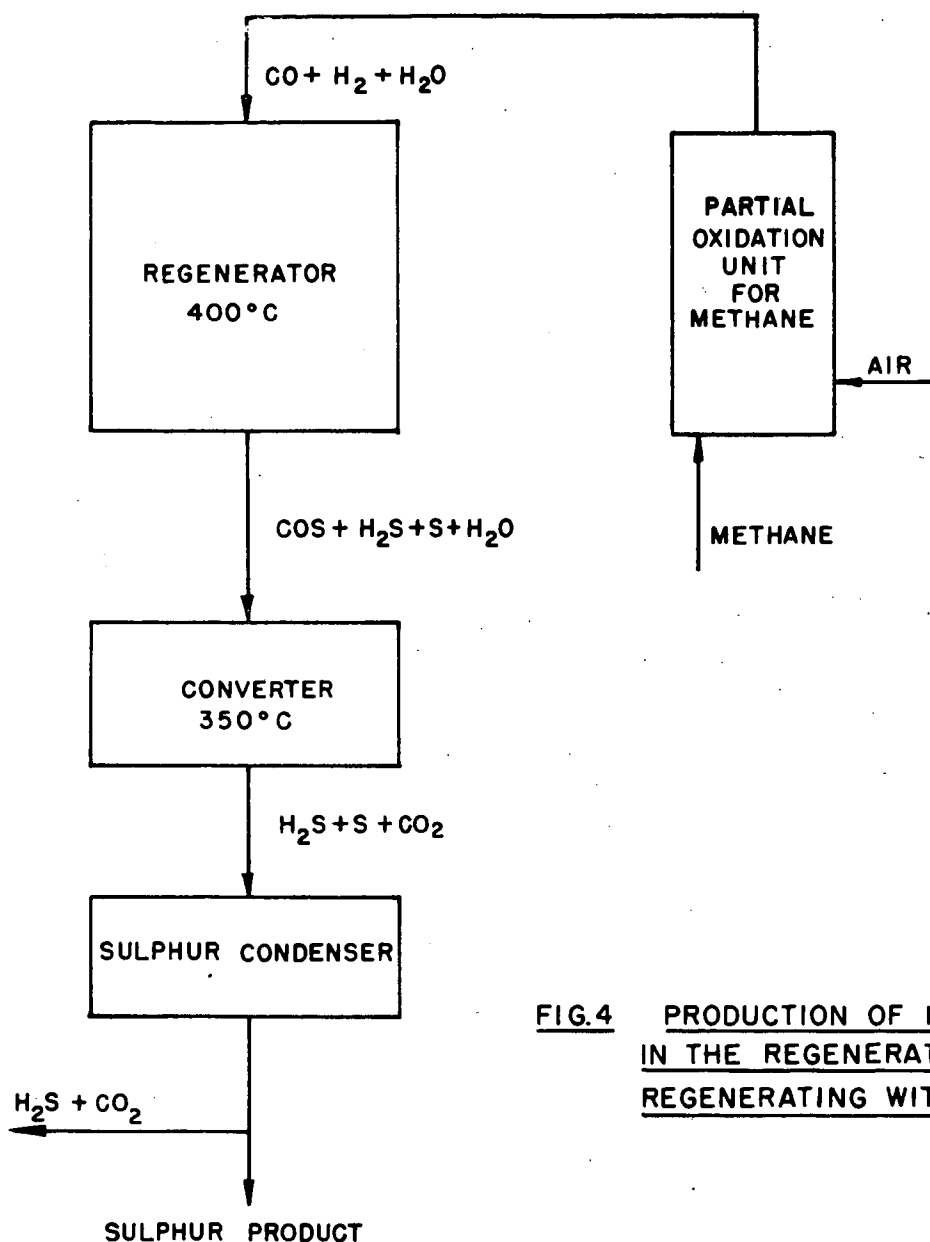


FIG.4 PRODUCTION OF H_2S
IN THE REGENERATOR BY
REGENERATING WITH CO/H_2

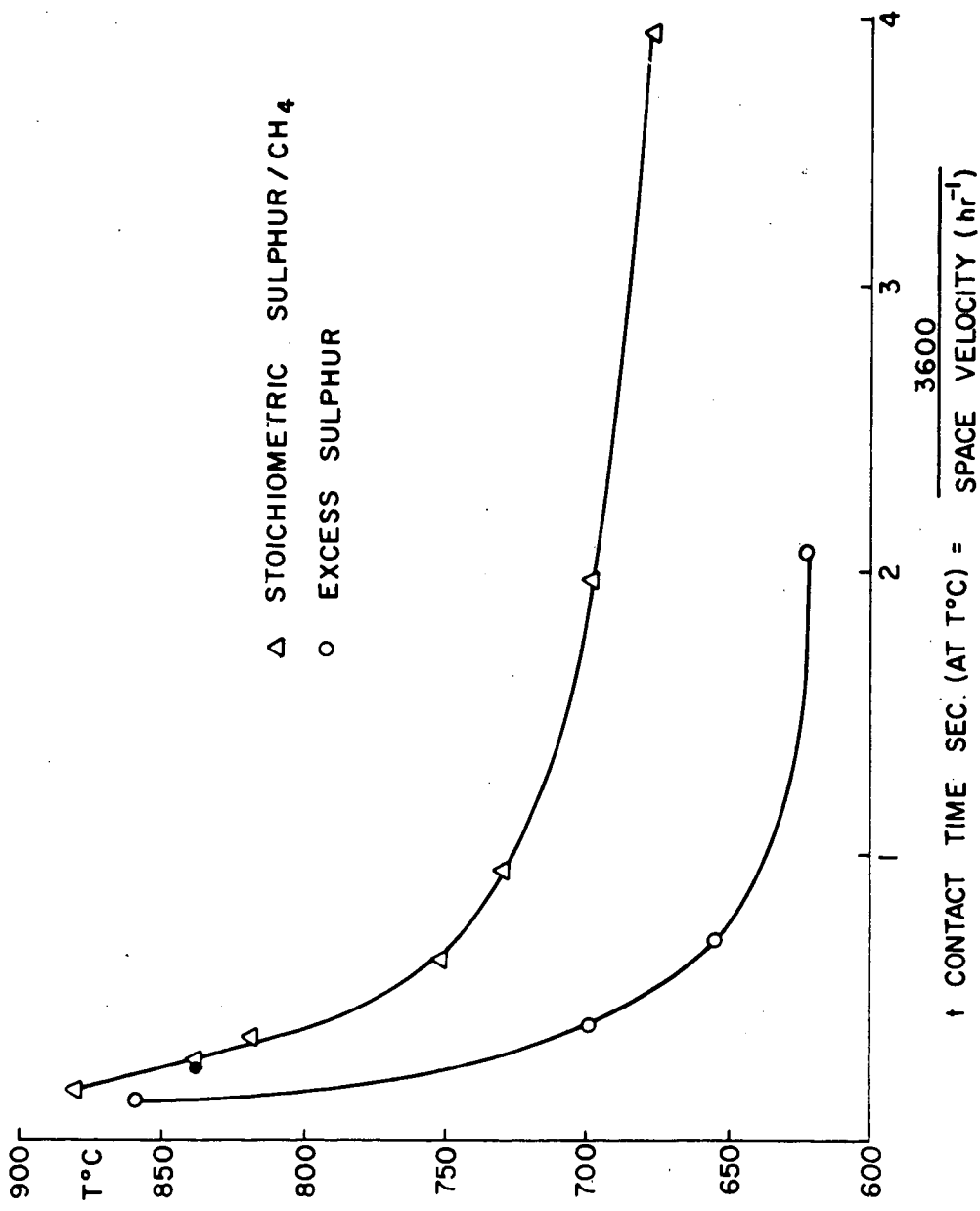


FIG. 5
THE EFFECT OF CONTACT TIME ON THE MINIMUM TEMPERATURE FOR COMPLETE REACTION OVER KA-21 CATALYST (8-16 MESH)

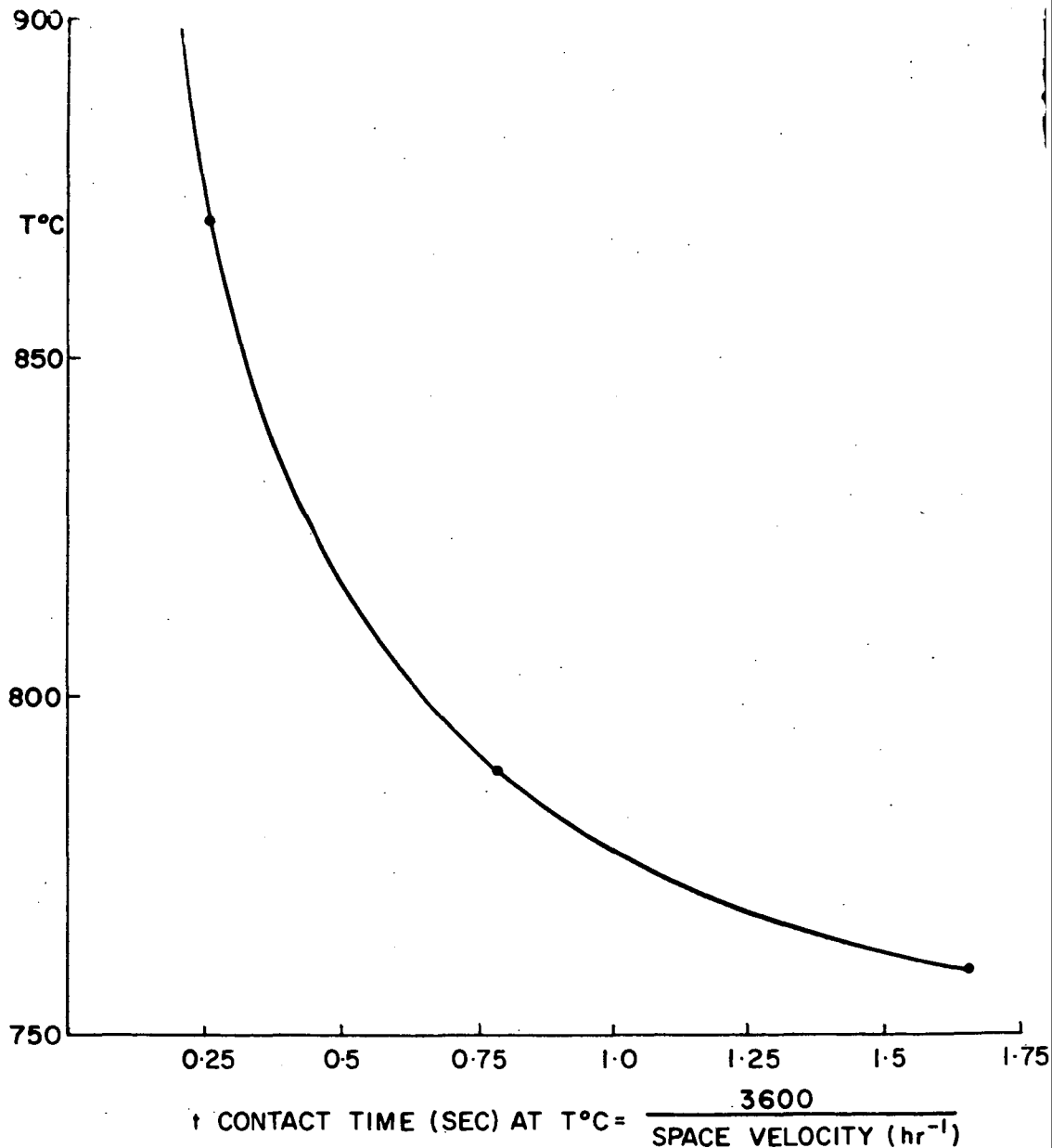


FIG. 6

THE EFFECT OF CONTACT TIME ON THE MINIMUM TEMPERATURE
FOR COMPLETE REACTION (MIXED $\text{S}/\text{SO}_2 + \text{CH}_4$) OVER KA-201
CATALYST (8-16 MESH)

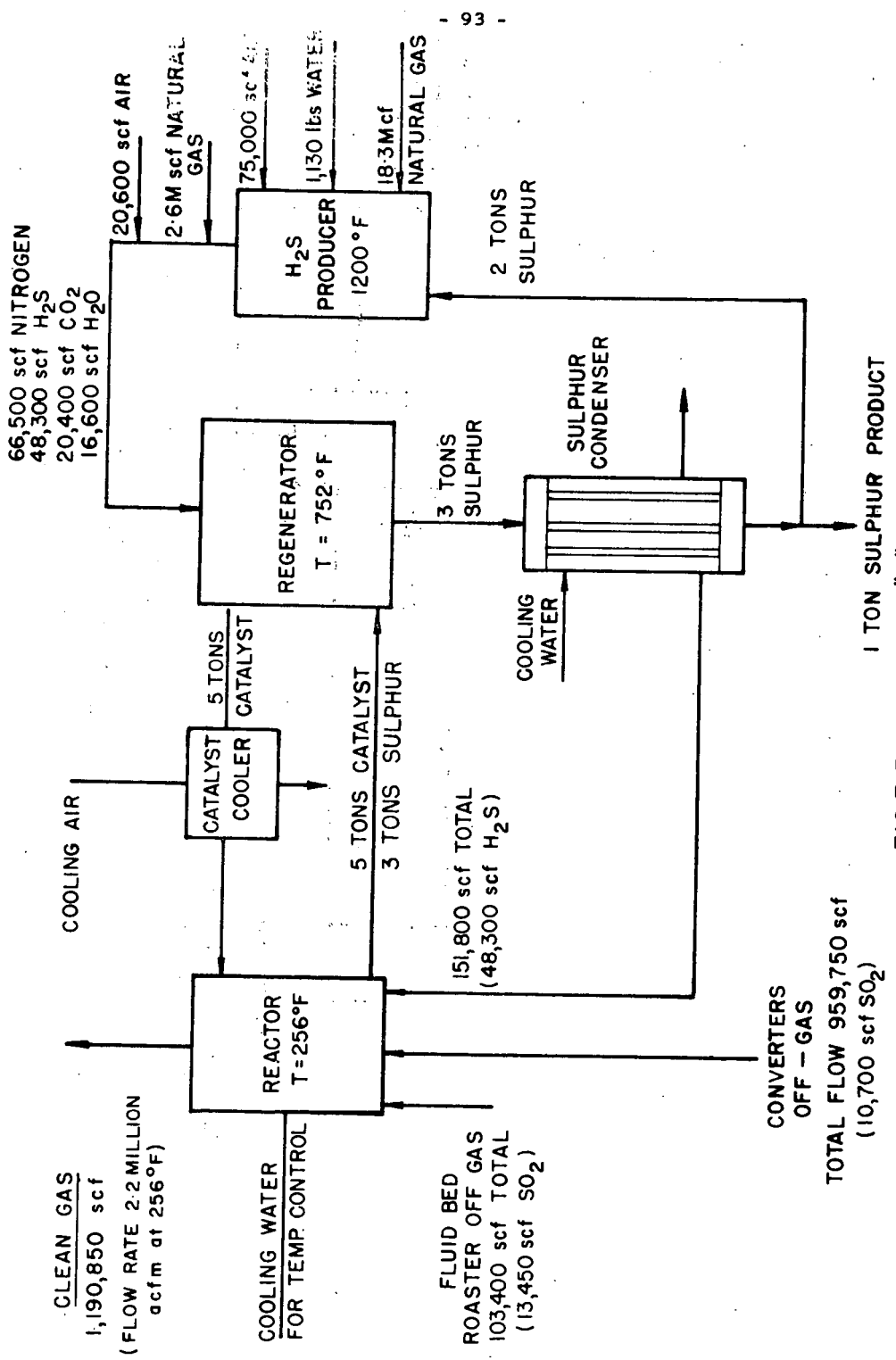


FIG. 7 FLOW SHEET "A"
CONVERTER AND ROASTER STREAMS TREATED IN THE REACTOR
BASIS 1 TON SULPHUR PRODUCT

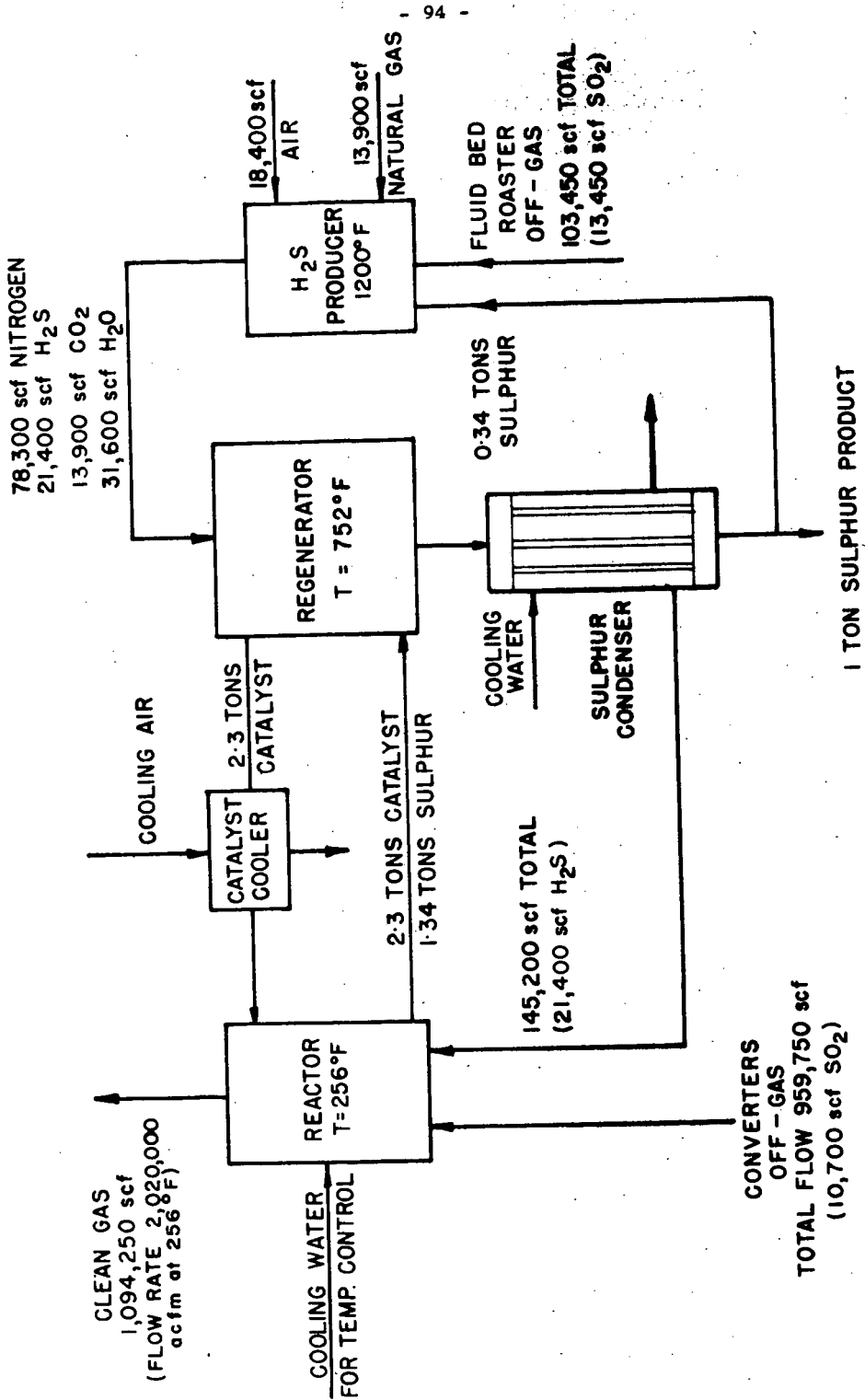


FIG. 8 FLOW SHEET "B"
FLUID BED ROASTER STREAM USED FOR H₂S PRODUCTION
BASIS 1 TON SULPHUR PRODUCT

FIG. 9 ESTIMATED PROCESS COSTS

BASIS COSTS PER TON OF SULPHUR PRODUCED (NO CREDIT FOR SULPHUR SALES.)

PRODUCTION RATE 82 tons SULPHUR /hour .

	<u>SCHEME A</u>	<u>SCHEME B</u>
CAPITAL CHARGES (25 % of investment Depreciation 10 % Interest 8 % Maintenance 4.5 % Taxes + Insurance 2.5 %)	8.90 - 10.70	8.90 - 10.70
NATURAL GAS COST (at 50¢/M.C.F.)	10.20	7.00
CATALYST REPLACEMENT (0.2 % cycle at \$ 300/ton)	3.00	1.40
LABOUR (4 men/shift at \$ 5.00/man - Supervision at \$ 7.00/man - + 50 % overhead)	.50	.50
UTILITIES (Power at 0.8¢/KWhr Cooling water at 5¢/1000 gals.)	3.00	2.50
	<hr/>	<hr/>
	\$ 25.60 - \$ 27.40	\$ 20.30 - \$ 22.10

COMBUSTION OF PULVERIZED CHAR

C.R. McCann, J.J. Demeter, A.A. Orning, and D. Bienstock

U. S. Department of the Interior, Bureau of Mines,
Pittsburgh Energy Research Center, Pittsburgh, Pa.

Introduction

The increasing demand for natural gas stems from its freedom from emissions of particulate matter and sulfur oxides and its adaptability to relatively inexpensive and automatic combustion equipment. Many studies of fuel resources in the U.S. have indicated an impending shortage of natural gas. Fish^{1/} concludes that development of coal gasification is essential for the survival of the gas industry and indicates wellhead prices of natural gas will reach 50¢/MCF within 15 years.

Several coal gasification processes are being developed for production of pipeline gas. These generally yield a char residue that must be recovered for use as a solid fuel. The heating value in the char residue can amount to 50% of the heating value of the coal feed, depending on the process.

The combustion properties of chars are quite variable. A study based on the Coal Research Laboratory Reactivity Indices^{2/} shows a close correlation with the volatile matter content of cokes, reactivity decreasing with decreasing volatile matter content. The reactive properties of chars may differ, for material of the same volatile matter content, from those of cokes to those of active carbons. The reactivity of char residues from gasification will probably be nearer that for coke.

Walker^{3/} reported that chars from a fluidized bed process can be burned in pulverized form in furnaces normally used for anthracite or in conventional bituminous-type units with supplemental fuel. Craig and Smith^{4/} have burned the product of fluidized-bed coking of petroleum fractions in a slagging furnace without supplemental fuel. The furnace used opposed firing inclined downward to give flame impingement on the slag pool and very stable ignition.

Experience is limited, but indicates that char residues from gasification can be burned efficiently provided the furnace is designed for the particular fuel or an auxiliary fuel is used.

Tests such as those for the CRL Reactivity Indices or burning profiles, developed by Wagoner and Duzy^{5/}, can be used to estimate relative ease of combustion, but may not be sufficient to predict combustion efficiency in a particular type of unit not designed primarily for handling low-volatile matter fuels. Also, the tests are not standardized nor are they generally available. This has resulted because data have not appeared that justify standardized reactivity tests in consideration of the close correlation between reactivity indices and the proximate analyses of solid fuels.

The present paper reports on the combustion experience with three chars of different volatile matter contents in a front-wall-fired, dry-bottom furnace capable of burning 500 lb of bituminous coal per hour.

Supplemental fuel was needed for stable combustion of low-volatile-matter chars in this unit. The proportion of supplemental fuel required, other operating variables held constant, is then a measure of the combustion properties of the given char. The percent carbon conversion in gasification should be optimized in relation to utilization of fuel value in the residual char, which in turn depends upon combustion properties of the char.

Experimental Apparatus

Combustion research has long been hampered by the unavailability of suitable equipment which could be used for experimental purposes. Present day industrial furnaces are too large, costly, and unwieldy to be used for experimentation, while results obtained from smaller experimental combustion units are difficult to interpret and extrapolate for use on full-scale furnaces. To overcome these liabilities, a multipurpose combustion unit was designed to simulate the performance of an industrial steam-generating furnace. The combustor, a dry bottom unit, is capable of burning 500 lbs of pulverized fuel per hour with an exit gas temperature of 2000°F. A photograph of the furnace is shown in Fig. 1. A simplified flowsheet of the combustion system including the pulverizing and feeding system is shown in Fig. 2. A cross-sectional view of the principal components, the combustor, convective heat transfer section, a duct designed for emission measurements, and a recuperative air heater is shown in Fig. 3. A detailed description of the furnace has been reported earlier.^{6/}

Operation

The four front-wall burners were designed to fire natural gas and/or pulverized solid fuel. Prior to each test period, the experimental furnace was fired with natural gas to preheat the refractory and to provide a source of preheat for the secondary air. During this period, combustion air flows were established and necessary secondary-air swirl adjustments were made to provide flames that were attached to the burners, but not drawn into the burner tubes. Preheating was then continued until the secondary air temperature reached about 550°F. Natural gas flow to each burner was then reduced by 50%, and pulverized-char feed was started at a rate of about 250 lbs per hour. From this point, oxygen content of the flue gas was used as a guide in the changeover. As the char feed rate was increased, natural gas to each burner was decreased to maintain a constant oxygen level in the flue gas. All of the chars fired in this investigation required supplemental fuel to provide stable flames. Since the burners are capable of burning pulverized solid fuels and natural gas, the latter was used as the supplemental fuel. Thus, the next operation was determination of the minimum amount of natural gas to provide stable flames.

When the desired char feed rate, nominally 400 lbs per hour, was reached, natural gas provided about 25% of the total thermal input to the furnace. Natural gas feed to each burner was then gradually decreased to the minimum amount necessary to produce stable flames, as determined by observation of the burners. Final adjustments were then made on char feed rate and secondary air to provide the desired excess air level for the test period.

Char used in this investigation was produced in an entrained carbonizer using Utah King HVBA as the parent coal. About 50 tons of coal were processed in 3 batches, each batch yielding a different volatile-level char, nominally 5, 12, and 15 percent by weight. During each combustion test, a char sample was taken from the primary air-fuel stream using a small cyclone sampler, the tip of which extended into the center of the recirculation loop. A typical analysis of char of each volatile level and of the parent coal is given in Table I.

TABLE I--Typical analyses of chars and parent coal

	Low volatile char	Medium volatile char	High volatile char	Utah King mine coal
<u>Proximate, wt-pct, as received</u>				
Moisture	0.8	2.8	2.6	4.9
Volatile matter	5.1	12.0	15.1	44.0
Fixed carbon	80.9	73.2	72.0	45.9
Ash	13.2	12.0	10.3	5.2
<u>Ultimate, wt-pct, as received</u>				
Carbon	81.6	75.9	75.5	72.3
Hydrogen	1.0	2.3	3.0	5.8
Nitrogen	1.4	1.7	1.8	1.3
Sulfur	0.5	0.6	0.6	0.5
Oxygen	2.3	7.5	8.8	14.9
Ash	13.2	12.0	10.3	5.2

Discussion of Results

Supplemental fuel requirements varied for each volatile level and, to a lesser degree, for each set of combustion conditions within a volatile level. Minimum fuel requirements, determined as percent of total enthalpy input are shown graphically in Fig. 4. The plot shows that minimum supplemental fuel depends somewhat upon the amount of preheat in combustion air. Extrapolation of the curves indicates that volatile matter content in excess of 20% is required for combustion of this char without supplemental fuel addition.

Combustion tests were performed according to a factorially designed program using three independent variables, each at two levels, as follows:

Variables* Levels

Excess air	5 and 20%
Secondary air preheat	600° and 700°F
Degree of pulverization	80 and 95% thru 200 mesh

*Supplemental fuel, as percent of total heat input, was also a variable, but as indicated above, it was not an independent variable.

When minimum auxiliary fuel requirements were met, chars of each volatile level burned with very stable flames. Table II is a summary of the experimental data from the combustion tests. Carbon combustion efficiencies greater than 99% were obtained with char containing 15% volatile matter. Even with the more undesirable combustion variables--low air preheat, low excess air, and large fuel particle size, the low volatile char yielded about 94% carbon combustion efficiency.

Figure 5 shows the effect of volatile matter content on carbon combustion efficiency, with excess air and fuel particle size as combustion parameters. While the experiments were factorially designed for each volatile level of char individually, the data were subjected to regression analysis, since this type of analysis permitted addition or transformation of variables, and analyses of all of the data as a single block. The analyses yielded an equation as follows:

TABLE II. - Summary of experimental data

Observation No.	Excess air, pct	Degree of pulverization; pct, thru 200 mesh	Air preheat temp., °F	Volatile matter content percent, as fired	Carbon combustion efficiency, pct	Percent of total heat input in natural gas
31	19.6	95.2	700	5.2	97.5	15.4
32	5.4	95.2	695	5.2	95.5	15.0
33	10.6	94.9	600	4.7	97.2	14.6
34	5.4	94.9	600	4.7	95.2	15.2
35	19.0	80.1	605	5.0	95.3	15.2
36	4.9	80.1	600	5.0	93.8	14.8
37	19.6	80.3	690	5.6	95.7	15.2
38	4.9	80.3	695	5.6	94.0	14.7
91	19.6	95.1	700	12.5	98.7	12.0
92	4.9	95.1	695	12.5	97.5	11.9
93	20.2	95.0	605	11.9	98.3	13.0
94	5.0	95.0	600	11.9	97.2	13.2
95	20.3	79.8	600	12.1	97.3	13.9
96	4.9	79.8	600	12.1	95.7	13.8
97	20.3	80.2	690	11.5	97.5	11.8
98	4.9	80.2	690	11.5	96.0	12.3
151	19.6	95.0	700	15.3	99.8	8.9
152	5.4	95.0	700	15.3	99.5	9.6
153	18.2	94.9	600	16.0	99.5	10.9
154	4.9	94.9	600	16.0	99.2	10.4
155	18.9	79.9	600	14.9	99.1	10.8
156	4.9	79.9	600	14.9	98.1	11.0
157	19.6	80.0	705	14.9	99.4	9.2
158	4.9	80.0	695	14.9	98.5	9.5

$$\text{Carbon combustion efficiency} = 85.5 + .077A + .067B + .00347C + 1.3 \times 10^{-6} D^2 + .0007E$$

where A = excess air, percent

B = degree of pulverization, percent thru 200 mesh

C = heating value of volatile in char, Btu/lb char as fired

D = (C - 1400)

E = thermal input in preheated air, Btu/lb char.

Heating value of volatile in the char, C, was calculated by difference in the heating value of the char and the heating value of the fixed carbon in the char, assuming 14,500 Btu/lb of fixed carbon.

Of interest in the equation is the absence of a term showing the effect of the natural gas used to provide flame stabilization. As the volatile matter content of the char was decreased, it was necessary to increase the percent of total heat input supplied by natural gas in order to maintain a stable flame. The percent of heat input supplied by natural gas was not an independent variable. Accordingly, the effect of natural gas is included in the effect of the heating value in the volatile of the char.

Analyses of the data indicate that excess air, degree of pulverization, heating value of the volatile in the char, and the quadratic effect of the heating value of the volatile in the char are about equally important, while air-preheat temperature is of marginal significance. Over 95% of the variation in carbon combustion efficiency is explained by the equation.

Conclusions

The combustor used in this investigation simulated the operation of a dry-bottom, horizontally-fired, pulverized-coal furnace. When fired in this unit, chars with about 5% volatile matter yielded 94-97.5% carbon combustion efficiency, while 12% volatile char yielded 95.7-98.7%, and 15% volatile char yielded 98.1-99.8% carbon combustion efficiency. The ranges of carbon combustion efficiency were the effect of the combustion parameters--excess air, fuel particle size, and secondary air preheat. As expected, higher excess air and higher preheat with fine particle size yielded higher efficiencies. All of the chars fired required supplemental fuel to provide flame stabilization. The amount required, based on percent of total enthalpy input, was about 10, 13, and 15% natural gas for chars containing 15, 12, and 5% volatile matter, respectively. It appears that a volatile matter content in excess of 20% is necessary for combustion of these chars without supplemental fuel.

References

- 1/ Fish, L.W., Am. Gas Assoc. Monthly 53, 8-9 (March 1971).
- 2/ Orning, A.A., Ind. Eng. Chem. 36, 813-16 (1944).
- 3/ Walker, J.B., Jr., Steam from By-Product Fuels, Paper presented at A.S.M.E. Annual Meeting, New York, N.Y., Dec. 1-6, 1957, (57-A-126).
- 4/ Craig, O., and Smith, E.H., Mech. Engr. 78, 921-25 (1956).
- 5/ Wagoner, C.L., and Duzy, A.F., Burning Profiles for Solid Fuels, Paper presented at A.S.M.E. Winter Annual Meeting and Energy Systems Exposition, Pittsburgh, Pa. Nov. 12-17, 1967, (67-WA/FU-4).
- 6/ McCann, C.R., Demeter, J.J., Orning, A.A., and Bienstock, D., NO_x Emissions at Low Excess-Air Levels in Pulverized-Coal Combustion, Presented at the A.S.M.E. Winter Annual Meeting, New York, N.Y., Nov. 29-Dec. 3, 1970, (70-WA/APC-3)..

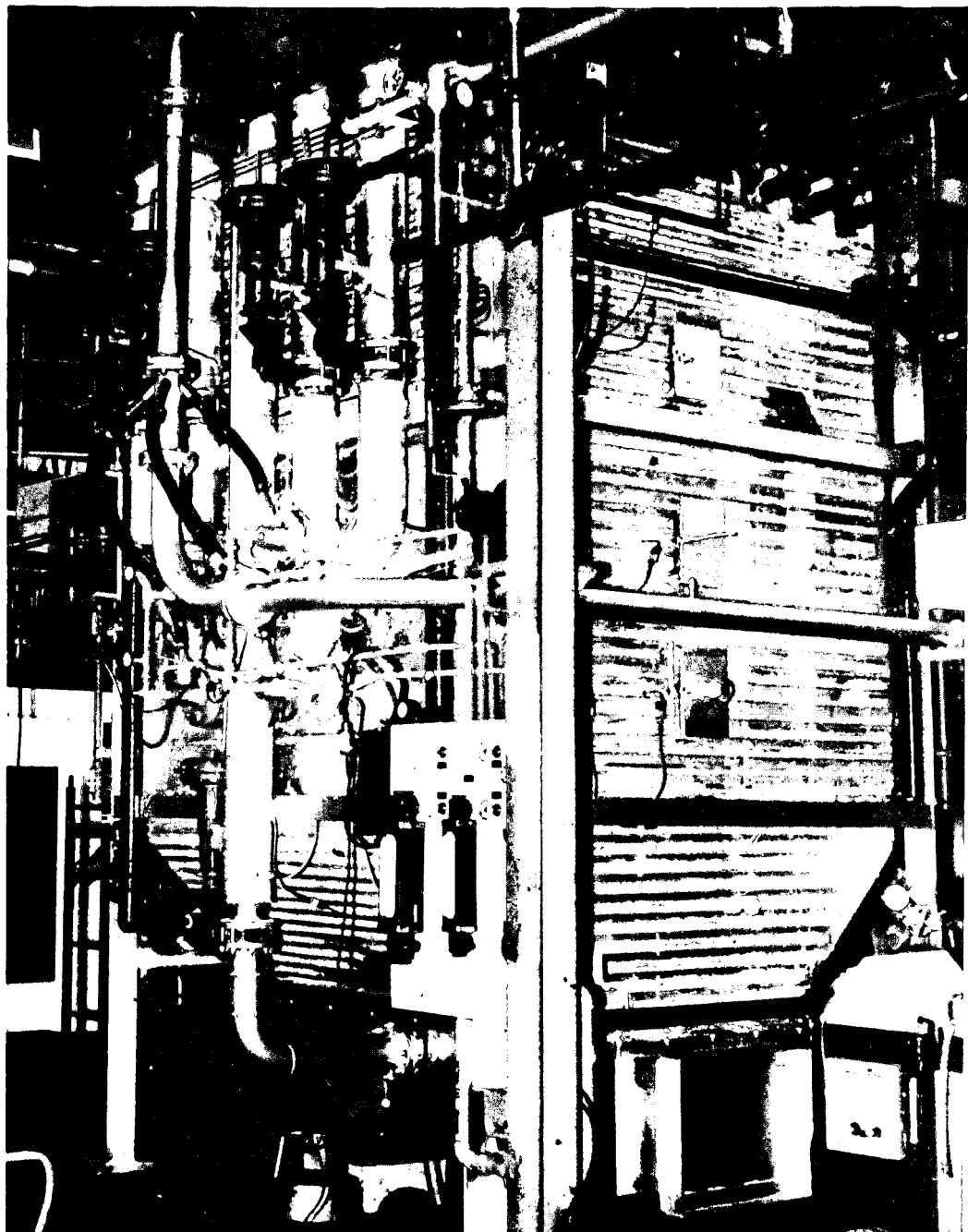


Figure 1.- Pulverized-Coal-Fired Combustor.

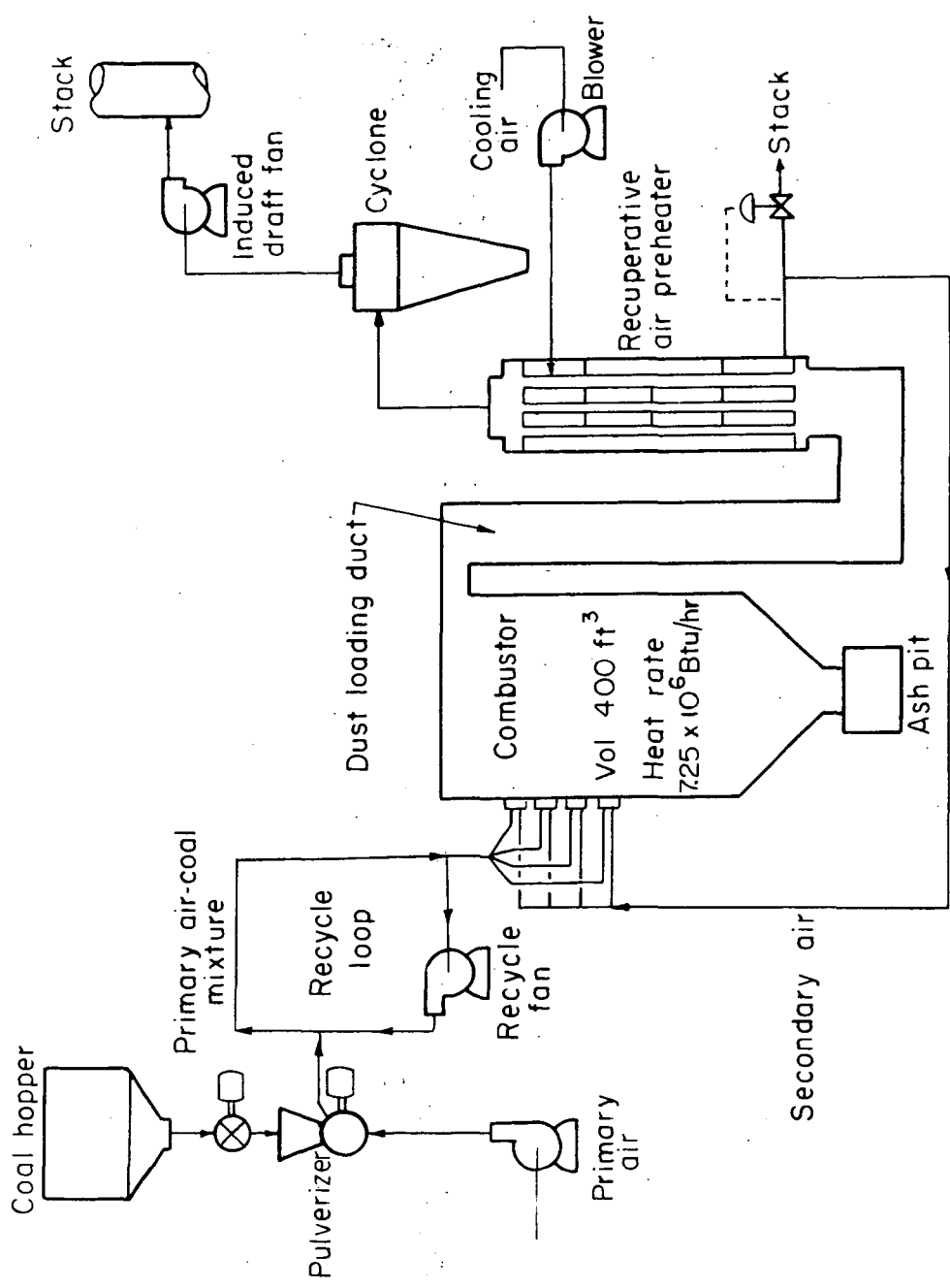


Figure 2—Simplified flowsheet of 500 lb/hr pulverized-fuel-fired furnace.
L-11323

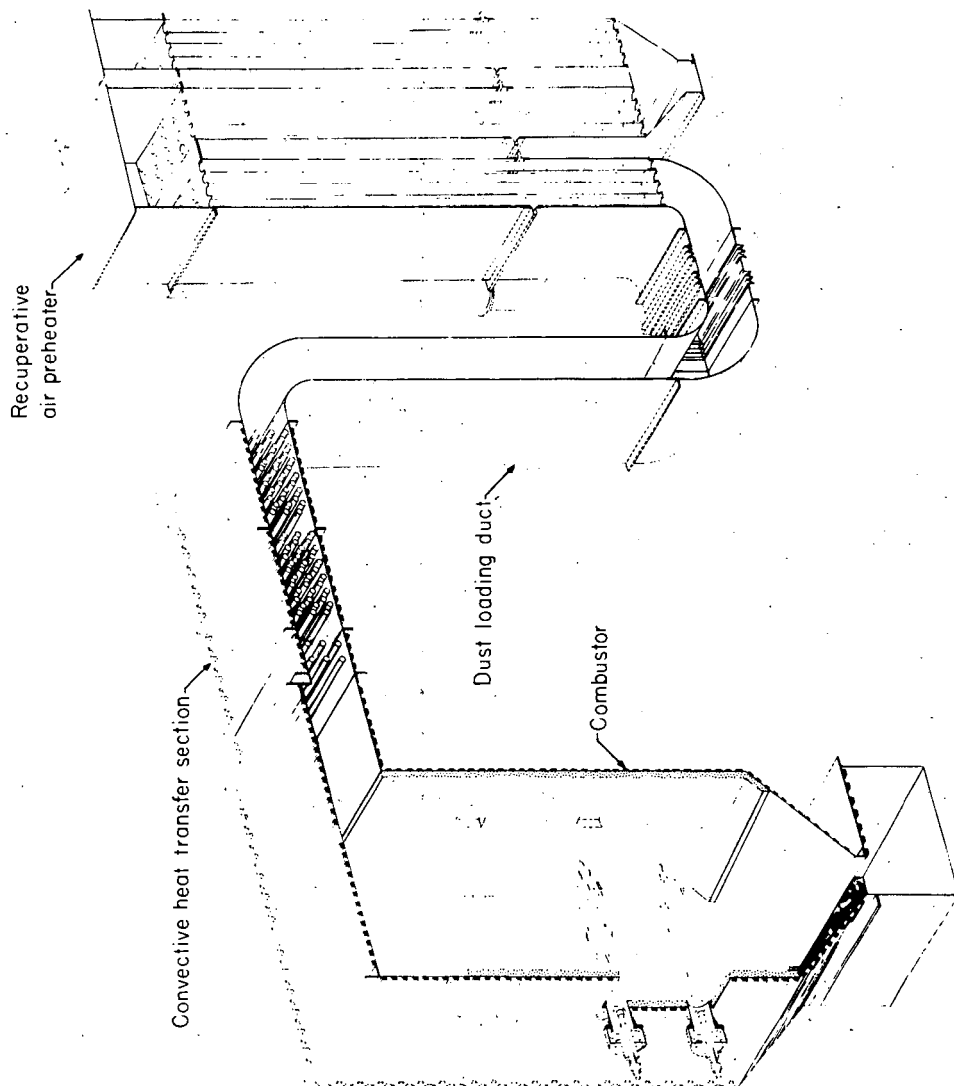


Figure 3.- Cross-sectional view of 500 lb/hr pulverized-fuel coal combustor.

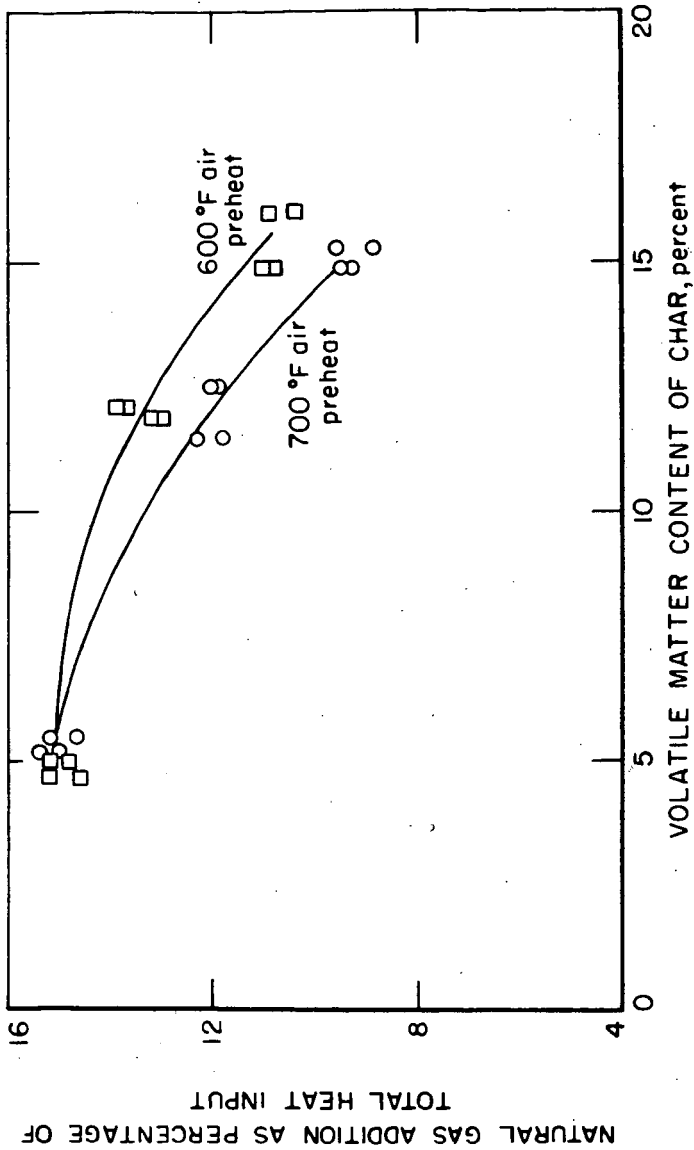


Figure 4—Supplemental fuel requirement as a function of volatile matter content.

L-12249

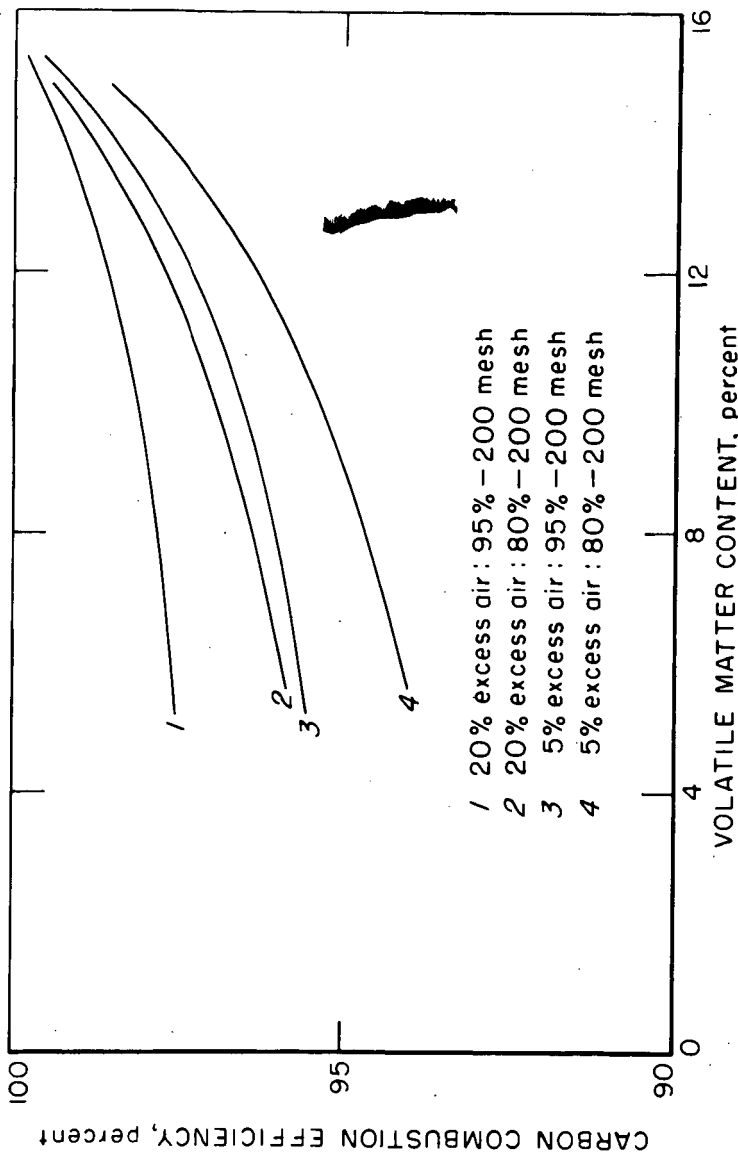


Figure 5—Carbon combustion efficiency as a function of excess air with 700° F preheat.

Sufficient natural gas added to stabilize combustion (See figure 4)

L-12248

DETECTION OF METHANE COMBUSTION WITH APPLICATIONS TO
QUENCHING COAL MINE EXPLOSIONS

By J. E. Nealy* and W. L. Grose**

NASA Langley Research Center, Hampton, Virginia

ABSTRACT

A device developed by the U.S. Bureau of Mines for the detection and quenching of coal mine explosions suffers from the inability to discriminate between the light emitted from hydrocarbon combustion and that emitted by electrical sparks and miner's cap lamps. Since the quenchant device is activated by an internal explosive charge, the possibility of serious injury to nearby personnel demands a detector which can reject false signals. Described herein is a device which can provide a rapid response signal upon the emission of radiation from hydrocarbon combustion and concurrently reject spurious signals from such sources as sparks and cap lamps.

NOMENCLATURE

B_λ	Planck blackbody function - watts/cm ² - μ
I	intensity - watts/cm ²
$j_{\Delta\lambda}$	spectral emission coefficient for bandpass $\Delta\lambda$ - watts/particle
n_{OH}	number density of OH particles - particles/cm ³
V	volume - cm ³
μ_λ	absorption coefficient - cm ⁻¹ particle ⁻¹
ω	solid angle - steradians

*Aerospace Engineer, Hypervelocity Impulse Facilities Section, Hypersonic Vehicles Division.

**Aerospace Engineer, Flow Field Kinetics Section, Hypersonic Vehicles Division.

INTRODUCTION

The accumulation of methane gas in a coal mine constitutes an ever present explosion hazard. The methane is a by-product of the decomposition process which forms the coal. If the concentration of methane in air reaches the critical range of approximately 5-12 percent an explosion can occur. Methane levels are customarily controlled by forced ventilation, but this is not completely successful in preventing localized concentrations in the critical range.

An explosion takes a finite time period (on the order of milliseconds) to develop after ignition of the methane. The U.S. Bureau of Mines has developed a device for detecting and quenching the developing explosion by discharging potassium bicarbonate in its path (refs. 1 and 2). However, the device is unable to discriminate between light emitted from methane combustion and that emitted by electrical sparks or miner's cap lamps. Since the quenchant device is dispersed by an internal explosive charge, the possibility of serious injury to nearby personnel demands a detector which can reject false signals. It was suggested by R. L. Trimpi, Assistant Chief, Hypersonic Vehicles Division, Langley Research Center, that this difficulty might be surmounted by developing a detector which would operate on the principle of monitoring the radiation intensity emitted from two separate spectral regions and ratioing the intensities. Such a detector would provide a rapid response signal after sensing the emission of radiation from the hydrocarbon combustion and concurrently reject spurious signals from sparks and cap lamps due to the differences in the spectral characteristics of the emissions.

A series of experiments are described for methane-air combustion which illustrate the validity of such an approach. Estimates of the spectral irradiance of the combustion event are presented, thereby determining the required sensitivity of the device.

EXPERIMENTAL APPARATUS

A cylindrical (3.8" diameter x 12") stainless steel shock tube test section was used as a combustion chamber. The test section was equipped with quartz windows (2" diameter) on either side, a piezoelectric pressure transducer, and two steel electrodes. A 10 kilovolt capacitor discharged across the electrodes provided a sub-microsecond duration spark to ignite the gas mixture within.

The desired partial pressures of methane and air were obtained by using a Wallace and Tiernan 0-800 mm Hg pressure gauge with which pressures could be determined to an accuracy of 1/2 mm Hg. All tests were conducted with a total pressure of 1 atmosphere in the chamber. The time history of the wall pressure was measured during combustion with a Kistler Model 701 Quartz Pressure Transducer and Charge Amplifier.

The radiation emitted during combustion was observed with Jarrell Ashe 1/4 meter monochromators placed symmetrically on either side of the test section. The monochromator dispersion was 33 Å/mm and both entrance and exit slits were 500 μ in width. Radiation emerging from the exit slits was detected with RCA 1P28 photomultiplier tubes. A Philbrick Model Q3M1P operational amplifier was used to ratio the output voltage from the two spectral channels. All signal voltages were recorded on Tektronix Models 551 and 556 oscilloscopes.

A schematic diagram of the experimental apparatus is shown in figure 1.

RESULTS

A survey of the flame spectrum of methane showed that a particularly strong emission occurred from the OH O-O band head at 3064 Å, and that a region of relatively low emission existed nearby at 3000 Å. Several ignitions were performed with the monochromators set on these channels to check consistency, and in all cases were found to repeat well, with an approximate intensity ratio of 6:1, and a peak wall pressure of 75 psia. An oscilloscope trace made during one of these tests in a stoichiometric mixture of methane and air is shown in figure 2.

Next, a series of ignitions was carried out in which the initial partial pressure of methane was varied through the combustion range of 5-12 percent. In these tests, it was found that the 6:1 intensity ratio was approximately maintained, even though the relative intensities varied considerably with initial CH_4 concentration. A plot of relative peak intensity for both channels as a function of initial partial pressure of methane is shown in figure 3, along with the peak wall pressure variation.

Figures 4 and 5 illustrate the electronic ratio of the signals of the two spectral channels. The records of figure 4 were made with the monochromators at the normal test configuration 6 inches from the test section centerline, while those of figure 5 correspond to a position 18 inches from the centerline. It is seen that even though the relative intensities have been greatly reduced, use of the operational amplifier to divide the incoming phototube signals minimizes the variation of output signal as a function of source detector distance.

For light sources emitting radiation in both channels, such as the incandescent lamp continuum or the many-line spectrum of iron, the signal ratio should be significantly reduced. Figure 6 shows the individual channel outputs for a 200 watt tungsten lamp and the corresponding ratioed signal from the operational amplifier. Similar results are obtained for an iron arc source, as shown in figure 7.

The components used in the "bread-board" experiment immediately suggest the use of more compact and less expensive spectral ratioing devices as a hydrocarbon combustion detector. For example, narrow band interference filters placed in front of solid-state photodetectors equipped with an electronic divider circuit could be operated from a central power supply or optionally from a self-contained battery pack. Electronic dividers are commercially available in wafer size integrated circuits, as are 25 Å bandpass filters in this wavelength region.

In order to assess the sensitivity requirements of such a prototype, the intensity, I , received at the detector may be approximated by the following:

$$I \approx \frac{n_{OH} \omega V}{4\pi} \int_{\Delta\lambda} \mu_\lambda B_\lambda d\lambda \equiv \frac{n_{OH} \omega V}{4\pi} j_{\Delta\lambda}$$

where $j_{\Delta\lambda}$ is the integral over the specified bandpass (.3064 - .3089 μ) of the emission coefficient of an OH particle and is a function of temperature only. This function has been calculated from the absorption coefficient tabulations of reference 3 and is presented in figure 8.

This information, along with the number density of OH particles in burning volume V at temperature T , and the solid angle, ω , subtended

by the detector, may be used to approximately determine the sensitivity requirement of a photodetector. Reference 4 gives typical mole fractions of OH as .02 at flame temperature 1960° K for a methane-air mixture at 1 atm. pressure. Choosing a representative volume of 28400 cm³ (1 ft³) and solid angle of 10⁻⁵,

$$I \approx \frac{1}{4\pi} [7.5(10)^{16} \cdot 10^{-5} \cdot 2.84(10)^4 \cdot 10^{-23}] \approx 10^{-8}$$

The RCA 1P28 photomultipliers used have a photosensitivity rating of about 50 ma/watt at .3μ and a current gain of 2 (10)⁵. This results in a cathode current of .1 ma, which through a 10 K output resistor supplies 1 volt signal to the divider, which is more than adequate.

CONCLUSIONS

It has been demonstrated that methane combustion produces much greater emission near .3064 μ than at .3000 μ, whereas electric sparks and incandescent lamps possess nearly constant emission levels in these spectral regions. Therefore, a detection scheme based on the ratio of the emission at these wavelengths can discriminate between methane combustion and the interjection of an incandescent lamp or an electric spark in the optical field of view. Estimates of the spectral irradiance of methane combustion have been made and indicate adequate detector sensitivity for representative conditions.

Although these experiments were conducted for CH₄ combustion, the detection apparatus should respond similarly for other hydrocarbon combustion processes due to formation of the OH radical.

REFERENCES

1. Mitchell, D. W.; Nagy, J.; Murphy, E. M.: Preventing Explosions from Gas Ignition at the Face. Bureau of Mines Report, Sept. 1967.
2. Kamenski, E. M.; Nagy, J.; Conn, J. W.: Further Development of an Explosion Quenching Device. International Conference of Safety in Mines Research, Tokyo, Japan, Nov. 1969.
3. Golden, S. A.: Spectral Absorption Coefficients of Electronic Transitions in Diatomic Molecules. Vol. 2, Part C, ARPA Report.
4. Gaydon, A. G.; and Woldhard, H. G.: Flames - Their Structure, Radiation and Temperature. Chapman and Hall, Ltd., 1960.

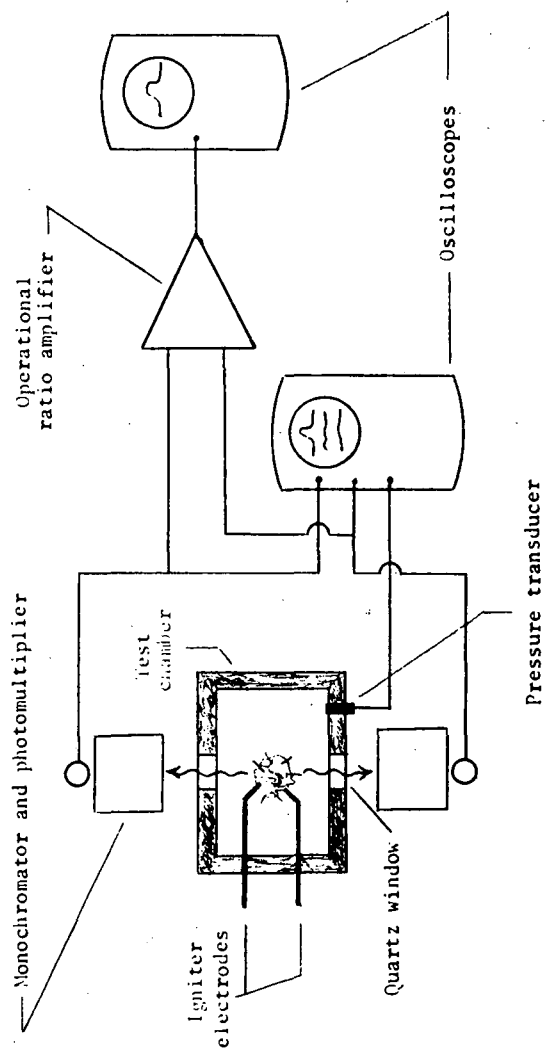


Fig. 1. Schematic diagram of experimental apparatus.

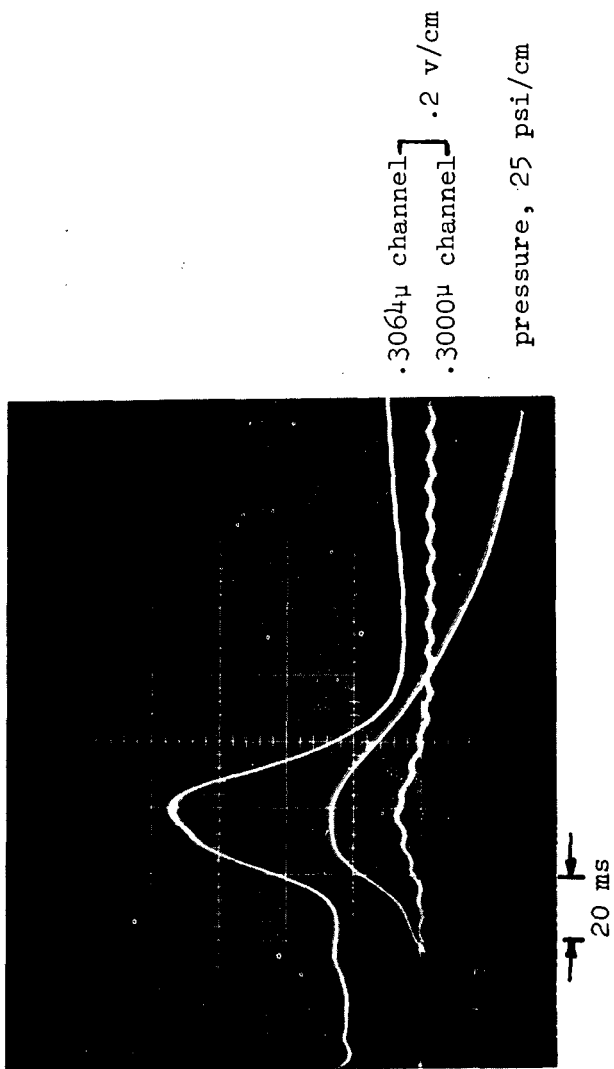


Fig. 2. Photomultiplier outputs and pressure transducer signal for typical combustion.

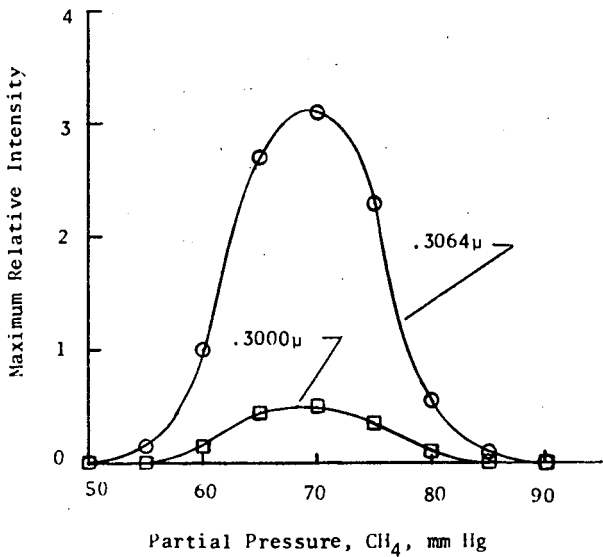
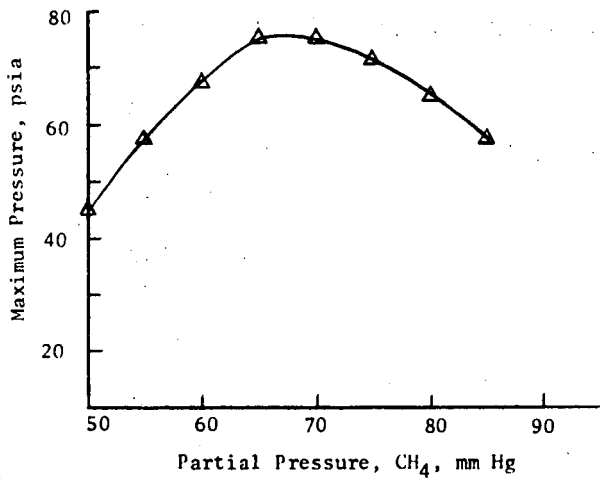


Fig. 3. Plots of peak spectral intensities and maximum pressures as functions of initial partial pressure of CH_4 in air.

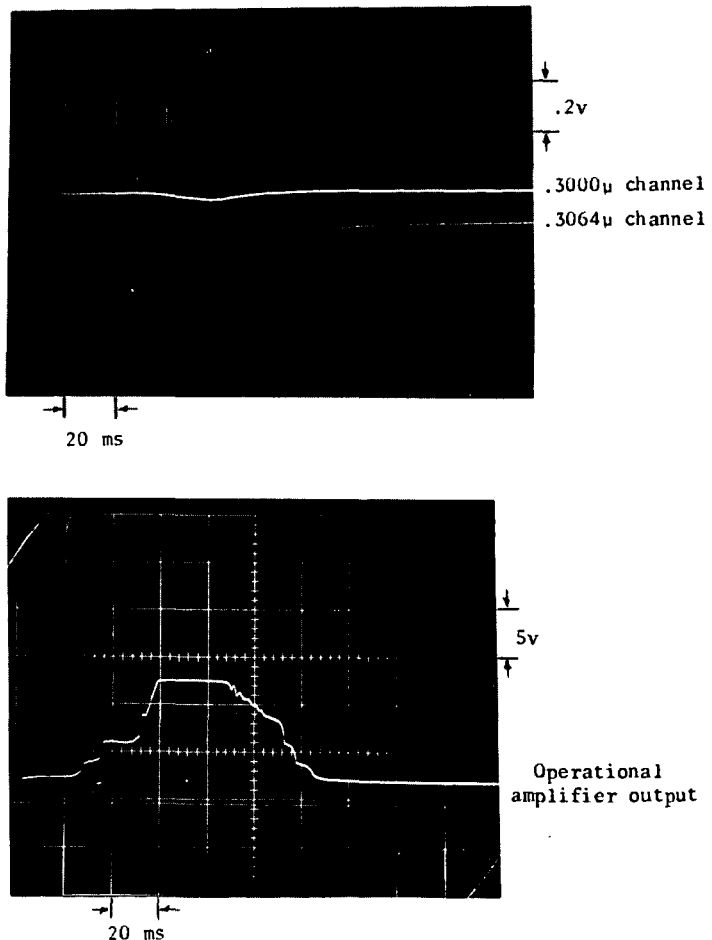


Fig. 4. Record of spectral intensities and output of electronic ratio amplifier during typical combustion test.

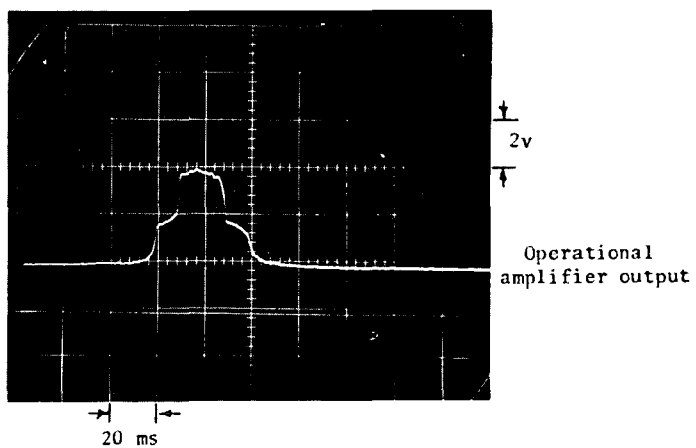
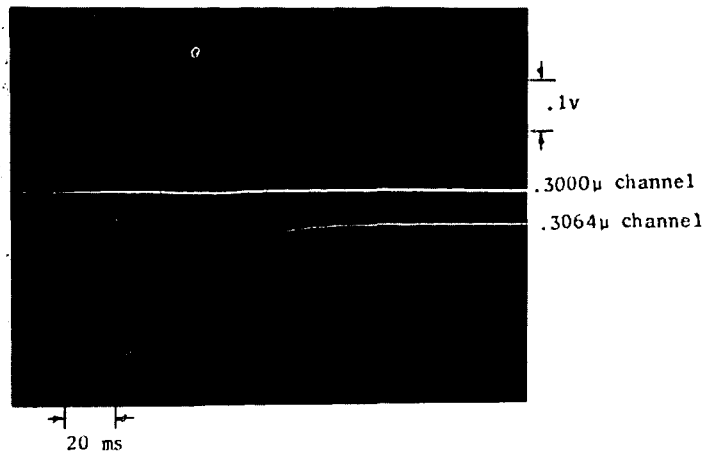


Fig. 5. Record of spectral intensities and output of ratio amplifier with reduced intensity on spectral channels.

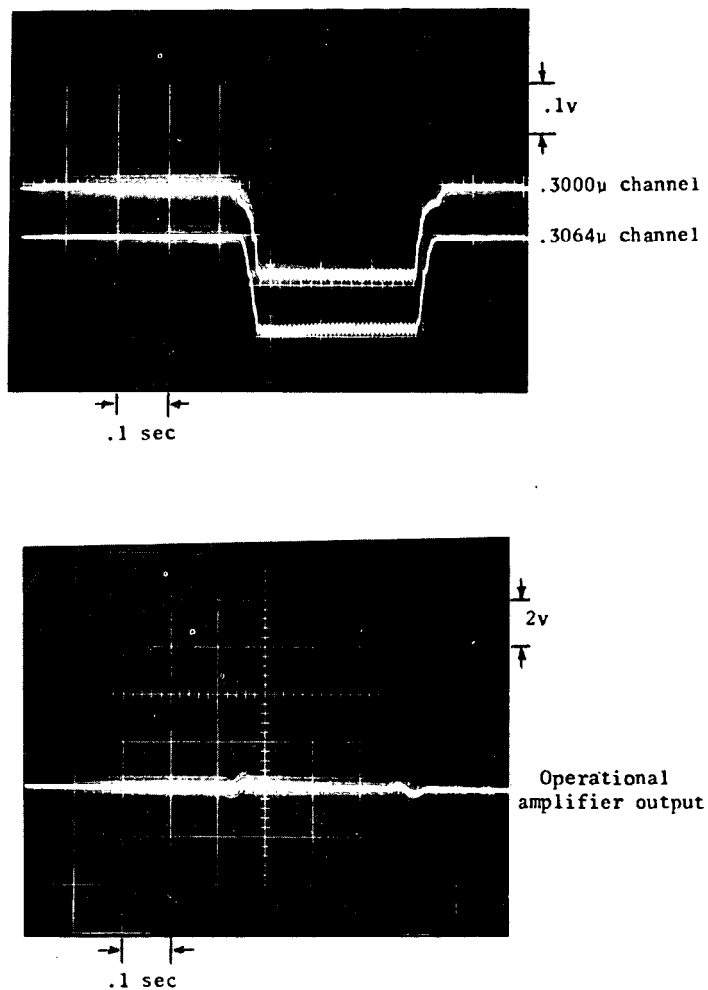


Fig. 6. Spectral signals and output of ratio amplifier for incandescent lamp.

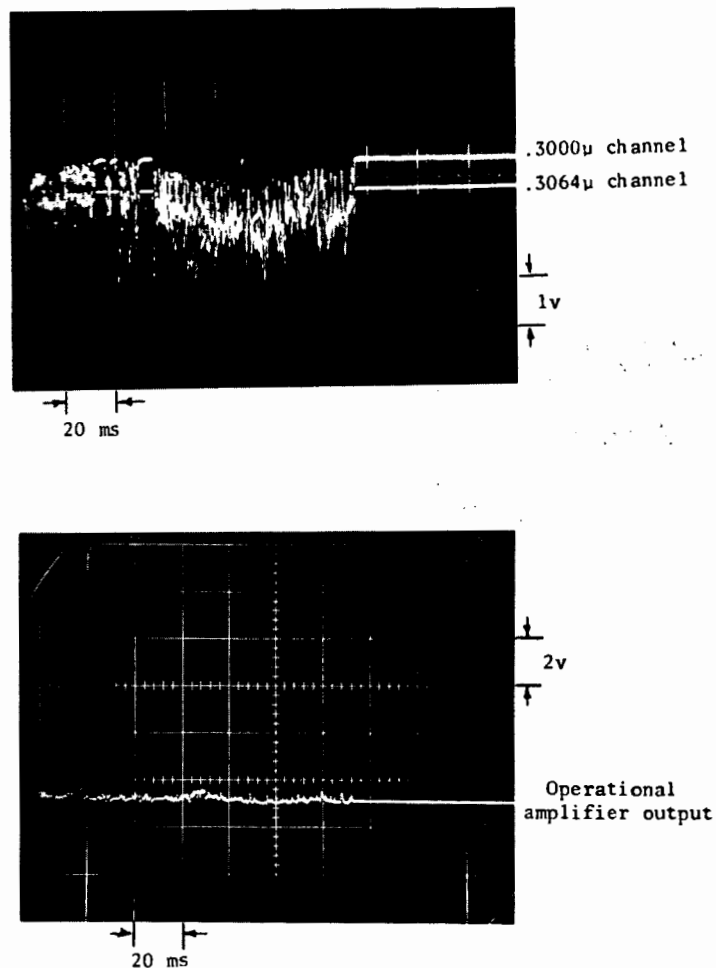


Fig. 7. Spectral signals and ratio amplifier output for iron arc source.

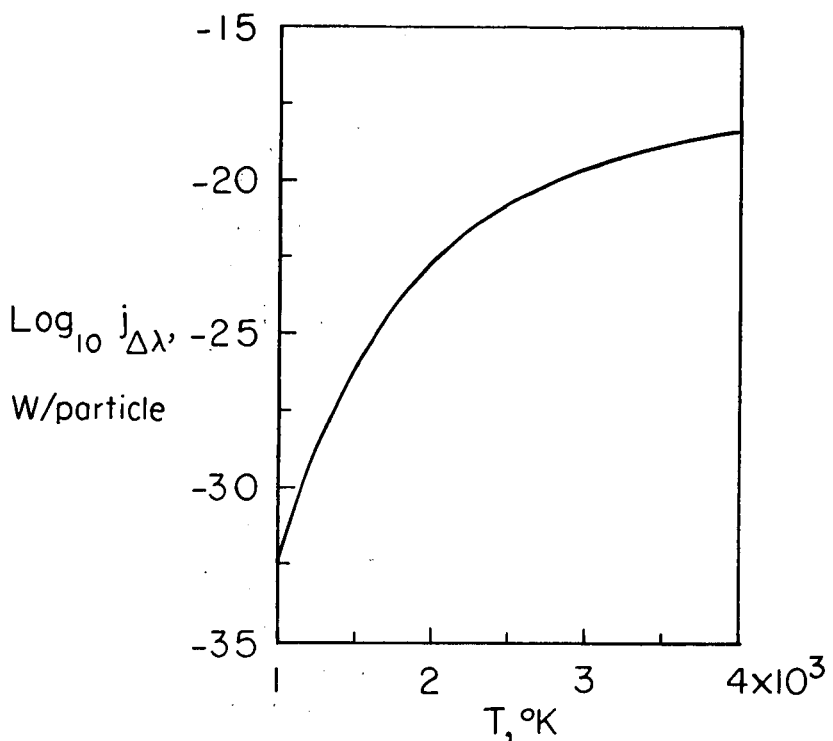


Fig. 8. Spectral bandpass energy per OH particle
as a function of temperature.

ANALYTICAL RELATIONSHIPS FOR THE INFLUENCE OF
PARTICLE SIZE ON PRECIPITATOR DESIGN

by

Robert G. Kunz and Owen T. Hanna

Introduction

The realistic design of many types of particulate collection devices involves consideration of the influence of particle size distribution. For an electrostatic precipitator, this influence is appropriately expressed by the integration of the Deutsch equation for a log-normal particle size distribution. The integral which must be evaluated in such cases depends on several parameters and cannot be evaluated exactly in terms of elementary functions. A numerical tabulation of the integral for all parametric cases of interest, while feasible, poses a considerable numerical interpolation problem and is not very suitable for computerization.

In order to express the integral simply and accurately, asymptotic methods are employed in this paper. These methods produce analytical approximations which are expressed in terms of well known functions and the solution of a certain nonlinear algebraic equation. Results of these calculations are given here in forms suitable for either hand or computer calculations. Comparison with numerical calculations shows that the results of the asymptotic analysis are applicable for virtually all cases of practical interest.

Electrostatic Precipitator Theory

In an electrostatic precipitator, suspended dust particles in a gas are electrically charged and migrate to collecting surfaces where they are captured. A force balance on a single charged particle in a quiescent gas under the influence of an electric field produces the following expression for the particle migration velocity:

$$w = \frac{E_0 E_p d_p}{4\pi\mu} \quad (1)$$

The collection efficiency of a precipitator in turbulent flow is then given by the Deutsch equation

$$n = 1 - e^{-A_p w/Q} \quad (2)$$

However, the value of w calculated according to first principles from eqn. (1) with its underlying simplifying assumptions may be several times too high because of effects unaccounted for in its derivation. These include multiple particles, uneven gas distribution, particle reentrainment, and high dust resistivity, as comprehensively discussed by White.^{11, 12} Therefore, to predict the operation of an actual precipitator, the theoretical migration velocity is replaced by a precipitation rate constant based on experience.⁶

Log-Normal Particle Size Distribution

Moreover, the particles encountered in practice are not uniform in size as we have so far tacitly assumed, but rather are made up of a continuous distribution of sizes. Specifically, most powders of industrial significance are log-normally distributed. The frequency of occurrence of a given diameter particle plotted against the logarithm of that size produces the familiar bell-shaped curve. Alternatively, the logarithm of the particle diameter (d_p) graphs as a straight line against cumulative weight percent less than that size. An example of the latter plot is shown in Figure 1. Two parameters, the mass median diameter (\bar{d}_p) and the geometric standard deviation (σ) completely specify the distribution. The mass median diameter is the diameter at the 50% point, and σ is given by either of the following ratios:

$$\bar{d}_p/d_p \text{ at } 15.9\% \text{ or } d_p \text{ at } 84.1\%/\bar{d}_p$$

A more complete explanation of fine particle statistics is contained elsewhere.⁵

Collection Efficiency Log-Normal Distribution

By lumping all non-size related quantities into one parameter

$$k = \frac{E_o E_p A}{4\pi\mu Q} \quad (3)$$

eqn. (2) can be written

$$\eta = 1 - e^{-kd_p} \quad (4)$$

Eqn. (4) is exponential in character although k, like w, is empirical. This function, shown in Fig. 2, is an example of the so-called grade efficiency curve discussed by Stairmand.⁸⁻¹⁰ Typically, larger particles are collected much more readily than smaller ones.

With the grade-efficiency function defined, the collection efficiency for each individual particle size in the distribution is completely determined. The overall efficiency of collection (η) is obtained by summing up these individual contributions

$$\eta = 1 - \frac{1}{\sqrt{2\pi}} \int_{-\infty}^{+\infty} e^{-\frac{t^2}{2}} -ae^{bt} dt \quad (5)$$

where $a \equiv kd_p$ and $b \equiv \ln \sigma$

Although attention has been focused on electrostatic precipitators, the technique to be outlined below applies as well to other types of particulate collection devices whose grade-efficiency curves can be approximated

by eqn. (4). Typical grade-efficiencies replotted on semi-logarithmic coordinates from Stairmand's tabulations and curves are shown in Fig. 3 for several such devices. Increasingly efficient collection is reflected by a larger value of k .

Numerical Integration

The integral of eqn. (5) can be computed directly by numerical quadrature, resulting in the curves presented in Fig. 4. For some purposes, these curves will be entirely satisfactory. More than likely, however, collection efficiency will be desired for a set of input parameters a and b not corresponding exactly to any of these curves, requiring either an interpolation or a complete numerical re-evaluation of the integral. In other words, the functional dependence of the efficiency on the input parameters is not shown explicitly. For this reason, simple and accurate analytical approximations for this integral have been developed.

Approximate Representation of $\frac{1}{\sqrt{2\pi}} \int_{-\infty}^{\infty} e^{-\frac{t^2}{2}} - ae^{bt} dt \approx I$

This infinite integral is seen to converge for all values of a and b . The integrand $\rightarrow 0$ for both $t \rightarrow -\infty$ and $t \rightarrow \infty$ and thus, since the integrand is always positive, it must have a maximum value at some point t^* . At the maximum point t^* , the usual condition for an interior maximum requires that

$$t^* + abe^{bt^*} = 0 \quad (6)$$

It is easily verified that there can be but one maximum point t^* for any given set of values of a and b . Thus, t^* depends on both a and b . However, by changing the variables to $t^* \equiv a^{1/2} u^*$ and $C \equiv a^{1/2} b$, eqn. (6) is reduced to a form involving the single parameter C as follows:

$$u^* + Ce^{Cu^*} = 0 \quad (7)$$

Since the integrand involves exponentials, it is natural to hope that by investigating the maximum of the integrand and suitably changing variables, the original integral might be transformed to one of the Laplace type, which could then be evaluated approximately for certain limiting values of a or b .² However, in this problem a transformation of this type does not yield the desired Laplace integral, but the transformation is nevertheless extremely useful since it does lead ultimately to a resolution of the original problem.

Some details of the analysis involved in approximating the integral are given in the appendix for the reader who is interested. Here we will present the essential results of the analysis. First we note that the approximation formulas depend on the solution of nonlinear eqn. (7). The solution of this equation is indicated graphically in Fig. 5. Approximate analytical solutions of this equation accurate to better than 5% are developed in Appendix I. These approximations may be used directly, or, if more accuracy is desired, they may be used as first guesses for iteration schemes that are also outlined in this appendix. This approach is very attractive for use on the digital computer.

The most useful approximation of the original integral I is as follows:

$$I \doteq \frac{e^{-\frac{A^2 b^2}{2}} - A}{(1+Ab^2)^{1/2}} \quad (a \rightarrow \infty, a \rightarrow 0, b \rightarrow 0) \quad (8)$$

The quantity A in eqn. (8) is related to the solution of nonlinear eqn. (7) since $Ab^2 \equiv -Cu^*$ and the solution of eqn. (7) is expressed in terms of this quantity.

Eqn. (8) is a simple expression which approximates the original integral very well, as shown in Table 1. In Appendix II, it is proved that eqn. (8) is valid in the limit of either $a \rightarrow \infty$, $a \rightarrow 0$, or $b \rightarrow 0$. The fact that eqn. (8) applies for so many limiting cases gives some reason for its excellent agreement with numerical results over such a wide range of a and b values. Except for the impractical case of large b(log-normal probability particle size distribution approaching a vertical line), the approximation would produce results coincident with the curves of Fig. 4.

Eqn. (8) represents the first approximation of an asymptotic expansion for the limiting cases quoted, and it is generally possible to increase the accuracy of the approximation by adding in some correction terms. However, adding only the next uniformly valid contribution for $a \rightarrow 0$, $a \rightarrow \infty$, $b \rightarrow 0$ causes the formula to become very much more complicated. Moreover, the comparison between eqn. (8) and the numerical results shown in Table 1 indicates that correction terms are not really necessary.

Although eqn. (8) seems to represent an appropriate approximation to the original integral I for current needs, it is difficult to anticipate whether some cases that seem unimportant now will prove to be significant at a later time. For this reason and for the sake of completeness, certain other approximations to I are given in Appendix III.

Approximate Representation of $\frac{1}{\sqrt{2\pi}} \int_{-\infty}^z e^{-\frac{t^2}{2}} dt \equiv J$

Frequently an estimate of the particle size distribution of the uncollected material is required in addition to an overall efficiency prediction. This would be important where several collecting devices are to be installed in series. For example, it is not uncommon for cyclones to be installed upstream of a precipitator. In this case, the quantity and distribution of the particulates escaping from the cyclones would be used as the feed to the precipitator, and the calculation repeated.

To calculate the particle size distribution, it is desirable to approximate the above integral where $z = \ln(dp/dp)/b$ is now a parameter in addition to a and b . It appears possible to do this in a manner analogous to that for the previous case ($z \rightarrow \infty$). Again, the details are indicated in the appendix (Appendix IV). The result is

$$(z < t^*) \quad J \doteq \frac{\frac{-z^2}{2} - E + \frac{(z+bE)^2}{2(1+b^2E)}}{\pi^{1/2} (1+b^2E)^{1/2}} \int_s^{\infty} e^{-s^2} ds = \frac{z+bE}{2^{1/2} (1+b^2E)^{1/2}} \quad (9)$$

where $E \equiv a e^{+bz}$.

Eqn. (9) holds only for $z < t^*$. For $z > t^*$, we have instead

$$(z > t^*) \quad J \doteq I - \frac{\frac{-z^2}{2} - E + \frac{(z+bE)^2}{2(1+b^2E)}}{\pi^{1/2} (1+b^2E)^{1/2}} \int_s^{\infty} e^{-s^2} ds = \frac{z+bE}{2^{1/2} (1+b^2E)^{1/2}} \quad (10)$$

The approximation given for J in eqns. (9) and (10) involve the well known error function which is widely tabulated and for which there are simple computer approximations.¹ Formulas (9) and (10) are shown in example 1 following to approximate well to the integral J .

Typical Applications of the Results

The above functions provide an analytical tool to evaluate the effect of inlet particule size distribution on collection efficiency at constant precipitator flow and field conditions. This treatment is intermediate between the simplified Deutsch equation based on a uniform particle size, eqn. (2), and a detailed systems analysis.⁶ The use of these asymptotic relationships will be demonstrated in the numerical examples given below.

Example 1

Problem:

Compute the overall efficiency of the precipitator whose grade-efficiency curve is given in Fig. 2 operating on the inlet dust distribution shown in Fig. 1. Evaluate the particle size distribution of the uncollected material.

Solution:

By replotting Fig. 2 on semi-logarithmic coordinates as in Fig. 3 and determining the slope, one finds $k = 0.46$ reciprocal microns. From Fig. 1, $\bar{d}_p = 12$ microns and $\sigma = 2.8$. Therefore, $a = k\bar{d}_p = 5.52$, $b = \ln \sigma = 1.03$, and $C = a^{1/2}b = 2.42$. From Fig. 5, $Ab^2 = 1.42$ giving $A = 1.34$. From eqn. (8),

$$n = 1 - \frac{e^{-\frac{A^2 b^2}{2}}}{(1+Ab^2)^{1/2}} = 1 - 0.0654 \approx 93.4\% \quad (\text{rounded down})$$

A refinement of these calculations including a computer solution of eqn. (7) gives an efficiency of 1-0.065436 compared to the above figure. An efficiency of 1-0.065370 is obtained by direct numerical integration of eqn. (5). Agreement of these results is excellent.

The particle size distribution in terms of the fraction lost below a given size can be found by considering the integral J with upper limit given by $z = \ln (\bar{d}_p / d_p) / b$. J can be approximated by eqns. (9) or (10) depending upon the value of z . To obtain the cumulative particle size distribution, J must be divided by I , the infinite integral. The results of these calculations, set forth in Table 2, show quite good agreement for this example.

In addition, the preceding calculations can be compared with a more commonly employed method. The inlet dust distribution is broken up into a finite number of narrow size ranges, the amount collected for each range is determined, and these values are summed to find the overall collection efficiency. An example of this procedure is given by Stairmand.^{8, 10} The calculations are summarized in Table 3. The overall collection efficiency is again 93.4%. The distribution of escaping material is slightly finer than the distribution obtained by direct numerical integration of the function I , shown previously in Table 2. The "exact" numerical integration distribution, with \bar{d}_p of 2.7 microns and σ of 1.9, lies between this approximate distribution and the one obtained using the asymptotic expressions.

For this illustrative calculation, entries in Table 3 corresponding to the inlet particle size and collection efficiency have been computed from the appropriate functional forms rather than graphically as might normally be done for a routine calculation. The differences in efficiency and distribution are therefore caused only from taking a series of finite intervals in which the collection efficiency is assumed to be constant at its midpoint value.

In this example, the asymptotic analytical expressions derived in this paper have been shown to produce an overall efficiency equivalent to that obtained from direct numerical integration and a commonly employed approximate technique. In addition, the particle size distributions of all three methods are roughly comparable, with differences of the order of a few percent. The asymptotic functions are especially attractive for hand calculations when only the overall efficiency is desired. When a complete particle size distribution is required, the calculations involving eqns. (9) and (10) are more tedious than the method outlined by Stairmand, which would probably be used. When computer facilities are available, the asymptotic functions represent a savings in computer time over a standard numerical quadrature and are expected to require about the same order of magnitude of time as that used by the Stairmand type of calculation.

Example 2

Problem:

To increase collection efficiency, the precipitator of example 1 is to be doubled in size by increasing the length of its plates in the direction of gas flow. Calculate the new efficiency accounting for particle size distribution and by using the simplified Deutsch equation.

Solution:

To account for a change in plate length, one must vary k which is directly proportional to this dimension. In example 1, the parameters of the inlet dust and $k = 0.46$ led to an efficiency of 93.4%. When the size is doubled, k becomes 0.96 and the computation proceeds in a similar manner, giving an efficiency of 97.9%.

This calculation can be compared to an entirely different technique. As is sometimes done, eqn. (2), the simplified Deutsch equation for a monodisperse particulate, can be employed and thereby circumvent the use of an integral and all the difficulties involved in its evaluation. In this procedure, the observed 93.4% efficiency can be used to fix the value of the argument of the exponential at 2.7. Doubling the plate length makes this parameter 5.4 and gives an efficiency of 99.5%. Although the two efficiencies, 97.9% and 99.5%, appear close, the loss rates differ significantly by a factor of 4.

The efficiency as a function of length is plotted in Fig. 6. The asymptotic expression gives the efficiency shown by the solid curve, while the simplified Deutsch equation produces the broken line. The two provide equivalent results only in the vicinity of 93.4% efficiency where the Deutsch equation exponent was fitted.

Thus, the Deutsch equation predicts a greater efficiency at a given increment in length or a shorter additional length required to achieve a given increase in efficiency. This is the same sort of behavior demonstrated

Solution:

To account for a change in plate length, one must vary k which is directly proportional to this dimension. In example 1, the parameters of the inlet dust and $k = 0.46$ led to an efficiency of 93.4%. When the size is doubled, k becomes 0.96 and the computation proceeds in a similar manner, giving an efficiency of 97.9%.

This calculation can be compared to an entirely different technique. As is sometimes done, eqn. (2), the simplified Deutsch equation for a monodisperse particulate, can be employed and thereby circumvent the use of an integral and all the difficulties involved in its evaluation. In this procedure, the observed 93.4% efficiency can be used to fix the value of the argument of the exponential at 2.7. Doubling the plate length makes this parameter 5.4 and gives an efficiency of 99.5%. Although the two efficiencies, 97.9% and 99.5%, appear close, the loss rates differ significantly by a factor of 4.

The efficiency as a function of length is plotted in Fig. 6. The asymptotic expression gives the efficiency shown by the solid curve, while the simplified Deutsch equation produces the broken line. The two provide equivalent results only in the vicinity of 93.4% efficiency where the Deutsch equation exponent was fitted.

Thus, the Deutsch equation predicts a greater efficiency at a given increment in length or a shorter additional length required to achieve a given increase in efficiency. This is the same sort of behavior demonstrated

TABLE I
COMPARISON OF APPROXIMATE METHOD WITH NUMERICAL INTEGRATION

$$I = \frac{1}{\sqrt{2\pi}} \int_{-\infty}^{1/2} e^{\frac{-t^2}{2}} -ae^{-bt} dt$$

$\alpha=1, b=t, c=0$				$\alpha=1, b=0.1032, b=0.1$				$\alpha=2, b=0.6931$				$\alpha=3, b=1.0986$				$\alpha=10, b=2.3026$				$\alpha=22.026, b=10$			
APPROX.	Num.	Int.	APPROX.	Num.	Int.	APPROX.	Num.	Int.	APPROX.	Num.	Int.	APPROX.	Num.	Int.	APPROX.	Num.	Int.	APPROX.	Num.	Int.			
0	1.0000	1.0000	1.0000	1.0000	1.0000	1.0000	1.0000	1.0000	1.0000	1.0000	1.0000	1.0000	1.0000	1.0000	1.0000	1.0000	1.0000	1.0000	1.0000				
1	0.3679	0.3679	0.3679	0.3679	0.3679	0.3757	0.3757	0.3733	0.3892	0.3848	0.4230	0.4196	0.4359	0.4773	- 133 -								
2	0.1353	0.1353	0.1367	0.1367	0.1367	0.1847	0.1838	0.2278	0.2263	0.3173	0.3185	0.4009	0.4500										
3	0.04979	0.04979	0.05126	0.05127	0.05126	0.1036	0.1031	0.1526	0.1520	0.2618	0.2643	0.3818	0.4241										
4	0.01832	0.01832	0.01941	0.01941	0.01941	0.06302	0.06279	0.1099	0.1097	0.2259	0.2288	0.3690	0.4229										
5	0.006738	0.006738	0.007416	0.007415	0.007416	0.04061	0.04049	0.08301	0.08293	0.2001	0.2032	0.3593	0.4143										
6	0.002479	0.002479	0.002859	0.002858	0.002859	0.02732	0.02726	0.06484	0.06484	0.1804	0.1835	0.3515	0.4072										
7	0.0009119	0.0009118	0.0011111	0.0011111	0.0011111	0.01902	0.01698	0.05195	0.05199	0.1648	0.1678	0.3451	0.4013										
8	0.0003355	0.0003354	0.0004356	0.0004355	0.0004356	0.01361	0.01359	0.04247	0.04253	0.1520	0.1549	0.3397	0.3962										
9	0.0001234	0.0001234	0.0001721	0.0001721	0.0001721	0.009362	0.009351	0.03328	0.03335	0.1412	0.1441	0.3349	0.3917										
10	0.00004340	0.00004340	0.00006854	0.00006854	0.00006854	0.007436	0.007429	0.02971	0.02977	0.1321	0.1349	0.3307	0.3877										
11	0.00001670	0.00001670	0.00002753	0.00002751	0.00002753	0.005645	0.005640	0.02530	0.02536	0.1241	0.1269	0.3269	0.3841										
12	0.000006144	0.000006144	0.00001113	0.00001113	0.00001113	0.004347	0.004345	0.02176	0.02182	0.1172	0.1198	0.3236	0.3808										
13	0.000002260	0.000002260	0.000004536	0.000004534	0.000004536	0.003391	0.003390	0.01887	0.01893	0.1111	0.1136	0.3205	0.3778										
14	0.0000008315	0.0000008315	0.000001862	0.000001861	0.000001862	0.002676	0.002675	0.01649	0.01654	0.1056	0.1081	0.3176	0.3750										

TABLE 2

COMPARISON OF APPROXIMATE AND NUMERICALLY INTEGRATED UNCOLLECTED
PARTICLE SIZE DISTRIBUTIONS FOR EXAMPLE 1

d_p (microns)	J (approx.) *	Cum. Wt.%	J (numerical)	Cum. Wt.%
1	0.00557	8.5	0.00563	8.6
2	0.0209	32.0	0.0219	33.5
3	0.0347	53.1	0.0372	56.9
4	0.0471	72.0	0.0481	73.6
5	0.0537	82.1	0.0550	84.1
6	0.0579	88.5	0.0592	90.5
7	0.0607	92.8	0.0618	94.5
8	0.0624	95.4	0.0632	96.6
9	0.0635	97.1	0.0641	98.0
10	0.0642	98.2	0.0646	98.8
∞	0.065436	100.	0.065370	100.

In this example, $d_p \approx 2.96$ corresponds to $z=t^$ and is therefore where we switch from eqn. (9) to eqn. (10).

TABLE 3

CALCULATION OF OVERALL COLLECTION EFFICIENCY FOR EXAMPLE 1 USING METHOD OUTLINED BY STAIRMAND

<u>Size of Grade (microns)</u>	<u>% in Grade at Inlet</u>	<u>Collection Efficiency at Mean Size (%)</u>	<u>Overall Collection (%)</u>	<u>Cum. Wt.% Collected</u>	<u>Cum. Wt.% Escaping</u>
0-1	0.8	20.6	0.165	0.18	9.7
1-2	3.3	49.8	1.64	1.9	34.9
2-3	4.7	68.3	3.21	5.4	57.7
3-4	5.4	80.0	4.32	10.0	74.1
4-5	5.6	87.4	4.89	15.2	84.9
5-6	5.2	92.4	4.80	20.4	91.0
6-7	5.0	95.0	4.75	25.5	94.9
7-8	4.7	96.8	4.55	30.3	97.1
8-9	4.3	98.0	4.21	34.8	98.5
9-10	4.0	98.7	3.95	39.1	99.3
10-15	15.6	99.7	15.55	55.7	100
15-20	10.5	100	10.5	67.0	100
20+	30.9	100	30.9	100	100
			<u>93.435</u>		

Figure 1

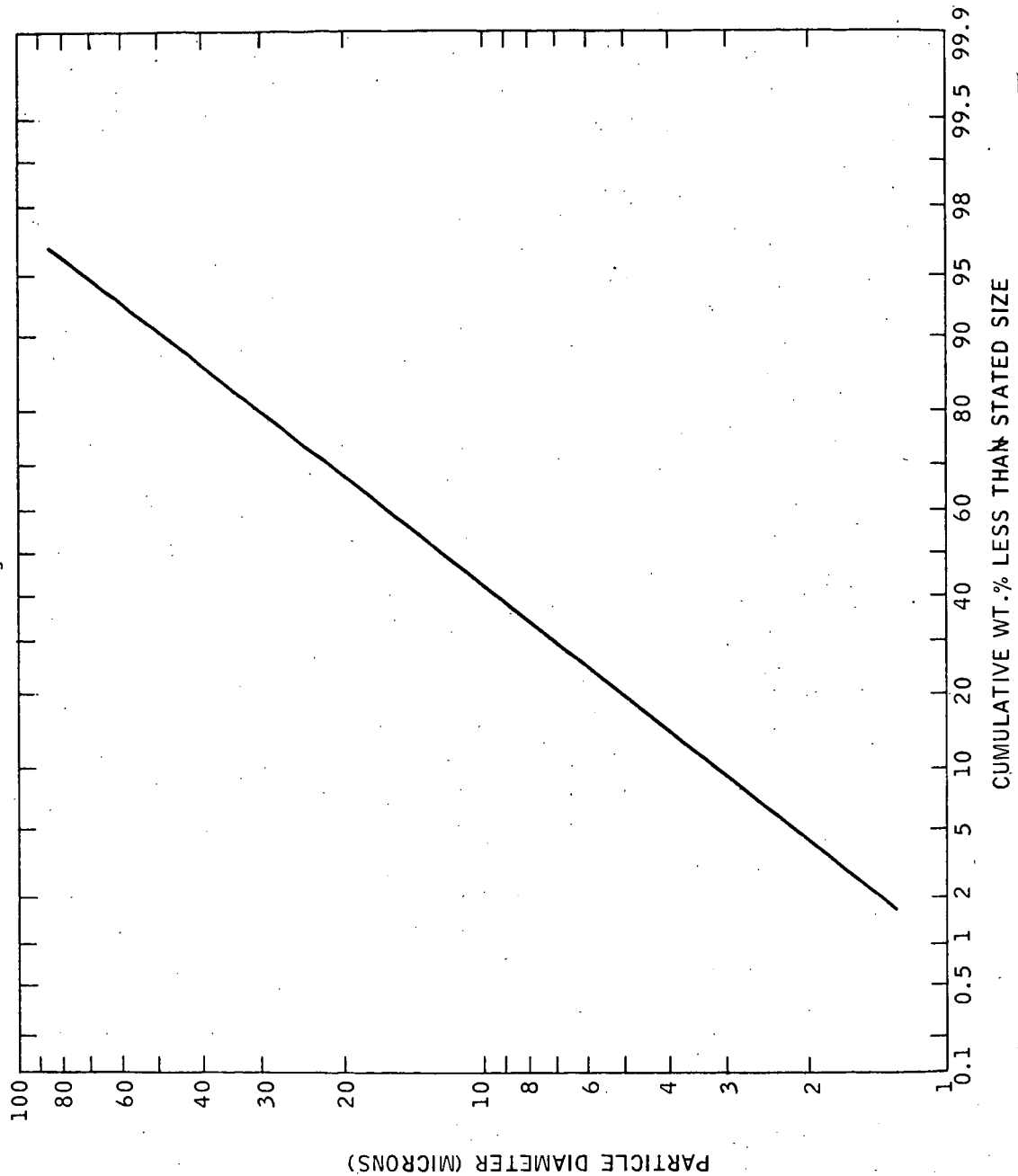


Figure 2

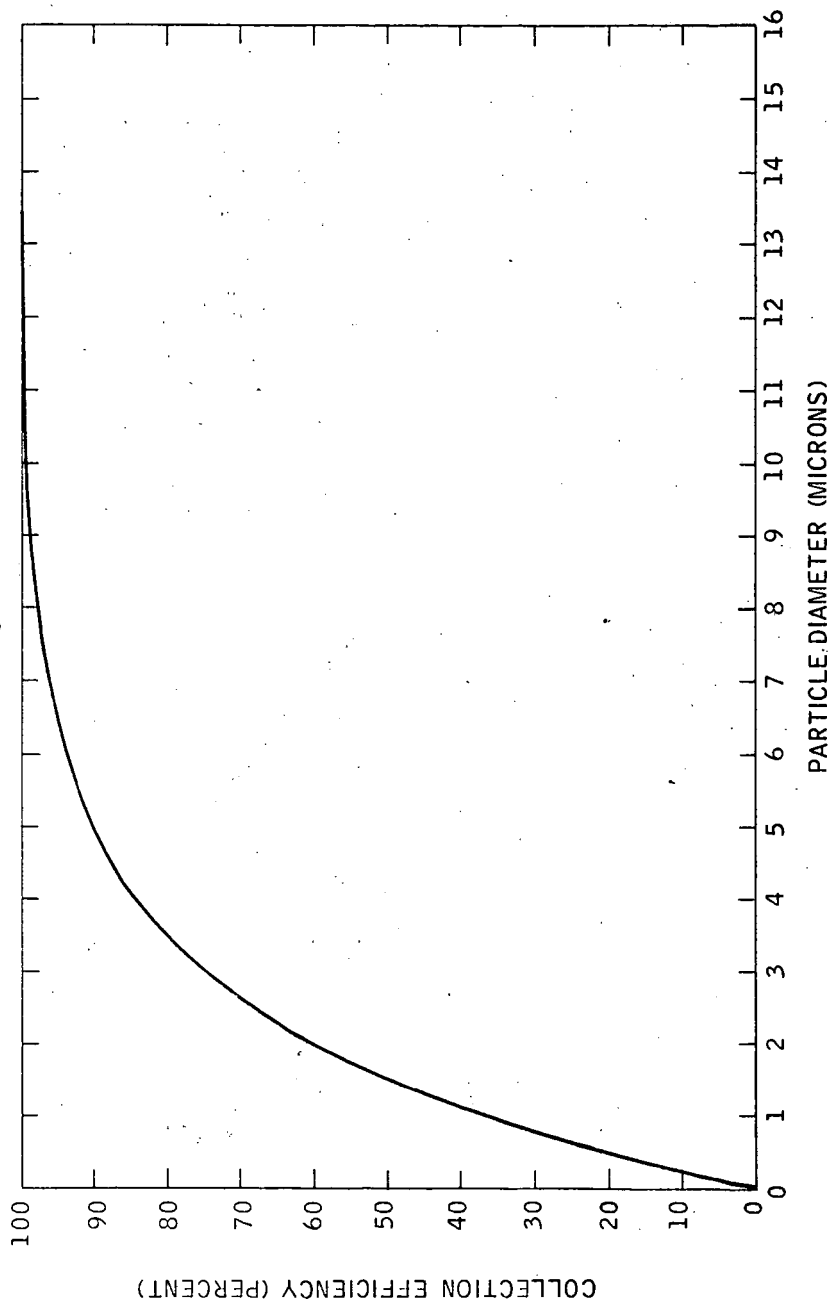


Figure 3

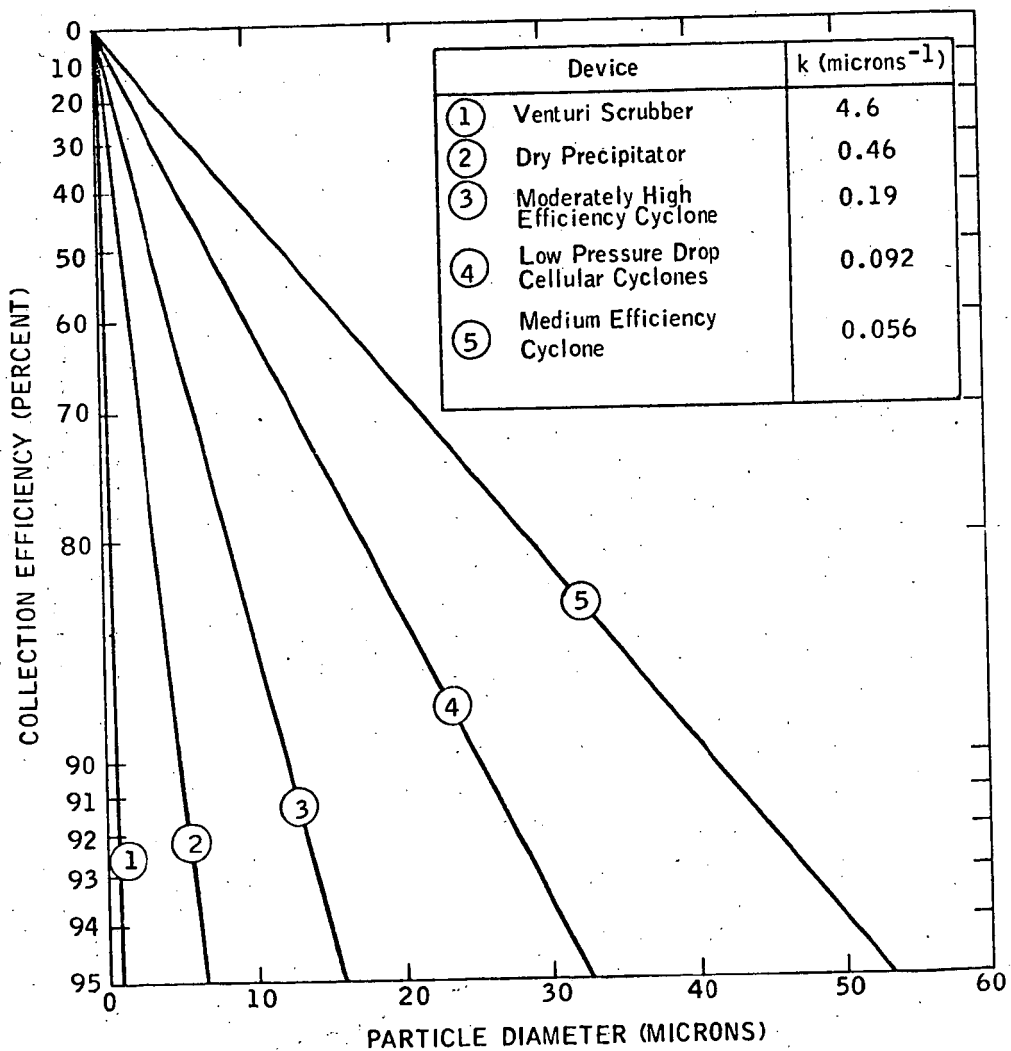


Figure 4

COLLECTION EFFICIENCY (PERCENT)

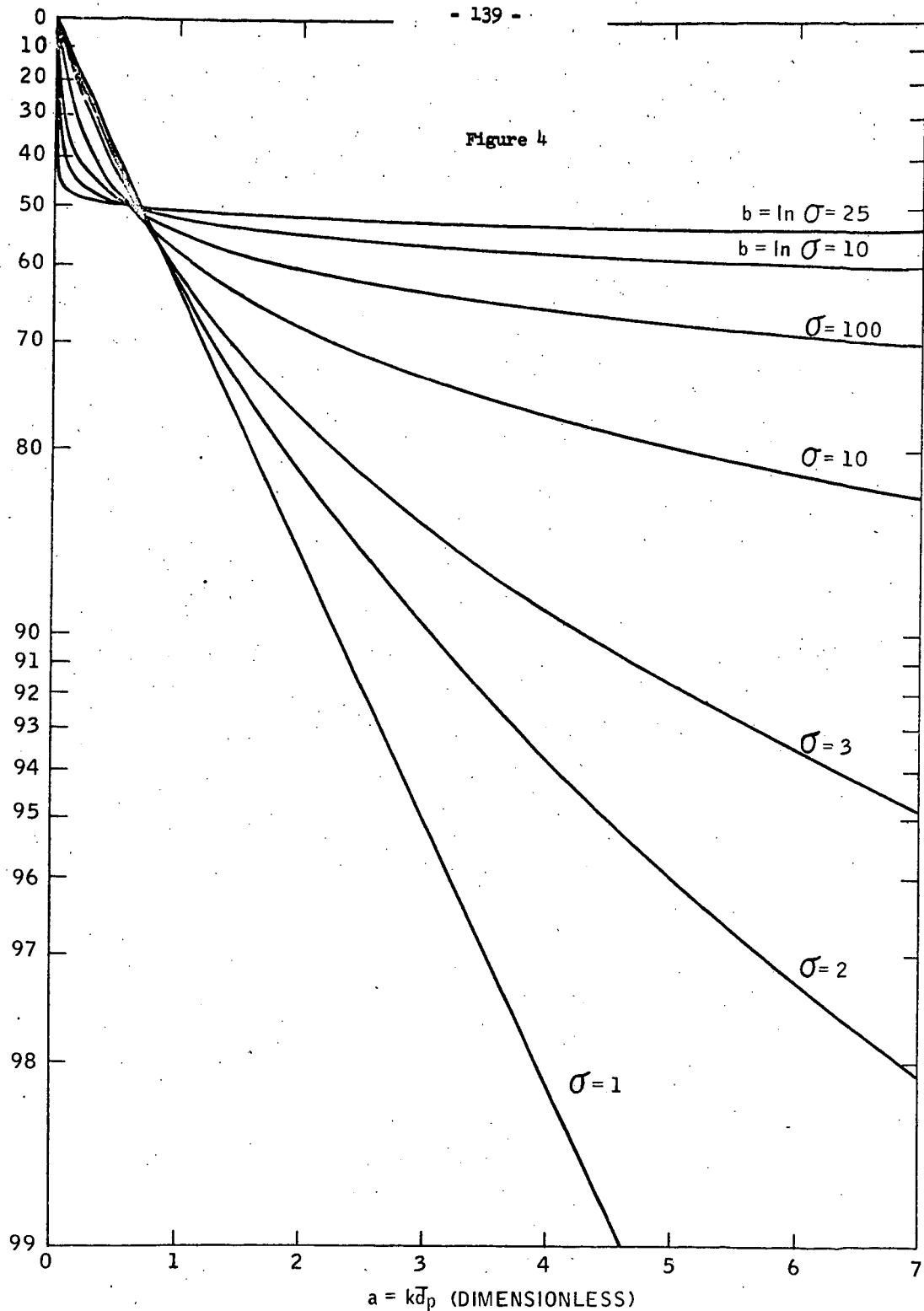
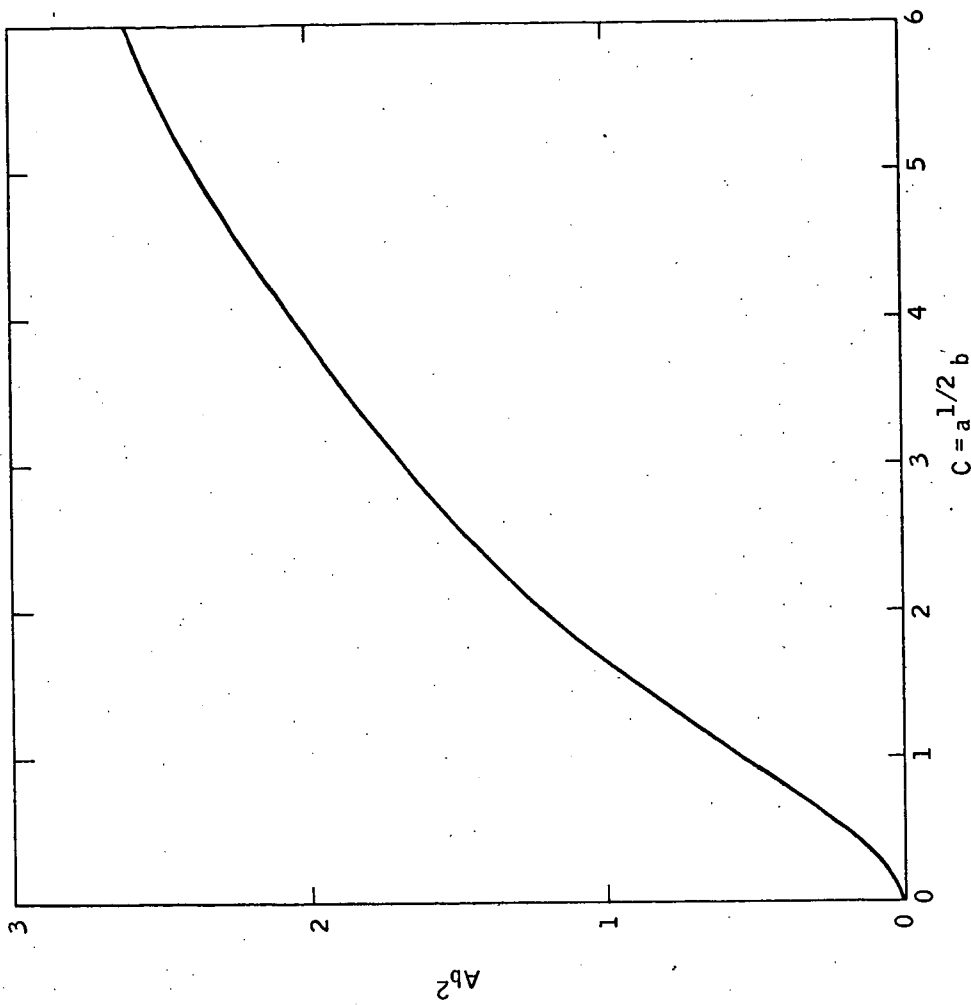
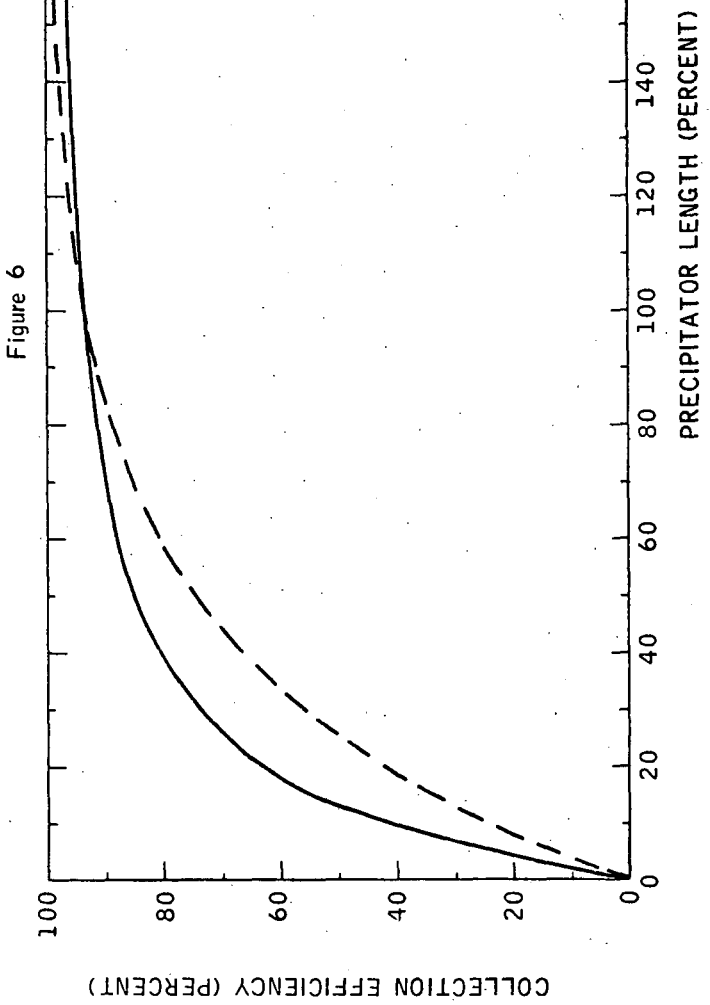


Figure 5





Notation

$$a = \frac{kd}{p}$$

$$A = ae^{bt^*} = -Cu^*/b^2 = -t^*/b$$

A_p = area of collection plates

b = $\ln \sigma$

$$C = a^{1/2} b$$

d_p = particle diameter

\bar{d}_p = mass median diameter

e = base of natural logarithms

$$E = ae^{bz}$$

E_o = charging electrical field intensity

E_p = collection electrical field intensity

I = infinite integral in eqn. (5)

J = integral I with variable upper limit

k = collection parameter

Q = gas volumetric flow

s = variable of integration

t = variable of integration

t^* = location of maximum point

$$u^* = t^*/a^{1/2}$$

w = effective migration velocity

z = variable upper limit of integral J = $\ln(d_p/\bar{d}_p)/b$

Greek Letters

η = collection efficiency

μ = gas viscosity

π = numerical constant

σ = geometric standard deviation

LITERATURE CITED

1. Abramowitz, M. and Stegun, I. A., "Handbook of Mathematical Functions," NBS AMS 55, U. S. Government Printing Office, Washington, D. C. (1964).
2. Erdeleyi, A., "Asymptotic Expansions," Dover, New York (1956).
3. Finney, J. A., Jr., Power Eng., 72 (12), 26 (1968).
4. Henrici, P., "Elements of Numerical Analysis," Wiley, New York (1964).
5. Irani, R. R. and Callis, C. F., "Particle Size: Measurement, Interpretation, and Application," Wiley, New York (1963).
6. Nichols, G. B. and Oglesby, S. Jr., Paper presented at the 63rd Annual Meeting A.I.Ch.E., Symposium on Particulate Control Device Measurement, Paper 4a (1970).
7. Penney, G. W., J. Air Pollut. Contr. Ass., 19, 596 (1969).
8. Stairmand, C. J., J. Inst. Fuel (London), 29, 58 (1956).
9. _____, The Chemical Engineer (London), 194, CE310 (1965).
10. _____, Filtration & Separation, 7(1), 53 (1970).
11. White, H. J., Ind. Eng. Chem., 47, 932 (1955).
12. _____, "Industrial Electrostatic Precipitation," Addison-Wesley, Reading, Mass. (1963).

Appendix I

The solution of $u^* + Ce^{Cu^*} = 0$.

This equation is easily solved numerically by means of a suitable iteration method if appropriate starting values are used. Suitable procedures include the Newton method or the ordinary iteration method accelerated by means of the δ^2 process.⁴ The latter method was used to obtain the numerical values shown in Fig. 5 and Table A-1. Asymptotic solutions of the equation were used to yield reasonable starting values.

The two asymptotic solutions for $-Cu^* \approx Ab^2$ are

$$G_1(C) = \frac{2C^2(1+C^2)}{2(1+C^2)^2-C^4} \quad (C \rightarrow 0) \quad (A1-1)$$

and

$$G_2(C) = 2\ln C - \ln(2\ln C) \quad (C \rightarrow \infty) \quad (A1-2)$$

These two asymptotes are compared with the numerical values in Table A-1. Since the $C \rightarrow \infty$ solution, eqn. (A1-2) involves a logarithmic scale, it only becomes accurate at extremely large (and impractical) values of C. However, it was observed that the difference between the numerical values and eqn. (A1-2) is nearly constant for $C \geq 2.5$, and thus in the table values of $G_2(C)+0.3$ are seen to yield accurate results for $C \geq 2.5$.

The asymptotic solutions given above are very useful in the asymptotic analysis of the integral I. Eqns. (A1-1) and (A1-2) show the asymptotic behavior of the quantity A with respect to a and b. For $a \rightarrow 0$, $A \rightarrow a$ and for $a \rightarrow \infty$, $A \rightarrow 2 \frac{\ln(a^{1/2}b)}{b^2}$.

TABLE A-1

COMPARISON OF NUMERICAL AND ASYMPTOTIC SOLUTIONS OF EQN. (7)

C	<u>Numerical</u> <u>-Cu* = Ab²</u>	<u>Asymptotic</u>		
		<u>G₁(C)</u>	<u>G₂(C)</u>	<u>G₂(C) + 0.3</u>
0	0	0		
0.1	0.0099	0.0099		
0.3	0.0828	0.0828		
0.5	0.2039	0.2040		
1	0.5671	0.5614		
2	1.202	1.176	1.060	1.360
2.5	1.456	1.372	1.227	1.527
3	1.679	1.513	1.410	1.710
4	2.053		1.753	2.053
5	2.360		2.050	2.350
6	2.620		2.307	2.607
8	3.045		2.734	3.034
10	3.386		3.078	3.378
20	4.490		4.201	4.501
1000	11.38		11.19	11.49
10,000	15.67		15.51	

$$G_1(C) = \frac{2C^2(1+C^2)}{2(1+C^2)^2-C^4}, \quad G_2(C) = 2\ln C - \ln(2\ln C)$$

Appendix II

$$\text{Evaluation of } \frac{1}{(2\pi)^{1/2}} \int_{-\infty}^{\infty} e^{-\frac{t^2}{2}} dt = ae^{bt}$$

We proceed by splitting the integral by means of $\int_{-\infty}^{\infty} = \int_{-\infty}^{t^*} + \int_{t^*}^{\infty}$ where t^* is the solution of eqn. (6). Thus $I = I_1 + I_2$ where $I_1 = \int_{-\infty}^{t^*}$ and $I_2 = \int_{t^*}^{\infty}$. First consider I_2 , which turns out to be much easier to analyze than I_1 (it happens that to the first approximation, I_1 and I_2 are equal). By translating the origin of coordinates to t^* through $t-t^* = u$, we get:

$$I_2 = \frac{e^{-\frac{b^2 A^2}{2}}}{(2\pi)^{1/2}} \int_{u=0}^{\infty} e^{-\frac{u^2}{2}} + Abu - Ae^{bu} du \quad (\text{A2-1})$$

Since the new integrand, by way of its construction, is a maximum near $u=0$, it is natural to approximate to the integrand in this vicinity in hopes that though the approximation may not be good in other regions, these regions contribute only a small part to the integral. The best procedure seems to be the following. Write

$$e^{bu} = 1 + bu + \frac{b^2 u^2}{2} + e^{bu} - 1 - bu - \frac{b^2 u^2}{2}.$$

Then expand the exponential in eqn. (A2-1) to get

$$I_1 = \frac{e^{-\frac{b^2 A^2}{2}} - A}{(2\pi)^{1/2}} \int_{u=0}^{\infty} e^{-\frac{(1+b^2 A)u^2}{2}} \left[1 - A(e^{bu} - 1 - bu - \frac{b^2 u^2}{2}) \right] du \quad (\text{A2-2})$$

where the error incurred by taking 1 for the quantity in square brackets is negative and less in magnitude than the next term.

By performing the integration we get

$$I_2 = \frac{e^{-\frac{b^2 A^2}{2} - A}}{(2\pi)^{1/2}} \left[\frac{\pi^{1/2}}{(2g)^{1/2}} - A \left\{ \left(\frac{2}{g} \right)^{1/2} e^{\frac{b^2}{2g}} \int_{s=-b}^{\infty} e^{-s^2} ds - \left(\frac{\pi}{2g} \right)^{1/2} - \frac{b^2 \pi^{1/2}}{(2g)^{3/2}} \right\} \right] \quad (A2-3)$$

where $g \equiv (1 + b^2 A)$

The error made by approximating the quantity in square brackets by the first term is negative and less in magnitude than the next term. It is easily shown eqn. (A2-3) that the relative error associated with using just the first term in square brackets goes to zero for either $a \rightarrow 0$, $a \rightarrow \infty$ or $b \rightarrow 0$. The integral I is transformed by means of $t^* - t = s$ and becomes

$$I_1 = \frac{e^{-\frac{b^2 A^2}{2} - A}}{(2\pi)^{1/2}} \int_{s=0}^{\infty} e^{-\frac{s^2}{2}} - Abs - Ae^{-bs} ds \quad (A2-4)$$

Here again the integrand is approximated near its maximum ($s=0$) and to a first approximation for either $a \rightarrow 0$, $a \rightarrow \infty$ or $b \rightarrow 0$

$$I_1 \rightarrow \frac{e^{-\frac{b^2 A^2}{2} - A}}{2g^{1/2}}$$

However, in the case of I_1 , the demonstration of the validity of this result is much more involved than it was in the case of I_2 and the lengthy details are omitted.

Appendix III

Other Asymptotic Expansions to I = $\frac{1}{(2\pi)^{1/2}} \int_{-\infty}^{\infty} e^{-\frac{t^2}{2}} - ae^{bt} dt$

For $b \rightarrow \infty$, $I \rightarrow 1/2$ in accordance with

$$I = 1/2 + R_1, |R_1| \leq \frac{1}{\sqrt{2\pi}} \max \left[\frac{a}{b}, \frac{e^{-a}}{ab} \right] \quad (A3-1)$$

Note the curve for $b=25$ of Fig. 4 is approaching this limit.

For $b \rightarrow 0$ we have

$$I = e^{-\frac{A^2 b^2}{2}} - A \left[1 - A \left(\frac{b^2}{e^2} - 1 \right) \dots \right] \quad (A3-2)$$

Eqn. (A3-2) is useful since it has the property that the error made by taking the term in square brackets equal to 1 is negative and less in magnitude than $A \left(\frac{b^2}{e^2} - 1 \right)$.

For $a \rightarrow 0$

$$I \sim \sum_{i=0}^{\infty} \frac{(-1)^i a^i e^{-\frac{b^2 i^2}{2}}}{i!} = 1 - ae^{-\frac{b^2}{2}} + \frac{a^2 e^{-2b^2}}{2!} - \frac{a^3 e^{-\frac{9b^2}{2}}}{3!} \dots \quad (A3-3)$$

This series diverges for any $b > 0$, but it is asymptotic in the sense that the error is of the same sign as the first neglected term and less than it in magnitude. Therefore, the series is of use computationally for sufficiently small values of a .

Appendix IV

Evaluation of $\frac{1}{(2\pi)^{1/2}} \int_{-\infty}^z e^{\frac{-t^2}{2}} dt = J$

It is convenient to consider separately the cases $z < t^*$ and $z > t^*$. For $z < t^*$, the maximum of the integrand is at z and accordingly we move the origin of coordinates to z and approximate to the integrand in this vicinity. Thus J becomes

$$J = \frac{e^{-\frac{z^2}{2}}}{(2\pi)^{1/2}} \int_{w=0}^{\infty} e^{zw - \frac{\omega^2}{2}} - E e^{-bw} d\omega \quad (A4-1)$$

where $E \equiv ae^{bz}$

By approximating the exponential near $\omega = 0$, we get

$$J \approx \frac{e^{-\frac{z^2}{2}} - E}{(\pi)^{1/2} (1+b^2 E)^{1/2}} e^{2(1+b^2 E)} \int_{s=\frac{(bE+z)}{2^{1/2}(1+b^2 E)^{1/2}}}^{\infty} e^{-s^2} ds \quad (z < t^*) \quad (A4-2)$$

The integral appearing in eqn. (A4-2) is just the complementary error function which is widely tabulated and for which there are simple computer approximations.

For $z > t^*$, it is convenient to calculate J by means of $K = \int_{-\infty}^z - \int_z^{\infty}$.

Then an approximation of the type discussed in the previous paragraph gives

$$J \approx I - \frac{e^{-\frac{z^2}{2}} - E}{\pi^{1/2} (1+b^2 E)^{1/2}} e^{2(1+b^2 E)} \int_{s=\frac{bE+z}{2^{1/2}(1+b^2 E)^{1/2}}}^{\infty} e^{-s^2} ds \quad (z > t^*) \quad (A4-3)$$

Note that for $z = t^*$ the sum of the approximations to $\int_{-\infty}^z$ and \int_z^{∞} just adds up to the approximation given for $\int_{-\infty}^{\infty}$.

A STUDY OF FLY ASH REACTIONS AND DEPOSIT FORMATION
IN A LARGE, CYCLONE-FIRED STEAM GENERATOR

A. A. Orning

U. S. Department of the Interior, Bureau of Mines,
Pittsburgh Energy Research Center, Pittsburgh, Pa.

Introduction

Many, if not most, of the problems peculiar to the use of coal as a fuel are related to its mineral matter content. The ash and slag products cause fouling and sometimes corrosion of heat transfer surfaces, are hard to remove when slag deposits become massive, are difficult to contain when the slag is fluid, and are costly to remove as particulate matter in the stack gases. The purpose of this paper is to discuss the release of mineral matter in burning coal and to present data on reactions of ash deposits with combustion product gases in a large cyclone-fired steam generator. Conclusions will be drawn that must be interpreted as pertinent to the particular unit though based in part on observations in other units. The intent is to demonstrate that valuable information can be gained by systematic sampling and analysis of fly ash and ash deposits.

The Release of Mineral Matter

Ash, as formed from the mineral matter of coal in the ASTM Standard Method,^{1/} has analyses as illustrated by samples 8 and 9 of Table I for two Illinois coals. Several things are noteworthy: 1) Carbonates are converted to oxides; 2) sulfur is retained as sulfate to the extent that sulfate formation precedes carbonate decomposition, and 3) the weight percentages of ash components, represented as oxides, add approximately to 100%. When the ash is formed under high-temperature conditions, as in the steam generator furnace rather than the temperature-controlled muffle furnace used for the ash determination, a lesser proportion of the sulfur is retained as sulfates and the alkali metals are at least partially volatilized. Vapor pressures for various alkali materials are given in Table II. The free alkali metals are most volatile, but equilibria favor conversion to the hydroxides. The oxides should be considered, although equilibria also favor their conversion to the hydroxides. Little information is available on the kinetics of such high-temperature, gas-phase reactions. Acid-base reactions are fast in water solution but may be slow in the gas phase. HCl gas seems relatively inert. Alkaline mists have been observed to fall out of the plume from incineration of organic wastes with high NaCl content. These considerations suggest that the hydroxides are the probable mode of transport of alkali metals in the hot combustion gases.

TABLE I. - Analyses of ash and slag samples, weight percent

No.	Location	SO ₃	Fe ₂ O ₃	Al ₂ O ₃	SiO ₂	CaO	MgO	Na ₂ O	K ₂ O	Total
1	Slag tank	0.25	19.7	17.6	45.8	8.67	0.95	2.16	1.99	97.1
3	Reheat superheater	10.2	21.0	16.4	32.5	10.95	.80	2.80	2.19	96.8
4	Primary superheater	2.2	18.6	18.3	47.1	5.96	.86	2.47	2.04	97.5
5	Economizer hopper	5.0	20.6	17.4	43.2	5.79	.75	2.56	2.13	97.4
6	Air heater hopper	2.2	21.7	17.6	45.4	7.61	.86	2.12	2.05	99.5
7	Precipitator hopper	3.5	18.9	17.6	45.8	5.04	.90	2.91	2.82	97.5
8	Coal ash, A	7.5	28.2	15.5	35.7	7.68	.78	2.43	1.83	99.6
9	Coal ash, B	8.0	17.2	18.9	44.5	7.55	.91	1.98	1.83	100.9

TABLE II. - Temperatures at selected vapor pressures

Component	T °C		
	1 mm	10 mm	100 mm
Na	439	549	701
K	341	443	586
NaOH	739	897	1111
KOH	719	863	1064
NaCl	865	1017	1220
KCl	821	968	1164

Iron sulfide, FeS, and metallic iron tend to appear with deficient air supply. This is aggravated in wet bottom furnaces when pyrite (FeS_2) impinges on the slag surface. The iron in coal is present primarily as pyrite. Bailey and Ely²⁷ have shown that iron tends to segregate into slag and into furnace deposits. The author has observed a furnace with front wall burners and a plan area too small to prevent flame impingement on the wall surfaces. Iron content of the wall slag was over three times that expected from the coal ash analysis. It appeared that oxygen was deficient in the area of flame impingement and that liquid droplets of FeS were preferentially adhering to the wall, although intermittent oxidation gave an oxidized slag.

Fireside corrosion associated with segregated deposits high in alkali-iron sulfates were first found on furnace wall tubes of wet bottom furnaces.^{3,4} Presence of CO in the local gas stream was indicative of local oxygen deficiency and flame impingement with preferential adherence of FeS droplets and high local heat transfer rates. However, the segregated deposits were found to be sulfates with detectable sulfide only at the interface between the deposit and the tube metal. Intermittent oxidizing conditions convert sulfides to sulfates. With tube surface temperatures on the order of 400°C, the complex alkali-iron pyrosulfates become stable liquids. While these liquids in part may be corrosion products, they in turn are cause for electrolytic corrosion if not the active corrosive agents.

Reactions between sulfur oxides and fly ash have been the subject of study and speculation for many years. Johnstone⁵ concluded that fly ash from stoker-fired boilers had a little catalytic action on the oxidation of sulfur dioxide in flue gas. Crossley, Poll and Sweett⁶ studied these reactions to explain findings of the Boiler Availability Committee that firing of pulverized coal over the back end of mechanical stokers was effective in controlling acidic deposits in the boiler. The appearance of the typical alkali-iron-aluminum sulfates on superheater tubes brought renewed interest in the reactions between fly ash and combustion gases. The extensive literature has been reviewed by Reid.⁷ The deposits are characterized by water solubility, a low pH, high content of alkali, iron, aluminum and sulfate, and relatively low contamination by other constituents of fly ash. These deposits underlie typical ash deposits. They have an amorphous or microcrystalline appearance when cold but sometimes show signs of having been liquid. They appear where gas temperatures, the thickness of the overlying ash deposit, and the steam conditions are such that the resulting heat transfer produces temperatures near the tube surface approaching 650°C. The segregated deposit may be separated from the tube metal by a poorly consolidated oxide scale. The author has also found samples where liquid wetted the metal tube and penetrated under the oxide scale so as to bend it away from the tube surface. Relatively low occlusion of fly ash in the segregated deposit indicates that components not soluble in the deposit are mechanically ejected by cyclic melting and solidification. The resulting deposit, from American bituminous coals, has a somewhat variable composition, particularly the

proportion of iron and aluminum sulfates, but is so characteristically different from the overlying fly ash deposits that it is visually detectable without need for chemical analysis.

Occurrence of the segregated deposit under typical ash deposits has caused speculation as to whether the deposit was formed first and the fly ash deposited later or whether the segregated material was synthesized beneath the fly ash deposit.

Synthesis of the complex sulfates requires a partial pressure of SO_3 higher than that found in the main stream of combustion gases. Anderson and Goddard⁸⁷ conclude that the $\text{SO}_2\text{-}\text{SO}_3$ reaction reaches equilibrium within the deposit and that solution phenomena at operating temperatures reduce the necessary partial pressure of SO_3 below that exhibited by pure phases of alkali-iron and alkali-aluminum sulfates that appear in the deposit after cooling.

While information on reactions between sulfur oxides and fly ash is sketchy, there is even less information on reactions involving the alkali metals. Weintraub, Goldberg and Orning⁹ found that the alkali content of fly ash, subjected to a temperature gradient in a flue gas atmosphere, migrated towards a cold surface at 375°C. The complex alkali sulfates did not appear. In the absence of a supply, beyond that of the original fly ash, there was insufficient alkali for the synthesis. Since the alkali components of the mineral matter of coal are volatile under combustion conditions, it seemed desirable to gather data on the reabsorption of alkali by fly ash and by deposits at various points within a coal-fired steam generator. A study of deposits in a cyclone-fired unit seemed preferable because the high temperatures within the cyclone would assure more complete volatilization of the alkali components.

The Steam Generator

The steam generator cross section is shown in Fig. 1. It was rated at 3,290,000 lb of steam/hr, 3625 psig and 1005°F superheat with 575 psig and 1005°F reheat. It had 10 cyclones, 10 ft in diameter, five each on the front and rear walls. Sampling points are shown by the circled numerals, except for the electrostatic precipitator hopper which is not shown. The furnace wall tubes were fully studded to a level about 5 ft below the gas recirculation ports. A thin, glassy slag coat was intact throughout the studded zone following shutdown. Slag shedding had occurred on all upper wall surfaces except in the corners just above the studding and on the walls under some of the gas recirculation ports.

Ash and Slag Samples

Two southern Illinois bituminous coals were used. Analyses of the ash and slag samples are shown in Table I. Data on the mole percent basis, shown in Table III, are more revealing. Unfortunately, the two coals that were used have somewhat different ash analyses. The SO_3 is equivalent to about 70% of the CaO for both coal ashes, while sulfur in ash accounted for 24.6% of the sulfur in coal A and 38.5% of the sulfur in coal B. Retention of sulfur in the coal ash, as produced at 700° to 750°C by the standard method for ash content, is related to the calcite content rather than to the sulfur content of the coal.

The composition of various slag, deposit, and fly-ash samples may be expected to depend upon opportunities for segregation, on temperatures at various points along the gas flow path, and on the readsorption of sulfur and alkali components. The temperatures were not measured but were probably on the order of over 1700°C in the cyclone, 1000°C in the secondary superheater, location 2, and 325°C at the air heater, location 6.

TABLE III.- Ash analyses, mole percent, and physical characteristics

No.	Location	Color ^a	Mag. ^b	SO ₃	Fe ₂ O ₃	Al ₂ O ₃	SiO ₂	CaO	MgO	Na ₂ O	K ₂ O
1	Slag tank	BL.	1	0.2	9.5	13.3	59.0	11.9	1.8	2.7	1.6
6	Air heater	BL.	3	2.1	10.4	13.2	58.0	10.4	1.6	2.6	1.7
4	Primary superheater	R.B.	2	2.2	8.9	13.9	60.4	8.2	1.6	3.1	1.7
5	Economizer hopper	B.R.	2	4.9	10.2	13.4	56.7	8.2	1.5	3.3	1.8
3	Reheat superheater	B.R.	0	10.2	10.5	12.9	43.6	15.7	1.6	3.6	1.9
7	Precipitator hopper	G.B.	2	3.4	9.2	13.4	59.4	7.0	1.7	3.6	2.3
8	Coal ash, A	-	-	7.6	14.3	12.3	48.3	11.1	1.6	3.2	1.6
9	Coal ash, B	-	-	7.5	8.0	13.8	55.2	10.0	1.7	2.4	1.4

^aColor code: BL., black; R.B., red-brown; G.B., gray-brown; B.R., brick-red.

^bScale of increasing magnetic character.

Sulfur content of the slag is almost immeasurably low. The 0.2 mole of SO₃ corresponds to 0.1 wt percent of sulfur, which is reported to the nearest 0.1%. The sodium and potassium contents of the slag are comparable to those of the coal ashes. Slag from the cyclones flows across the furnace floor to the slag drip. Either the alkali metals were not substantially volatilized in the cyclones or they were readSORBED as the slag flowed across the furnace floor.

Deposit samples were not taken from location 2, Fig. 1 (lead tube of the last platen of the secondary superheater). Visually identifiable complex alkali-iron-aluminum sulfate, covered by a thin shell of ash, was found on these tubes. The ash shell had partially shed on cooling of the furnace. Large sections could be removed intact with light finger pressure on the edge to expose the underlying sulfate deposit. The shell was so thin that clean separation from the underlying sulfate deposit could not be assured for the purpose of chemical analysis.

Deposits at location 3 (lead tube of the reheat superheater platen) were shaped like antlers jutting into the gas stream and were joined by a thin shell across the front of the tube. They were so hard that the author could not break them off by hand though they projected about 3 inches in front of the tube. The analysis gave an exceptionally high content of SO₃ and maximum values for the alkali metals, except K₂O in the precipitator hopper sample. The surface of the deposit was dusty, and fracture surfaces showed no indication of fusion, suggesting that the ash was cemented by formation of alkali sulfates within pores of the deposit.

The samples from location 4 (the top of the primary superheater) were hard nodules blown from an unknown location and too large to pass between the superheater tubes. While these nodules were as hard as sample No. 3, the sulfur content was not as high. The underlying tubes were free of deposits.

The economizer hopper (location 5) was located below the downflow section of convective heat transfer tubes. The air heater hopper was under the flow reversal duct between sections of the air heater. The classifying action of changes in flow direction, compared to electrostatic precipitation, may be responsible for the differences in analysis between samples from the economizer hopper, the air heater hopper, and the precipitator hopper, locations 5, 6, and 7. There is also a progressive drop in temperature between these locations.

The sample analyses are remarkably consistent except for the variation in SO_3 content and a disproportionation between lime and silica in sample No. 3. The iron content of the hopper and deposit samples is between those of the two coal ashes, while the silica contents, with the one exception, are higher than that of either coal ash.

The hopper and deposit samples showed remarkable differences in color and magnetic properties. Table III gives data from gross appearance. Microscopic examination showed heterogeneous character. The slag tank sample looked like pulverized black glass with a few translucent wedges and a few magnetic particles, presumably magnetite. The brick-red material from the reheat superheater tube had a very small number of magnetite particles. The economizer hopper and superheater nodule samples had increasing proportions of magnetite mixed with the brick red. The air heater sample appeared almost as black as the slag tap sample, and had a large portion of magnetite with a sprinkling of small red particles on the surface of the larger black particles. The precipitator hopper sample had a considerable portion of magnetite with enough whites (some opalescent beads) and reds to give a gray-brown appearance. Almost all black particles, except those from the slag tank, were magnetic, presumably magnetite. The analyses for iron are given in terms of Fe_2O_3 without regard to the actual state of oxidation. The brick red color is due to ferric oxide, and the color variations may be used to infer variations in ferric oxide content.

Discussion

Most of the ash from cyclone combustion is collected in the slag tank with almost negligible sulfur content. Deposits with high sulfur content are formed over long periods of time and represent a negligible part of the material balance. The fly ash has a significant sulfur content but represents a minor fraction of the mineral matter input. Most of the sulfur passes through the system as SO_2 , but oxidation to SO_3 and sulfate formation by reaction with other mineral matter components have considerable effect on deposit formation.

The behavior of iron is of particular interest. It is present in the coal almost entirely as pyrite, often distributed as very fine particles. Rapid heating to 2200°C produces liquid droplets approximating FeS , ferrous sulfide.^{10/} The sequence of melting, decomposition, and oxidation is unknown. Larger particles are probably thrown onto the slag within the cyclone. Smaller particles are converted in suspension to finely divided ferric oxide. The author has observed a cyclone-fired unit with a mechanical but no electrostatic precipitator. The stack plume was brick red. Had it been black it would have been rated number 4 smoke. The finely divided ferric oxide produces a dust coating on tube surfaces. At appropriate temperature levels, oxidation of SO_2 to SO_3 within the dust layer and reaction with adsorbed alkali metals produces the complex alkali-iron sulfates. Depending upon temperatures and temperature gradients, these sulfates may act as cementing agents or may accumulate as a segregated phase near the tube surface. Cyclic melting and freezing then causes ejection of non-soluble particulates and accumulation of the segregated deposit.

A systematic variation in alkali metal content was not apparent until the data were arranged in the sequence of Table III. Data for the slag tank sample are listed first. Those for the precipitator hopper sample and the coal ashes are listed last. Intervening data are in the sequence of increasing content of ferric iron as inferred from color. Variation from the sequence of positions along the flow path is a result of segregation of particulate matter and the action of retractable blowers used periodically to blow loose deposits off tube surfaces. The highest content of ferric iron was found in the hard deposit on the reheat superheater tube. Dusty deposits are blown off the tubes by the retractable blowers.

Depending upon agglomeration, these tend to fall out in the economizer hopper or carry through to the electrostatic precipitator. Absorption of the alkali metals appears to be favored by the finely divided ferric oxide with some effect of temperature on opportunities for sulfate formation. Temperatures are lowest in the precipitator. Conditions are most favorable for reaction with SO₃ within deposits on the secondary superheater, location 2, and the reheat superheater, location 3. Material balances are obscured by differences between the coals and the unknown times required for deposit formation. High SO₃ content in segregated deposits is negligible in comparison to total flow over the time of their formation. Relatively high content in the precipitator sample is offset by the larger portion of the total ash collected in the slag tank. Immeasurably lower content in the slag tank sample is sufficient to provide material balance. The disproportionation of MgO and SiO₂, in the deposit at location No. 3, the reheat superheater lead tube, is explainable in terms of the results of intermittent operation of retractable blowers. Acid formation and alkali adsorption extend through the interface between the cemented deposit and the dusty outer coat. Basic constituents, as against the acidic silica present in segregated particles, are preferentially retained when the dust coating is intermittently removed by the blower action.

Recommendations for Future Study

Data presented here are for samples taken from a cyclone-combustion-fired-unit. It has often been observed that these units produce reddish fly ash rather than the typical gray fly ash from pulverized-coal-fired systems, indicating the presence of finely divided ferric oxide. Nevertheless, the data indicate the possibilities for better understanding of the reactions involved in deposit formation. Supplemental data on temperatures, gas compositions, and particulate samples taken from the gas stream at various points along the gas flow path would be helpful. Preparation for taking samples from less accessible positions would also be helpful.

Laboratory studies of reactions between gases and mineral matter components become meaningful only when interpreted in relation to the conditions and materials that exist within actual steam generator systems. Laboratory studies should be encouraged, but they must be coordinated with actual conditions in large steam generators.

Conclusions

- 1) Samples of fly ash and deposits were obtained from various locations in a large, cyclone-fired steam generator.
- 2) Wide variations in color were due to variations in ferric oxide content.
- 3) Variations in alkali metal content were related qualitatively to variations in ferric oxide content and temperatures.
- 4) Typical segregated deposits of complex alkali-iron-alumina sulfates were visually identified within the secondary superheater.
- 5) A hard deposit on the reheat superheater probably was formed by the cementing action of sulfates formed within the pores of an overlying dusty deposit and incremental buildup of cemented material left after each cycle of retractable blower operation.

References

- 1/ ASTM Standard Method of Laboratory Sampling and Analysis of Coal and Coke, D271-64.
- 2/ Bailey, E.G., and Ely, F.G., Tr. Am. Soc. Mech. Engrs. 63, 465-71 (1941).
- 3/ Reid, W.T., Corey, R.C., and Cross, B.J., Tr. Am. Soc. Mech. Engrs. 67, 279-88 (1945).
- 4/ Corey, R.C., Cross, B.J., and Reid, W.T., Tr. Am. Soc. Mech. Engrs. 67, 289-302 (1945).
- 5/ Johnstone, H.F., Univ. of Illinois Eng. Exp. Sta. Bull. 228, 1931, pp. 44, 45.
- 6/ Crossley, H.E., Poll, A., Sweett, F., J. Inst. Fuel 21, 207-13 (Apr. 1948).
- 7/ Reid, W.T., External Corrosion and Deposits-Boilers and Gas Turbines, Elsevier, New York, 1971.
- 8/ Anderson, C.H., and Goddard, C.W., J. Inst. Fuel 61, 357-64 (1968).
- 9/ Weintraub, M., Goldberg, S.A., and Orning, A.A., Tr. Am. Soc. Mech. Eng., Series A, 83, 444-50 (Oct. 1961).
- 10/ Halstead, W.D., and Raask, E., J. Inst. Fuel 62, 344-49 (1969).

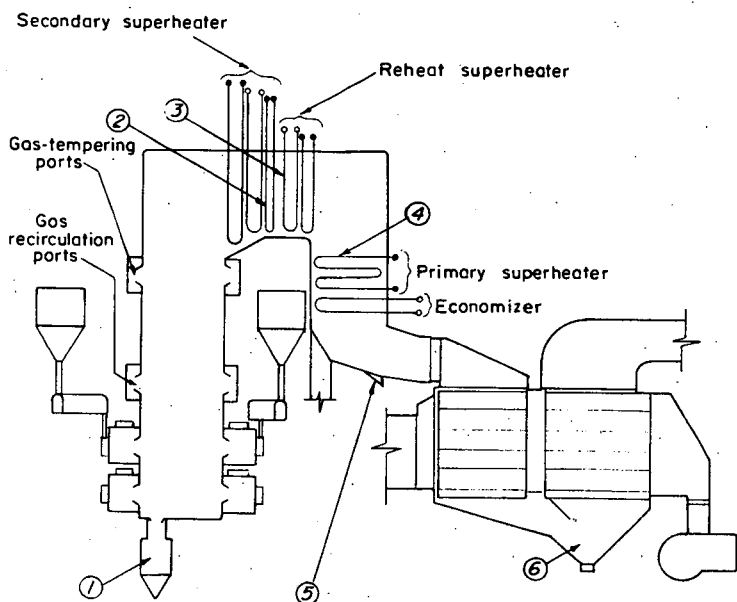


Figure 1.- Sampling locations in the cyclone fired steam generator.
Location 7, the precipitator hopper is not shown.